

# Engineering translational vaccine delivery systems with the polyphenol tannic acid

By

Morgan E. Janes

B.S. Bioengineering  
University of Maryland – College Park, 2019

Submitted to the department of Harvard-MIT Health Sciences and Technology in partial  
fulfillment of the requirements for the degree of

DOCTOR OF PHILOSOPHY IN MEDICAL ENGINEERING AND MEDICAL PHYSICS

at the

MASSACHUSETTS INSTITUTE OF TECHNOLOGY

May 2024

©2024 Morgan E. Janes. All rights reserved. The author hereby grants to MIT a nonexclusive, worldwide, irrevocable, royalty-free license to exercise any and all rights under copyright, including to reproduce, preserve, distribute, and publicly display copies of the thesis, or release the thesis under an open-access license.

Authored by: *Morgan E. Janes*

Harvard-MIT Health Sciences and Technology  
March 1, 2024

Certified by: *Samir Mitragotri, PhD*

Hiller Professor of Bioengineering  
Hansjorg Wyss Professor of Biologically Inspired Engineering  
Thesis Supervisor

Accepted by: *Collin M. Stultz, MD, PhD*

Director, Harvard-MIT Program in Health Sciences and Technology  
Nina T. and Robert H. Rubin Professor in Medical Engineering and Science  
Professor of Electrical Engineering and Computer Science

**Thesis Supervisor:**

Samir Mitragotri, PhD

Hiller Professor of Bioengineering, Harvard University

**Thesis Committee Chair:**

Darrell Irvine, PhD

Professor of Biological Engineering and Materials Science & Engineering, MIT

**Thesis Reader:**

David Avigan, MD

Professor of Medicine, Harvard Medical School

Chief of Division of Hematology/Hematologic Malignancy, Beth Israel Deaconess Medical Center

# Engineering translational vaccine delivery systems with the polyphenol tannic acid

By Morgan E. Janes

Submitted to the department of Harvard-MIT Health Sciences and Technology on March 15, 2024 in partial fulfillment of the requirements for the degree of  
DOCTOR OF PHILOSOPHY IN MEDICAL ENGINEERING AND MEDICAL PHYSICS

## ABSTRACT

Supramolecular biomaterials, which are capable of spontaneous assembly via diverse non-covalent interactions, represent an exciting frontier in drug delivery due to their ease of formulation and modularity. Tannic acid (TA) is a naturally-occurring compound that has a demonstrated ability to engage in supramolecular interactions with biological cargo, including proteins, nucleic acids, and cell membranes. In this thesis, we harnessed the broad bio-adhesive capacity of TA to develop scalable, modular systems for vaccine engineering across various applications.

Building upon previous work utilizing TA-containing metal phenolic networks for cell membrane engineering, we fabricated a cell membrane-bound formulation for local drug delivery to dendritic cell (DC) vaccines termed META (**M**embrane **E**ngineering using **T**annic **A**cid). DC vaccines hold great potential for a spectrum of diseases including cancer and autoimmune conditions, and combination drug delivery is an attractive strategy to manipulate their function and overcome *in vivo* plasticity. However, DCs are not compatible with particle-based local delivery approaches due to their broad phagocytic capacity. We showed that META preserved DC viability and critical functions such as migration, and then demonstrated the capacity of the system to incorporate and release protein cargoes with varying physical properties alone and in combination. Finally, we showed that META carrying either pro- or anti-inflammatory cargo could influence the carrier cell phenotype accordingly, underscoring the potential of META for the local control of phagocytic immune cells in a next step to advance DC therapies in the clinic.

In the main portion of this work, we used TA to modulate the delivery kinetics of subunit vaccines to enhance their immunogenicity against infectious disease. Subunit vaccines are a well-established and clinically scalable intervention, yet they have achieved limited success for weak or rapidly evolving antigens such as those associated with SARS-CoV-2. Delivery strategies that promote gradual release of subunit vaccines from the site of injection may improve humoral immunity by enhancing the duration of lymph node exposure, however, clinical implementation of this approach is challenging due to poor scalability and high costs. Here, we showed that TA acts as an “adhesive” to mediate deposition and retention of protein antigens at the subcutaneous injection site for over one week. In addition to enhancing the magnitude and duration of vaccine drainage to the lymph nodes, inclusion of TA induced lymph node accumulation of antigen-laden monocyte-derived dendritic cells (moDCs), eliciting durable antibody titers against the receptor-binding domain (RBD) of SARS-CoV-2 and variants of concern in mice. This system, termed TAPER (**T**issue-**A**dhesive **P**olyphenol-mediated **E**nhanced **R**etention), provides many benefits including one-pot synthesis, scalability, low cost, and modularity, which together may open the door for the realization of effective and clinically feasible vaccination strategies.

**Thesis Supervisor:** Samir Mitragotri, PhD  
Hiller Professor of Bioengineering, Harvard University

## Acknowledgments

This thesis would not have been possible without the support of so many individuals for whom I am incredibly grateful. Samir, thank you for taking me into the lab as an HST student and remaining open-minded to the many winding paths that my research projects would take. Your optimism in the face of uncertainty helped me to carry on in the face of many setbacks and pursue new avenues that ultimately led to exciting new findings. I would also like to thank my thesis committee members, Dr. Darrell Irvine and Dr. David Avigan, for their pertinent feedback on my research proposal and their support through the latter half of the PhD.

I extend my heartfelt appreciation to all the members of the Mitragotri Lab who have shaped me into the scientist and person who I am today. To Neha Kapate and Lily Li-Wen Wang, I am so lucky to have had you as scientific mentors, classmates, and friends. Lily, your enthusiasm and generosity are what motivated me to learn more about the lab, and it has been so exciting to see your work flourish. Neha, thank you so much for your insights on everything from experiments to career planning and more (and for allowing me to borrow reagents during the COVID supply shortage/when I simply forgot in the early days of the PhD). To Charles Park and Alex Gottlieb, our time as the “Cellnex Team” was by far the defining period of my PhD and the one I will remember the most fondly. Charles, thank you for teaching me just about everything I know about how to be not just a good scientist, but a great scientist. It is no exaggeration that everything I have accomplished would not have been possible without you. I cannot thank you enough for the time you have invested to teach me new techniques, collaborate on experiments, brainstorm, and everything in between. You have consistently pushed me to be my best and I am so grateful to have had you as a collaborator and friend. Alex G., I am so fortunate we were able to work together during the early days of our PhDs. I have always been impressed by your ability to quickly pick up and work with new concepts and techniques, and your wealth of knowledge about flow techniques and analysis helped elevate my work to the next level. Thank you for always lending a helping hand whenever I’ve needed it, near or far, and for making all the time we spent in the lab and the animal room much more enjoyable. To Ninad Kumbhojkar, Supriya Prakash, and Morgan Goetz, I am so glad I was able to join your “cohort” in the lab. Thank you for making the Mitragotri Lab such a fun place to work. To Danika Rodrigues, thank you for being the best deskmate, labmate, and roommate! To all the Mitragotri Lab members past and present, including Kolade Adebawale, Rick Liao, Vinny Chandran Suja, John Clegg, Zongmin Zhao, Jayoung Kim, Yongsheng Gao, Suyog Shaha, Maithili Joshi, and Alex Curreri, thank you for your mentorship, scientific discussions, and all the fun times we had throughout the years. To Bijay Singh and Claudia Stearns, thank you for all your efforts to keep the lab running and support our research, especially during difficult times.

I am so grateful for the support of my friends and family throughout the highs and lows of the PhD experience. To my HST cohort, I am so thrilled that we were able to learn and grow together, and I know we’ll do great things. Special shoutout to my friends and teammates in the MIT Biotech Group and Area Two Bio Fund; I am so proud of all we were able to build together. To my friends from UMD and back home, thank you for taking such an interest in my work and my progress. I am so excited to celebrate this milestone with you. To my parents and Ben, thank you for your support and enthusiasm through each step of this process, and a never-ending supply of comedic relief when needed. And finally, to Alex, I am beyond grateful to have had your support throughout my PhD. In addition to your sharp attention to detail as a scientist, your kindness, generosity, and humor have been so uplifting during difficult times. I love you!

I would like to extend a special thanks to Dr. Zongmin Zhao, Dr. Kolade Adebawale, Dr. Neha Kapate, and Dr. Alex Najibi for advice on experiment design and feedback on my writing. I would also like to acknowledge support from the Wyss Institute of Biologically Inspired Engineering and Harvard John A. Paulson School of Engineering and Applied Sciences, as well as the Harvard Center for Biological Imaging, Molecular and Cellular Biology (MCB) Core, Materials Characterization Core, and Harvard University Center for Nanoscale Systems (CNS) for research services and support. I would also like to acknowledge Biorender ([biorender.com](https://biorender.com)) for assistance creating figures.

# Table of Contents

<b>1. Chapter 1: Introduction.....</b>	<b>11</b>
1.1. Introduction to vaccines.....	11
1.2. Cancer vaccines.....	11
1.3. Cell-based vaccination.....	14
1.3.1. Dendritic cell cancer vaccines.....	14
1.3.2. Dendritic cell vaccines for autoimmune disease.....	16
1.3.3. Challenges and opportunities for DC vaccines.....	17
1.4. Subunit vaccines against infectious disease.....	18
1.4.1. Vaccines protect against infectious disease.....	18
1.4.2. Magnitude and timing of vaccine delivery governs immunogenicity.....	20
1.4.3. Approaches to modulate vaccine delivery kinetics.....	21
1.5. Polyphenols as drug delivery agents.....	23
1.5.1. Tannic acid and interactions.....	23
1.5.2. Biomedical applications of TA.....	24
1.5.3. Cellular engineering using TA.....	25
1.6. Aims and scope of thesis.....	25
<b>2. Chapter 2: Dendritic cell immune modulation via polyphenol membrane coatings.....</b>	<b>27</b>
2.1. Abstract.....	27
2.2. Introduction.....	27
2.3. Results.....	29
2.3.1. Formulation development and biocompatibility of protein networks.....	29
2.3.2. Cargo loading, release, and characterization.....	31
2.3.3. Bioactivity of loaded cargo.....	33
2.3.4. Cellular uptake of network components.....	33
2.3.5. Networked cells maintain capacity for migration and phagocytosis.....	34
2.3.6. Networks promote cell viability and maturation of carrier DCs.....	35
2.4. Discussion.....	37
2.5. Conclusions.....	38
2.6. Materials and Methods.....	38
<b>3. Chapter 3: Controlling Vaccine Kinetics Using Polyphenols for Enhanced Humoral Immunity.....</b>	<b>43</b>
3.1. Abstract.....	43
3.2. Introduction.....	43
3.3. Results.....	45
3.3.1. TA associates with protein antigens and nucleic acid adjuvants in vitro.....	45
3.3.2. TAPER vaccines extend antigen retention in vivo at the injection site.....	48
3.3.3. TAPER vaccines enhance lymph node accumulation of antigen and adjuvant.....	49
3.3.4. TAPER vaccines promote antigen acquisition and activation in multiple cell types in the lymph nodes.....	51
3.3.5. TAPER vaccination improves humoral immune responses to OVA.....	52
3.3.6. TA induces moDC apoptosis and modulates responses to CpG in a concentration-dependent manner.....	54

3.3.7.	TAPER vaccination enhances multiple aspects of the humoral immune response to the SARS-CoV-2 RBD antigen.....	55
3.4.	Discussion .....	59
3.5.	Materials and Methods .....	61
<b>4.</b>	<b>Chapter 4: Conclusions and Outlook.....</b>	<b>66</b>
4.1.	Overview.....	66
4.2.	Future Directions .....	66
4.2.1.	META Platform.....	66
4.2.2.	TAPER Platform.....	67
4.3.	Outlook .....	68
<b>5.</b>	<b>Chapter 5: References .....</b>	<b>69</b>
<b>6.</b>	<b>Chapter 6: Appendix .....</b>	<b>78</b>
6.1.	Appendix A: Methods .....	78
6.1.1.	Cancer vaccine trial analysis.....	78
6.2.	Appendix B: Figures .....	79
6.3.	Appendix C: Tables .....	91

## List of Figures

Fig. 1-1. Categories of cancer vaccines and associated mechanism of action. ....	12
Fig. 1-2. Summary of current landscape of cancer vaccine clinical trials .....	13
Fig. 1-3. Overview of clinical trials using antigen-presenting cell vaccines.....	15
Fig. 1-4. Induction of immunity by vaccination. ....	19
Fig. 1-5. Driving factors of enhanced humoral immunity arising from extended-release vaccination. ....	20
Fig. 1-6. Structural elements and interactions of tannic acid (TA). ....	23
Fig. 1-7. Affinity of TA for proteins of the extracellular matrix. ....	24
Fig. 2-1. Formation of META DCs.....	29
Fig. 2-2. Effect of TA concentration on viability of coated cells.....	30
Fig. 2-3. Confocal imaging of fluorescently labeled protein networks.....	31
Fig. 2-4. Loading and release of model protein cargo from networks. All assessments of loading and release were conducted using ELISA. ....	32
Fig. 2-5. Bioactivity of networked proteins. ....	33
Fig. 2-6. Uptake of proteins networked in META. ....	34
Fig. 2-7. Migration and phagocytosis capacity of META DCs.....	35
Fig. 2-8. Response of immature DCs to the activating stimulus CD40L or tolerogenic stimulus IL-10 in cell networks. ....	36
Fig. 3-1. Complexation of OVA and CpG with TA.....	46
Fig. 3-2. TA associates with model antigen OVA.....	47
Fig. 3-3. Complexation of OVA and CpG together with TA.....	48
Fig. 3-4. TA facilitates injection site retention and enhances lymph node accumulation of a model subunit vaccine. ....	49
Fig. 3-5. Key structural features of OVA are maintained upon TA binding. ....	51
Fig. 3-6. TA modulates immune cell activation and composition in the LNs.....	53
Fig. 3-7. The presence of TA modifies BMDC viability and phenotype.....	55
Fig. 3-8. TA enhances humoral immunity to RBD vaccines.....	56
Fig. 3-9. Retention of RBD and CpG at the injection site.....	57
Fig. 3-10. Retention of RBD modulates kinetics of the germinal center (GC) response.....	58
Fig. 3-11. Impact of TA on cellular immunity.....	59
Appendix Fig. 1. Hydrodynamic diameter of TA/BSA precursor solutions.....	79
Appendix Fig. 2. Confocal microscopy of backpack association with mature DCs after 24-hour incubation.....	79
Appendix Fig. 3. Effect of iron-containing metal phenolic networks on the viability of immature DCs. ....	80
Appendix Fig. 4. Effects of soluble network components on viability of immature DCs.....	80
Appendix Fig. 5. Loading of anti-CD40 in a combinatorial network with IL-15. ....	81
Appendix Fig. 6. Loading of IL-15 in networks at different TA concentrations.....	81
Appendix Fig. 7. Activity curves of networked human IL-15. ....	82
Appendix Fig. 8. Network stability after application of shear stresses associated with injection.....	82
Appendix Fig. 9. Viability of immature DCs with networks containing GM-CSF. ....	83
Appendix Fig. 10. In vivo imaging system (IVIS) images of fluorescent vaccine components in the lymph nodes 48 hours after vaccination. ....	84
Appendix Fig. 11. Lymph node accumulation of OVA at low TA ratios.....	85
Appendix Fig. 12. Vaccine accumulation and phenotype among other relevant cell types. ....	86
Appendix Fig. 13. Phenotype of BMDCs cultured with vaccine formulations containing TA. ....	88
Appendix Fig. 14. Mouse body weight following RBD vaccination. ....	89

Appendix Fig. 15. Representative flow cytometry gating plots of immune cells in the lymph nodes. .... 90

## List of Tables

Appendix Table 1. Examples of current clinical trials for DC/APC vaccines.....	91
Appendix Table 2. Indications for DC/APC vaccine clinical trials. ....	92
Appendix Table 3. DC/APC antigen identities. ....	92
Appendix Table 4. Antibodies used in the lymph node analysis study. ....	93
Appendix Table 5. Antibodies used in the germinal center analysis study. ....	94

# 1. Chapter 1: Introduction

Note: Part of this chapter is adapted from a review article published in *Bioengineering and Translational Medicine*: **M.E. Janes**, A.P. Gottlieb, K.S. Park, and Samir Mitragotri (2023). *Cancer Vaccines in the Clinic. Bioengineering and Translational Medicine*, e10588.

## 1.1. Introduction to vaccines

Vaccines are inarguably one of the most important advances in medicine. Vaccines are a critical public health tool for protection against infectious disease, as exemplified by the eradication of diseases including smallpox and polio, and recent efforts to develop effective, life-saving vaccines during the SARS-CoV-2 pandemic.<sup>1-4</sup> Despite over 100 years of widespread use, significant work remains to produce effective and accessible vaccines against a variety of infectious threats. In addition, recent advancements in immunology have highlighted the potential of vaccines as therapeutic interventions for non-infectious diseases including cancer and autoimmune disease.<sup>5-</sup>

<sup>8</sup> Although no FDA-approved vaccines are actively in use for these indications today, the ample number of novel interventions under both clinical and preclinical investigation suggests that the clinical utility of vaccines is on the cusp of a revolution.

## 1.2. Cancer vaccines

Vaccines are a critically important public health intervention that have yet to achieve landmark clinical efficacy in oncology.<sup>9,10</sup> Vaccination holds promise as a treatment modality due to the aberrant overexpression or unique expression of certain antigens on tumor cells. Accordingly, the purpose of a cancer vaccine is to educate a patient's immune system to recognize and attack malignant cells. The success of such vaccines necessitates highly regulated cooperation from many arms of the immune system, including antigen-presenting cells (APCs), helper and cytotoxic T cells, natural killer (NK) cells, and tumor-resident myeloid cells. The complex spatiotemporal factors governing such interactions, and the many mechanisms of local and systemic immune suppression and evasion, have long hindered clinical development of cancer vaccines.<sup>11,12</sup> Their journey has been challenging and wrought with many high-profile failures. However, an improved understanding of factors such as antigen immunogenicity, immune cell exhaustion, and combination therapy selection holds promise for the application of cancer vaccines in effective therapeutic regimens. Here, we provide an update on the status of cancer vaccines on the market and in the clinic, highlighting 360 active clinical trials (as of July 2022) and 8 globally approved products. We dissect the current space according to the materials used to deliver the antigen, antigen types, indications, phases, combination approaches, and other relevant metrics. We then discuss the challenges associated with clinical translation of cancer vaccines, as well as novel preclinical and clinical approaches to circumvent these challenges.

Cancer vaccines have been under intense clinical investigation for 40 years with only a select few successes in very narrow contexts. The earliest fruitful efforts to harness the immune system against cancer were carried out in 1891 by William Coley, who injected live and heat-killed bacteria into bone and soft tissue sarcomas and observed tumor shrinkage in some patients.<sup>13</sup> Over eighty years later, intravesical administration of tuberculosis vaccine *Bacillus Calmette-*

Guérin (BCG) demonstrated efficacy against non-muscle-invasive bladder cancer through local immune activation that impairs tumor cell survival and proliferation.<sup>14</sup> BCG therapy remains standard in bladder cancer and represents the first modern approved cancer immunotherapy. The early bacterial approaches resulted in localized immune activation against foreign antigens, spurring the development of anti-tumor immune responses. Today, most vaccines under clinical investigation involve the delivery of tumor antigens in combination with an adjuvant or other costimulatory factor. In this review, we focus on six major categories of cancer vaccines including peptides, RNA, DNA, tumor cells, and viral vaccines, and APC vaccines, most of which consist of dendritic cells (DCs) (**Fig. 1-1**).

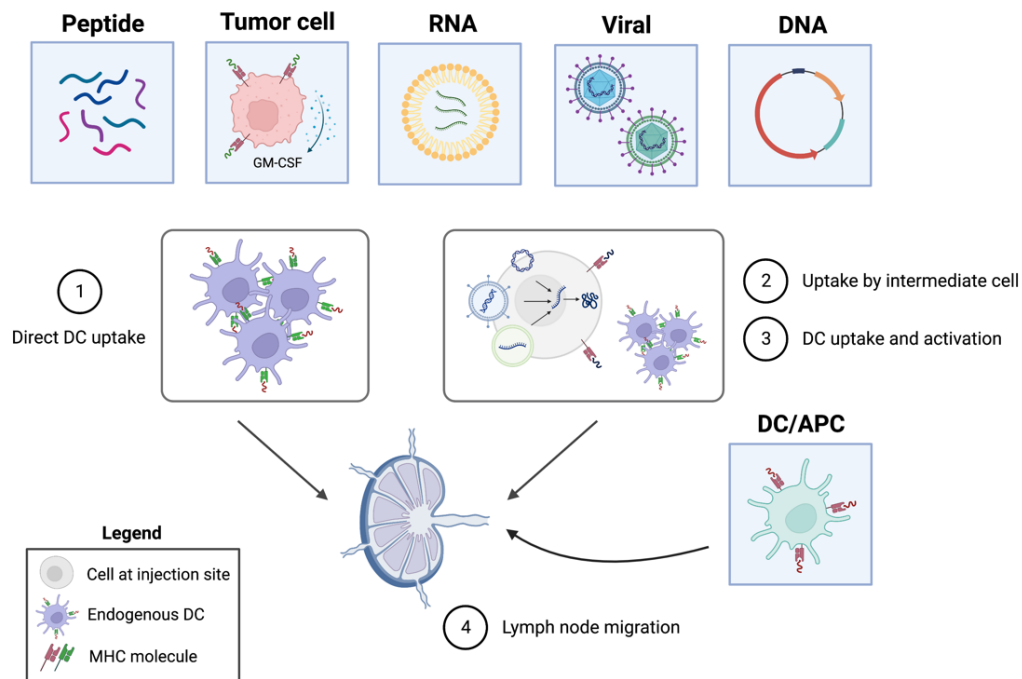


**Fig. 1-1. Categories of cancer vaccines and associated mechanism of action.**

Peptide, tumor cell, RNA, viral, DNA, and DC/APC vaccines comprise the major categories analyzed. Such constructs all have the potential for direct DC uptake and presentation of antigen (1). Alternatively, non-cellular constructs may be taken up by cells at the injection site (2), which in turn provides a source of antigen to endogenous DCs (3). Activated DCs then migrate to the lymph nodes, where they induce a CD8 T cell response (4). DC: dendritic cell, APC: antigen-presenting cell, GM-CSF: granulocyte-macrophage colony-stimulating factor, MHC: major histocompatibility complex.

A total of 360 cancer vaccine trials were analyzed in the present study. More detail about the analysis methodology can be found in the Appendix. Of the 360 trials analyzed, we identified 377 distinct vaccine interventions on a per-trial basis, comprising 235 soluble (62.3%) and 142 cellular (37.7%) vaccines. Peptide vaccines comprise more than half the soluble vaccine space (123/235, or 52.3%) and were the most dominant singular category overall (123/377, or 32.6%) (**Fig. 1-2A**). DC vaccines are the second most frequently investigated, and comprise the vast majority of the cellular vaccine space (108/142, 76.1%) and a large fraction of the total cancer vaccine space (28.7%). Viral (10.9%), DNA (6.9%), RNA (6.1%), and tumor cell vaccines (5.8%) followed DC vaccines. The majority of trials are at Phase 1 or 1/2 (68.9%), followed by Phase 2 (27.5%), and

Phase 2/3 and 3 (7 trials, 1.7%), reflecting both the difficulty of clinical advancement in the space and wealth of new products that continue to enter clinical trials (**Fig. 1-2B**).

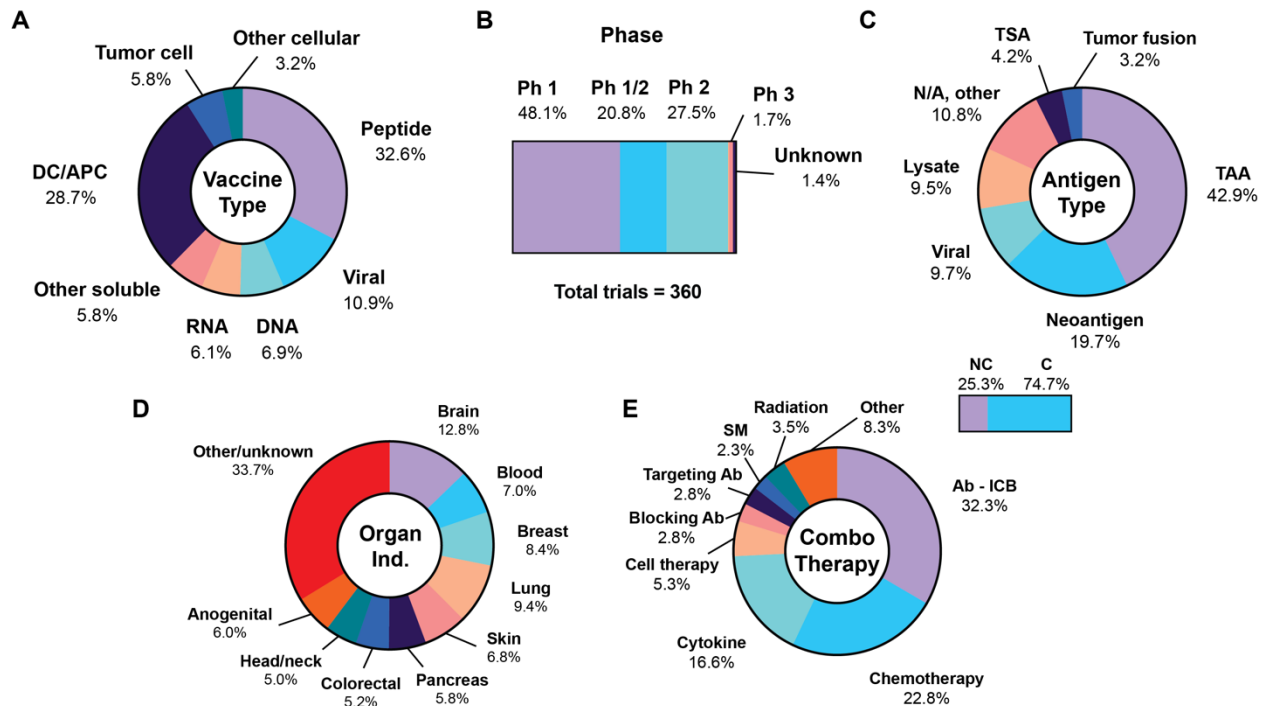


**Fig. 1-2. Summary of current landscape of cancer vaccine clinical trials**

(A) Overview of all captured interventions by type, (B) phases of 360 clinical trials, (C) landscape of antigen classifications, (D) most common indications segmented by organ/anatomic site, (E) percentage of trials using a combination therapy (top right bar), and combination therapies by category, among trials using a combination. DC: dendritic cell, APC: antigen-presenting cell, Ph: phase, TAA: tumor-associated antigen, TSA: tumor-specific antigen, N/A: not applicable, Ab: antibody, ICB: immune checkpoint blockade, SM: small molecule, NC: no combination, C: combination.

When broken down by the type of antigen, the most represented category is tumor-associated antigens (TAAs) (163/380, 42.9%), antigens that are overexpressed on tumor cells. Vaccines also target neoantigens and tumor-specific antigens (TSAs) (75/380 and 16/380, 23.9% combined) (**Fig. 1-2C**). These antigens are exclusively expressed on tumor cells and absent from healthy cells. In this review, TSA denotes a singular defined vaccine product targeting a “shared” mutation. For TSA vaccines, patients are screened to determine if they possess the mutation in question and are eligible for the therapy. “Neoantigen” denotes a vaccine consisting of patient-specific antigens that are absent from healthy cells. For neoantigen vaccines, the patient’s individual tumor is sequenced to identify these patient-specific antigens and produce a personalized product. Other antigen types include viral antigens (9.7%), indicated for virus-associated cancers, and antigens derived from tumor lysate (9.5%). Tumor fusion vaccines are DC vaccines fused with tumor cells prior to infusion (3.2%). Trials where the type was not applicable (N/A, **Fig. 1-2C**) refer to tumor cell and *in situ* vaccine trials.

The most commonly targeted organ is the brain, followed by cancers of the blood, breast, lung, skin, pancreas, and prostate (**Fig. 1-2D**). Of the 360 trials, 269 (74.7%) employ a combination approach (**Fig. 1-2E**). Among the combination strategies, the most common is ICB (32.3%),

followed by chemotherapy (22.8%), cytokines (16.6%), and cell therapies (5.3%). To generate these data, we counted the number of times a combination type was listed and calculated its frequency as a percentage of the total number of combination interventions in that category. Therefore, the data represent the prevalence of the combination type amongst all combination interventions, not the fraction of trials that use that type of therapy. Many trials use more than one approach together or in different arms of the trial, which is reflected in the large total number of identified interventions (419) compared to the number of combination trials (269).

### **1.3. Cell-based vaccination**

#### **1.3.1. Dendritic cell cancer vaccines**

Rather than delivering a source of tumor antigens and relying on endogenous APCs to initiate the immune response, DC vaccines instead aim to supply fully differentiated, mature DCs which theoretically possess all signals necessary to induce an anti-tumor immune response, including antigen presentation, costimulatory signals, and cytokine production.<sup>15–17</sup> Typically, monocytes are harvested from the patient via leukapheresis and cultured *ex vivo* with GM-CSF for at least one week to yield differentiated monocyte-derived DCs (moDCs). At this point, the cells are loaded with tumor antigens and matured with an activation cocktail before reinfusion, usually via the subcutaneous (SC) or intradermal (ID) route. While this approach is appealing because it can overcome endogenous DC dysfunction that is often observed in cancer, it bears major logistical hurdles and a high cost. Autologous DC vaccines have undergone rigorous clinical investigation, beginning in the 1990s with the identification of tumor-associated antigens suitable for vaccination.<sup>18</sup> A significant majority of past DC vaccine trials employed moDC, and modest research efforts were devoted to identifying optimal protocols for *ex vivo* activation of these cells.<sup>19</sup> Modern protocols precondition moDC with activation cocktails of cytokines and Toll-like receptor (TLR) agonists to elicit maximal expression of costimulatory receptors and production of key cytokines while preserving cell viability and migratory capacity. Various protocols for culturing, antigen loading, and maturing DC vaccines have been reviewed in depth elsewhere.<sup>20</sup>

Clinical responses to DC vaccines have been largely disappointing, with response rates rarely exceeding 15%.<sup>21</sup> Multiple Phase 3 trials have failed to produce desired results, with only a single APC-based approach (Sipuleucel-T) showing sufficient efficacy to support regulatory approval. Many DC vaccines have succeeded in eliciting measurable anti-tumor T cell responses, but these responses have been insufficient to consistently yield clinical benefit. These disappointments have been attributed to a variety of factors, including duration and stability of antigen presentation, suboptimal characteristics or exhaustion of anti-tumor CD8 T cells, insufficient priming of Th1-polarized CD4 T cells, and failure to repolarize the suppressive tumor microenvironment (TME) to enable T cell function.<sup>22,23</sup> Perhaps the primary limitation is the inability to differentiate and expand the most relevant DC subset for the activation of CD8 T cells, conventional type I DCs (cDC1), in an *ex vivo* setting. While moDC are easily obtained in large quantities, they are comparatively deficient in their cross-presentation and T cell stimulatory capacities.<sup>24,25</sup> The past decades of clinical research have produced a wealth of insights into the challenges facing DC vaccination, and ongoing preclinical and clinical studies aim to address the deficiencies of previous approaches. Chief among these strategies are combination with ICB, optimization of antigen loading methods, novel protocols to culture specialized DC, and inclusion of CD4

epitopes.<sup>26-28</sup> As with the entire cancer vaccine field, recent advances in gene sequencing and immunogenic neoantigen identification promise to enhance DC vaccines, and cutting edge approaches have focused on loading DCs with patient-specific neoantigens using messenger RNA (mRNA) transfection.<sup>20</sup> While hard-won clinical insights promise to bring ongoing and future approaches closer to their clinical potential, the time and resources required to generate these autologous cellular vaccines remain a barrier.

Antigen-presenting cell (APC) vaccines comprise the second-largest subclass of cancer vaccines, second only to peptide vaccines, with 108 references in clinical trial listings (**Fig. 1-2**). Of these, 103 are listed as DC, 1 as APC, 1 as PBMC, and 3 as monocytes. Although all of these products contain cells with antigen-presenting functions, DCs are the classical antigen-presenting cells and the subject of most clinical investigations (**Fig. 1-3**). A representative selection of trials can be found in **Appendix Table 1**. The most common indication category for DC vaccines is the brain (30/127, 23.6%); these trials almost exclusively were for treatment of glioblastoma (GBM) (**Appendix Table 2**). 64.1% of trials are in Phase 1 or 1/2, with almost one third (32.0%) at Phase 2, and four trials (3.9%) at Phase 3 (**Fig. 1-3A**). Of the Phase 3 trials, three are indicated for GBM and one for uveal melanoma. Antigen priming materials in these trials include tumor lysate, autologous total tumor RNA, and a tumor cell fusion (NCT03400917, NCT04277221, NCT00045968, NCT01983748).

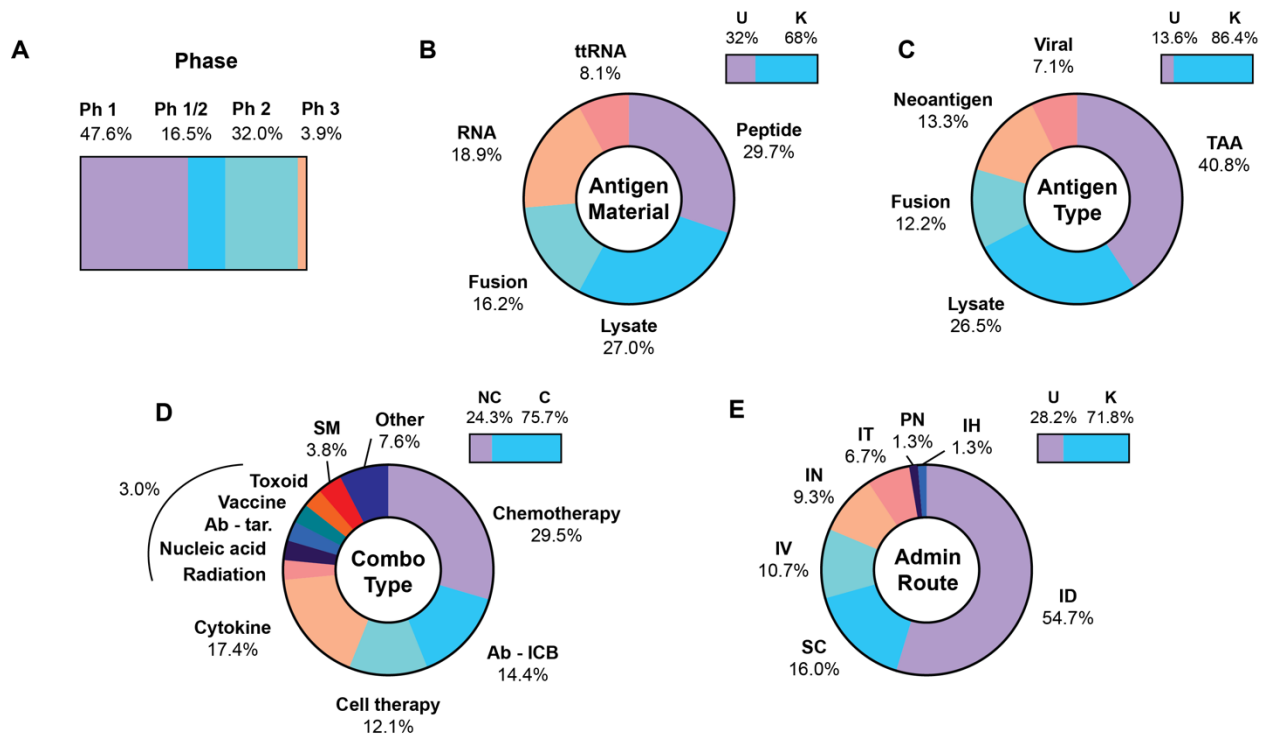


**Fig. 1-3. Overview of clinical trials using antigen-presenting cell vaccines.**

(A) Trial phases, (B) percentage of trials with a known material used to deliver antigen to cells ex vivo (top right bar), and summary of materials, (C) percentage of trials with a known antigen classification, and summary of antigen types (D) percentage of trials using a combination therapy (top right bar), and combination therapies by category, among trials using a combination, (E) percentage of trials with a known route of administration (top right bar), and breakdown of routes. ttRNA: total tumor RNA, U: unknown, K: known, TAA: tumor-associated antigen, Ab - ICB: antibody - immune checkpoint blockade, Ab - tar: antibody

- targeted, SM: small molecules, NC: no combination, C: combination, SC: subcutaneous, IV: intravenous, IN: intranodal, IT: intratumoral, PN: perinodal, IH: intrahepatic, ID: intradermal, Ph: phase.

Aside from the brain, the most common indications for DC vaccines include cancers of the blood, lung, skin (melanoma), and breast. While few vaccines in the overall space are indicated for liquid cancers, this was the second most common indication for DC vaccines (15/127, 11.8%). One of the more advanced candidates for liquid cancers is a tumor fusion vaccine indicated for patients in remission from acute myeloid leukemia (AML), and it is designed to prevent cancer recurrence. This candidate, known as DC/AML, is being investigated in multiple Phase 2 trials (NCT03059485, NCT01096602, NCT03679650).

An important consideration in DC vaccine development is the material used to load cells with the target antigen(s) *ex vivo*. Among trials with a listed material, peptides and lysate are the most frequently used, followed by RNA, tumor fusions, and total tumor RNA (**Fig. 1-3B**). The lysate, tumor fusion, and total tumor RNA approaches (combined 43% of all approaches) rely on the diversity of antigens present in biopsied tumor cells to initiate an immune response, as opposed to priming with defined antigens or neoantigens. The majority of approaches for defined antigens target TAAs (40.8% of known antigen listings), the most common including WT1 (leukemia) and HER2 (breast cancer), along with survivin, hTERT, and NY-ESO-1 (various solid tumors) (**Fig. 1-3C, Appendix Table 3**). A small fraction of trials includes viral targets, particularly for HPV- and cytomegalovirus (CMV)-associated cancers. Personalized neoantigen targets are also making their way into the DC space; 13.3% of trials use DCs loaded with neoantigen peptides. Although the standard cell source for DC generation is monocytes derived from autologous PBMCs and nearly all trials use autologous cells (99/103 trials, 96.1%), we identified four trials using allogeneic cells (NCT03371485, NCT03970746, NCT04739527, NCT03697707).

The majority of DC trials utilize a therapeutic combination (78/103, 75.7%) (**Fig. 1-3D**). Among these trials, chemotherapy is the most common (39/132, 29.5%), owing to the large proportion of trials targeting GBM, for which maintenance temozolomide chemotherapy is usually employed in combination with novel interventions. Cytokines are another common combination (23/132, 17.4%), due to the frequent addition of GM-CSF to promote the survival and function of injected DCs. Interestingly, cell therapies (16/132, 12.1%) are used as combinations about as frequently as ICB (19/132, 14.4%), in contrast to peptide and other categories which employ ICB much more frequently. Listed cell therapies include various types of T cells, including chimeric antigen receptor (CAR) T cells, tumor-infiltrating lymphocytes (TILs), and cytokine-induced killer cells (CIK). These striking differences are likely due to the prevalence of GBM and liquid indications, for which ICB is not usually effective.<sup>29,30</sup> The prevalence of T cell combinations is likely driven by the potential for the administered DC product to directly interact with and further expand T cells in the lymph nodes. Administration routes are highly variable, the most common being ID (**Fig. 1-3E**).

### 1.3.2. Dendritic cell vaccines for autoimmune disease

Although DC vaccines have been extensively explored for treatment of cancer, tolerizing DC vaccines hold promise to treat autoimmune disease. Unlike vaccines against infectious diseases or cancer, which aim to induce immune attack against disease-associated antigens, the goal of

tolerogenic vaccination is to quell pathogenic immune responses against self-antigens. Central tolerance, the initial process that involves elimination of self-reactive T and B cells in the thymus, is the first safeguard against autoimmunity. However, as many as 40% of self- and auto-reactive T and B cells escape elimination by central mechanisms.<sup>8,31</sup> Therefore, peripheral tolerance is a critical function. Dendritic cells are the key mediators of peripheral tolerance due to their ability to directly promote elimination and anergy of self-reactive T cells, and to promote differentiation and function of regulatory T cells.<sup>32,33</sup> DCs can modulate the three major signals that are required for antigen-specific T cell activation, including peptide-MHC binding (signal 1), receptor co-stimulation (signal 2) and cytokine signaling (signal 3). Dendritic cells in an immature or tolerogenic state can promote T cell anergy and deletion by presenting antigen to T cells in absence of signals 2 and 3 and in the presence of immunosuppressive signals.<sup>34</sup> Accordingly, the tolerogenic state is characterized by features including low expression of MHC molecules and co-stimulatory molecules such as CD86, secretion of anti-inflammatory cytokines such as IL-10, expression of inhibitory molecules such as PD-L1, and secretion of immunosuppressive metabolites.<sup>35</sup> The tolerogenic DC phenotype, which is transcriptionally distinct from the naïve phenotype, can be induced *ex vivo* by a variety of stimuli including low-level GM-CSF exposure, various anti-inflammatory cytokines, microbial metabolites, and vitamins A and D3. The capacity of DCs to mediate antigen-specific tolerance in the periphery provides an opportunity to develop therapeutics for autoimmune diseases.

Tolerogenic DC vaccines have been studied in the clinic for a variety of indications including rheumatoid arthritis,<sup>36,37</sup> multiple sclerosis,<sup>38</sup> and type I diabetes,<sup>39,40</sup> among others. TolDCs are typically derived from autologous monocytes in the presence of GM-CSF, then pulsed with antigens and exposed to tolerance-inducing stimuli prior to infusion. While multiple phase I trials have indicated that the therapy is well-tolerated and can improve disease biomarkers such as the frequency of effector and regulatory T cells, antigen-responsiveness of T cells, and systemic indicators of inflammation, very few phase II trials have been conducted.<sup>37,41,42</sup> Logistical and challenges associated with preparation of cellular vaccines are major obstacles in the execution of large-scale trials.<sup>6</sup> These factors limit enrollment, which hinders progression to larger trials with appropriate placebo and cellular controls. In addition, the ability to achieve primary endpoints related to disease remediation is hindered by high intra-patient variability in disease activity and flare. Together, these factors have limited our clinical understanding of the disease-modifying activity and durability of tolerogenic DC vaccines.

### **1.3.3. Challenges and opportunities for DC vaccines**

Dendritic cell vaccines offer an alternative way to control immune-activating signals to modulate both cancer and autoimmune disease. While the ability to prime cells *ex vivo* with antigens and maturation or tolerogenic stimuli is an attractive feature, these vaccines have multiple limitations. For therapies like DC vaccines that rely on antigen specificity, the identification of immunogenic antigens is a major challenge. Many autoimmune diseases present with a breadth of self-antigen targets, which are not fully understood and could be highly variable among patients. In cancer, tumor-intrinsic processes including downregulation of MHC I expression and immune editing may result in antigen loss, which limits the efficacy of cancer vaccines.<sup>43,44</sup> The maintenance of antigen presentation and optimal maturation state *in vivo* is another major limiting factor. Effective and

timely presentation of antigen peptides is critical for induction of durable immune responses. While DCs may be incubated *ex vivo* with protein antigens or peptides before infusion, peptide-MHC complexes are rapidly recycled, leading to transient expression and variable magnitude over time, which can unfavorably impact the immune response. An ideal cancer vaccine would consist of bona fide cDC1s, an APC subset capable of cross-presentation.<sup>17,45–47</sup> However, these cells are too rare to isolate from the bloodstream, and also difficult to recapitulate *ex vivo* using monocytes as starting material.<sup>48,49</sup> Phenotypic changes arising from signals *in vivo* may also compromise the efficacy of DC vaccines. While tolerogenic DCs may be optimally generated *ex vivo*, these cells are exposed to many inflammatory insults in the context of autoimmune disease, including systemic cytokines and costimulatory signaling from activated CD4+ T cells. Reprogramming of tolDCs to a mature state in concert with exposure to high concentrations of self-antigens *in vivo* has the potential not only to abrogate therapeutic effects, but to convert DCs into mediators of disease. Our understanding of these effects is further complicated by the challenges associated with running clinical trials, including devising trials with appropriate statistical power to directly measure disease-modifying effects in the long term. The ability to tune or maintain DC antigen presentation and phenotype *in vivo* following administration would be a major advantage in the future design of cellular vaccines across many relevant indications.

## **1.4. Subunit vaccines against infectious disease**

### **1.4.1. Vaccines protect against infectious disease**

Vaccines are a critical public health tool for protection against infectious disease, as exemplified by the SARS-CoV-2 pandemic.<sup>1–3</sup> Successful vaccines rely on development of humoral immune responses, which are characterized by the production of antibodies. Traditional vaccines typically include whole attenuated or inactivated pathogens, and have been effective for many indications.<sup>50</sup> Many vaccines in use today are subunit vaccines, which consist of immunogenic components of the disease target as opposed to whole pathogens. Examples of licensed subunit vaccines include those against pertussis, influenza, and hepatitis A and B.<sup>1</sup> These vaccines usually contain a protein or carbohydrate antigen to which the immune response is directed, along with an adjuvant. Adjuvants can greatly enhance vaccine immunogenicity by various mechanisms including direct stimulation of Toll-like receptors (TLRs) and pattern-recognition receptors (PRRs), activation of the NLRP3 inflammasome, and induction of tissue damage and subsequent inflammation at the injection site. Adjuvants may consist of soluble danger signals, such as lipids, single-stranded DNA, and other microbial products, or immunogenic depot or emulsion-forming agents such as alum and MF59.<sup>51,52</sup> The induction of an immune response to vaccination involves a highly coordinated process among cells in the lymph node that results in generation of protective antibodies (**Fig. 1-4**).

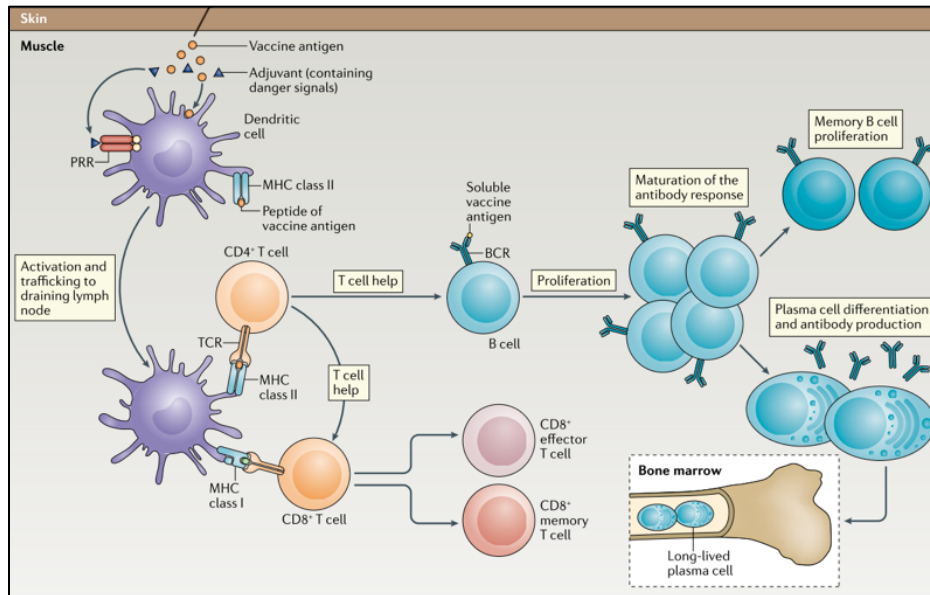


**Fig. 1-4. Induction of immunity by vaccination.**

Dendritic cells encounter antigen and adjuvant at the site of injection, which allows them to display antigen-specific peptides, become activated, and traffic to the draining lymph nodes to present antigen to T cells. CD4<sup>+</sup> helper T cells engage with cognate B cells that have encountered antigen to promote B cell survival, proliferation, and entry into germinal centers. Mature B cells differentiate into plasma cells and memory B cells, which secrete high-affinity antibodies against the vaccine antigen. Long-lived plasma cells accumulate in the bone marrow, while memory B cells patrol the periphery to initiate rapid responses upon second encounter. Adapted from Ref. 1.

The response is initiated when B cells with a cognate BCR bind the antigen, which is followed by antigen uptake and peptide presentation on MHCII. Antigens can reach B cells in the follicle in a variety of ways, including direct drainage through conduits, transfer by subcapsular sinus macrophages, and presentation by follicular dendritic cells (FDCs).<sup>53–56</sup> Antigen size and state generally govern the mode of presentation. Small, uncomplexed antigens (<70 kDa) can generally reach the follicle by soluble drainage, whereas antigens that are larger or complexed with complement or antibodies must be captured in the sinus or medulla and then presented.<sup>57</sup> Concomitantly, CD4<sup>+</sup> T cells in the lymph nodes become activated by DCs presenting antigen. Activated T and B cells are induced to migrate to the follicle periphery by upregulation of chemokine receptors CXCR5 and CCR7, respectively. The interaction of cognate T and B cells, driven in part by ligation of CD40 on B cells, facilitates B cell proliferation and formation of germinal centers (GCs).<sup>58</sup> In the GC, B cells undergo somatic hypermutation of the BCR and multiple rounds of selection by FDCs and T follicular helper (Tfh) cells. The interaction of high-affinity B cells with Tfh cells promotes reciprocal survival and maturation. ICOSL signaling from B cells promotes upregulation of CD40L on Tfh cells, which in turn potentiates B cell proliferation and further rounds of selection.<sup>59</sup> The nature of the immune response is determined in part by cytokine signaling from Tfh cells, which governs class switching from native IgM to IgG and other isotypes. Ultimately, the GC reaction produces antibody-secreting plasma cells and long-lived memory cells. Notably, the functional effectiveness of this process is highly variable according to antigen structure, which governs immunodominance of the antibody response.<sup>60</sup> Complex, weakly immunogenic, and/or rapidly evolving antigens such as those derived from HIV and SARS-CoV-

2 may fail to induce adequate or long-lived protection due to a deficiency in neutralizing antibodies targeting the epitopes that are most critical for protection.<sup>61,62</sup>

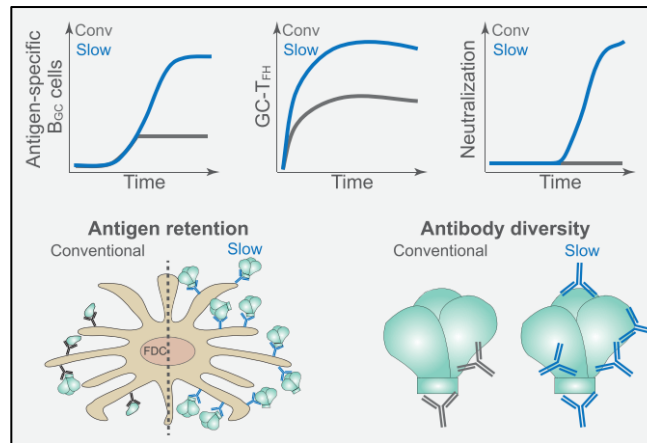


**Fig. 1-5. Driving factors of enhanced humoral immunity arising from extended-release vaccination.** Slow vaccine delivery enhances the generation of germinal center B cells ( $B_{GC}$ ) and T follicular helper cells ( $GC-T_{FH}$ ) to facilitate and/or enhance induction of neutralizing antibodies in cases where conventional bolus vaccination fails to do so. The enhanced availability of antigen in the lymph nodes during the germinal center reaction promotes improved deposition of immune complexes on follicular dendritic cells (FDC), which sustains  $T_{FH}$  and  $B_{GC}$  cells for additional rounds of selection. Adapted from Ref. 67.

#### 1.4.2. Magnitude and timing of vaccine delivery governs immunogenicity

Transport of antigen and adjuvant to the lymph nodes is a critical consideration for vaccine efficacy, as the temporal dynamics governing the magnitude and duration of antigen availability have significant implications for the resulting immune response.<sup>56,63,64</sup> Transport mainly occurs in one of two ways, via passive drainage through the lymphatics, or directed migration of cells from the injection site to the lymph node. Soluble vaccine formulations injected intramuscularly or subcutaneously offer little control over kinetics, and are rapidly cleared from the injection site and lymphatics.<sup>65</sup> In contrast, immunogenic components can persist on the order of weeks during a natural infection.<sup>63,66</sup> Recent studies have demonstrated that extended antigen availability on the order of weeks can dramatically enhance total antibody titers and promote the development of neutralizing antibody responses.<sup>67-69</sup> In terms of the magnitude of the immune response, prolonged exposure of antigen at the injection site and in the lymph nodes can improve uptake by migratory DCs and capture by FDCs, respectively. Enhanced activation and antigen uptake by conventional and monocyte-derived DCs can directly improve Tfh induction, which is critical for the germinal center reaction and subsequent class switching in B cells. Enhanced presentation of antigen by FDCs can both directly enhance initial B cell activation and engagement and survival of Tfh cells during the GC reaction. Extended antigen availability can also improve vaccine efficacy by modulating B cell immunodominance in the GC, which can enhance the diversity of the B cell repertoire and subsequent production of neutralizing antibodies. Extended delivery likely results in an increased likelihood of rare, non-dominant B cells undergoing selection and somatic hypermutation. Drivers of this effect include extended antigen presentation by FDCs and sustained T cell help during the peak of the germinal center reaction. At this stage, immune complexes form between immunodominant antibodies and antigen captured by FDCs. The masking of immunodominant epitopes along with sufficient availability of antigen at this critical

point is believed to increase the likelihood of non-dominant B cells receiving sufficient signal to undergo selection. Functionally, extended-delivery immunization results in a greater overall proportion of antigen-specific B cells in germinal centers, higher total IgG titers, and the induction of neutralizing antibodies against relevant epitopes (**Fig. 1-5**). These findings suggest the importance of tuning antigen kinetics for challenging antigen targets, which is difficult to achieve using conventional vaccine formulations. Although studies with extended-duration immunization have yielded significant insights, their execution requires surgical implantation of an osmotic pump and is not clinically translatable or scalable. Therefore, novel, simple, and translatable approaches are needed to enhance immune responses to challenging antigens, such as those derived from HIV and SARS-CoV-2.

### **1.4.3. Approaches to modulate vaccine delivery kinetics**

#### **Adjuvant selection**

From the perspective of formulation development, many types of strategies have been investigated to alter vaccine kinetics and prolong antigen exposure in the lymph nodes. One of the oldest approaches is the use of weakly immunogenic “depot-forming” adjuvants, such as alum and Montanide, which are two of the most common adjuvants in commercial formulations.<sup>51</sup> These components were once thought to promote extended antigen release; however, recent research suggests that it is instead their local immunogenicity that drives downstream immune responses.<sup>70</sup> For example, the oil-based adjuvant Montanide does not specifically interact with antigen, which is cleared rapidly after IM injection. Rather, Montanide facilitates local inflammation, which drives chemokine signaling followed by recruitment of immune cells and subsequent migration to the lymph nodes.<sup>71</sup> Alum similarly can initiate local inflammation, and in some cases may induce a depot effect.<sup>72</sup> However, such responses are difficult to tune given variability of vaccine adsorption to alum under physiologic conditions.<sup>73</sup> Overall, extant clinical approaches involving adjuvant selection are not sufficient to promote or tune sustained antigen delivery to the lymph nodes.

Biomaterial-based drug delivery approaches are an area of active investigation for vaccine delivery. Three prominent preclinical strategies to sustain or enhance vaccine delivery to the lymph nodes include chemical conjugation, nanomaterial formulation, and scaffolds.

#### **Chemical conjugation**

Chemical conjugation involves the tagging of vaccine moieties with factors such as lipids or proteins to endow them with affinity for a target and/or alter their biodistribution *in vivo*. For example, the conjugation of albumin-binding lipid tails to peptides and nucleic acid adjuvants has been shown to promote passive lymph node accumulation via albumin hitchhiking.<sup>74</sup> In addition, a generalizable chemical conjugation strategy has been developed to prolong retention of vaccine components on alum.<sup>73,75,76</sup> This approach has shown success in preclinical models by sustaining depot formation, enhancing the duration of lymph node exposure via gradual release on the order of weeks, and increasing the valency of antigen presentation to B cells. One limitation of chemical conjugation platforms is that they necessitate the modification of each vaccine component and optimization of necessary chemical reactions, which can be cumbersome for vaccines employing many components.<sup>77</sup>

## **Nanomaterials**

Nanoparticulate formulations are another delivery approach, and are beneficial because they enable co-loading of antigen and adjuvant and uptake by phagocytes. The ability to adjust the nanocarrier size, surface charge, and/or functionalization is valuable to facilitate passive transport to the lymph nodes and/or interaction with APCs.<sup>56,78</sup> Nanocarriers may also be used to stabilize sensitive components; for example, mRNA vaccines are encapsulated in lipid carriers for cargo protection.<sup>79</sup> With the exception of a select few lipid formulations, very few nanoparticles have progressed into the clinic despite extensive preclinical investigation.<sup>80</sup> Difficulties with NPs including physiologic stability and aggregation, formulation at scale, and modularity of cargo loading capacity preclude their facile application in the clinic.<sup>64,78</sup> For protein and peptide vaccines, investigators continue to opt for emulsion-based adjuvants in the clinic.

## **Scaffolds**

Biomaterial scaffolds are a delivery strategy that have gained significant traction over the past decade. Such strategies involve the use of three-dimensional materials to establish a niche for priming of robust APC-mediated responses.<sup>81,82</sup> Traditionally, these constructs include an antigen, adjuvant, and chemoattractant such as GM-CSF, and are designed to recapitulate innate responses to infection.<sup>55</sup> APCs are recruited to the scaffold, where they encounter the antigen and adjuvant simultaneously, become activated, and migrate to the draining lymph nodes to initiate an immune response. While these scaffolds were first studied as cancer vaccines, they are also capable of inducing robust antibody titers.<sup>83–85</sup> Scaffolds have multiple potential advantages, including tunable loading and release of vaccine components, component co-delivery, adjustable mechanical properties and pore sizes, and inherent immunogenicity, among others. Together, these properties can be adjusted to promote enhanced immune responses in the draining lymph nodes. While gradual release of vaccine components is an advantage, the immune responses are primarily driven by the recruitment and subsequent migration of APCs to the lymph nodes.<sup>84</sup> Many types of materials have been investigated and compared, including polymers, hydrogels and cryogels, and mesoporous silica rods. Such scaffolds may also be composed of elements with the aforementioned modifications, such as protein antigens tagged with a targeting moiety or encapsulated in a nanomaterial. For example, an injectable polymer-nanoparticle hydrogel composed of HPMC-C12 and PEG-PLA nanoparticles was shown to promote injection site retention of protein antigens, resulting in improved IgG titers and induction of neutralizing antibodies.<sup>85,86</sup> However, these materials pose multiple barriers to clinical translation. Because of their 3D structure, many scaffolds must be surgically implanted; additionally, their material composition and degradation profiles must be tuned to avoid toxicity. Some injectable, spontaneously assembling systems have been developed to circumvent this challenge. However, these constructs must be optimized to produce an ideal pore size and charge to facilitate adequate loading and release of diverse vaccine components, as well as cell infiltration and survival. To date, only one such scaffold has been investigated in a clinical trial, which was for the treatment of cancer.

These challenges highlight how clinical translation of novel vaccines is often hindered by their complexity; the requirement for multiple recombinant or engineered elements, diverse materials and chemistries, and specific formulation conditions is a major obstacle for translation at scale.<sup>77</sup>

An ideal vaccine delivery system would consist of a biomaterial that supports modular cargoes, is easy and inexpensive to assemble, and is retained at the injection site on the order of days to weeks to promote sustained soluble antigen delivery and/or uptake by APCs. These efforts will enable the development of translatable immunization platforms against challenging targets in infectious disease.

## 1.5. Polyphenols as drug delivery agents

### 1.5.1. Tannic acid and interactions

Drug delivery platforms assembled by supramolecular chemistry may provide novel solutions to many challenges in the vaccine delivery field. Supramolecular biomaterials are formed by diverse non-covalent interactions among participating molecular entities, including hydrogen bonds, non-specific hydrophobic interactions, pi-pi stacking, and electrostatic interactions, among others.<sup>87</sup> Rationally designed supramolecular biomaterials have many beneficial properties including tunability, reversibility, modularity, and environmental responsiveness, with relevant applications in drug delivery and medicine. For example, materials including polymers, proteins, and peptides may be subject to diverse chemical modifications to enable interactions including receptor-ligand binding, host-guest complexation, and chain extension or stacking. Polyphenols are a class of molecules characterized by the presence of more than one phenolic group, which can facilitate formation of supramolecular assemblies. The core building block of the phenolic compound is at least one hydroxyl group conjugated to an aromatic hydrocarbon ring. These moieties can facilitate hydrophilic interactions via hydrogen bonding and dipole-dipole interactions, and hydrophobic interactions due to various aromatic rings in the structure (pi-pi stacking and other nonspecific interactions) (Fig. 1-6).<sup>88-90</sup>

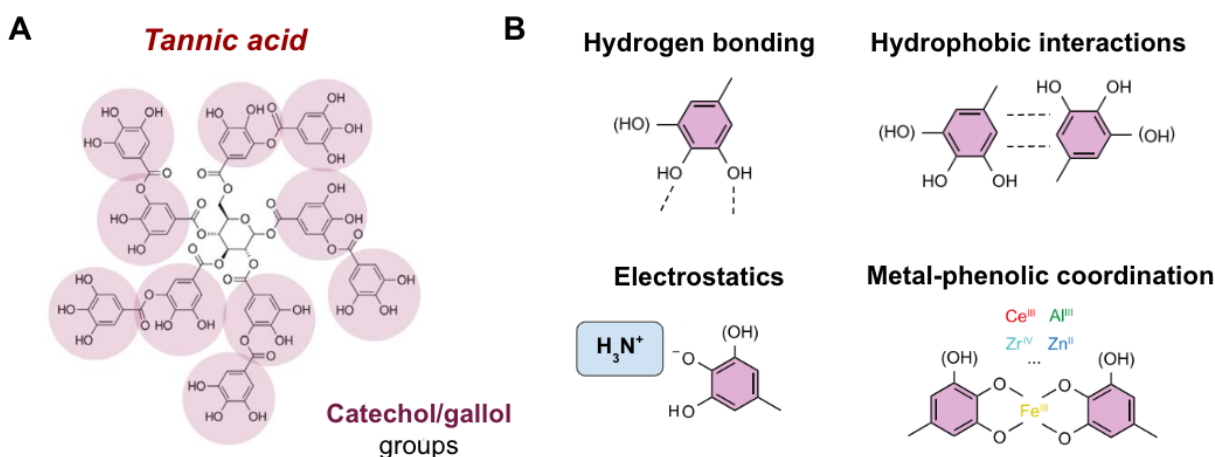


**Fig. 1-6. Structural elements and interactions of tannic acid (TA).**

(A) Structure of tannic acid. Phenolic groups (catechols and gallols) are highlighted in pink. (B) Noncovalent interactions of phenolic groups in TA. Adapted from Ref 94.

They can also participate in electrostatic interactions under favorable conditions, including ion-ion and ion-dipole interactions. One of the most well-studied polyphenols is tannic acid, a 1.7 kDa hydrolyzable tannin that is abundant in plant matter. Tannic acid consists of a central glucose molecule linked to 5 gallic acid groups, each composed of a catechol and gallol, which form a branched, multidentate structure.<sup>91</sup> The number and density of the phenolic groups in the

molecule facilitate strong cohesive and adhesive properties, which are favorable for formation of supramolecular assemblies with many organic and inorganic materials. One critical property of TA is that the proximity of hydroxyl groups in the phenolic rings enables formation of coordination complexes with transition metal ions. In 2013, Ejima et al introduced metal coordination of TA and  $\text{Fe}^{3+}$  as a simple, rapid, and scalable strategy for deposition of organic thin films on diverse particulate templates.<sup>92</sup> These properties have been leveraged to produce multilayer thin films of polyphenols on diverse substrates, with applications including anti-fouling, nanocapsule development, and nanoparticle stabilization.<sup>93–96</sup>

### 1.5.2. Biomedical applications of TA

Supramolecular assemblies incorporating TA both with and without transition metal ions have been prepared for a variety of biomedical applications, owing to favorable interactions of TA with biomolecules including proteins and nucleic acids.<sup>97–100</sup> In the drug delivery space, TA has been used to prepare adhesive hydrogels for tissue engineering applications, including the development of hemostats and drug depots for biologics.<sup>101,102</sup> Supramolecular interaction or direct conjugation of TA to polymers can facilitate formation of injectable hydrogels with tunable self-healing and mechanical properties to engineer compatibility with tissue.<sup>97,103–107</sup> TA is capable of interacting broadly with proteins of varying size, charge, and hydrophobicity to facilitate development of modular drug delivery systems including nanoparticles. By coating a sacrificial nanoparticle template with TA and protein cargo, nanocapsules of varying shape and size can be produced upon dissolution of the template. These capsules can be formulated to adjust factors such as permeability and pH-responsiveness to mediate favorable drug release.<sup>93,98,99,101,108</sup> Direct complexation of proteins and peptides with TA and other polyphenols has been explored for the generation and stabilization of nanoparticles for drug delivery.<sup>96,109–111</sup> TA/protein complexes without additional stabilization have also been investigated for systemic targeted drug delivery. Shin et al found that TA and the representative protein green fluorescent protein (GFP) formed heterogeneous complexes in vitro and could accumulate in ECM-rich tissue such as the heart upon intravenous injection, owing to the affinity of TA for ECM proteins including collagen and elastin (**Fig. 1-7**).<sup>112,113</sup> While TA has been extensively explored for creation of drug-encapsulating particles, gels, and films for antimicrobial, anti-cancer, and regenerative applications, it remains underexplored in the field of vaccine development and delivery.

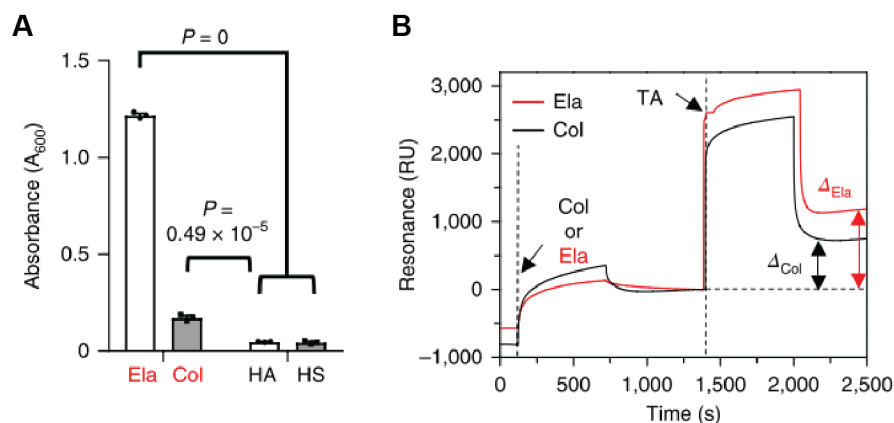


**Fig. 1-7. Affinity of TA for proteins of the extracellular matrix.**

(A) Solution turbidity as measured by absorbance at 600 nm of elastin (Ela), collagen (Col), and glycans hyaluronic acid (HA) and heparan sulfate (HS) upon complexation with TA. (B) Surface plasmon resonance upon binding of TA to gold surfaces coated with elastin or collagen. Adapted from Ref. 112.

### **1.5.3. Cellular engineering using TA**

The recent clinical success of cell-based therapies has opened the door for new drug delivery applications focused on manipulating adoptively transferred cells to direct therapeutic outcomes. The *in vivo* plasticity of many immune cells in the context of disease is a major challenge in the cell therapy field that will require new engineering approaches to overcome. Cellular hitchhiking is an emerging approach that involves anchoring therapeutic drugs to the cell membrane to **(i)** exploit unique cellular tropisms for targeted drug delivery, and/or **(ii)** manipulate the phenotype of the carrier cell. Engineering approaches developed preclinically to date include direct chemical conjugation mediated by biorthogonal chemistry, tethering of polymer or lipid-based nanoparticles to the cell membrane, and adhesion of microparticles.<sup>114–118</sup> Our lab has pioneered the innovation of backpacks, discoidal polymer-based particles that possess a high aspect ratio and are capable of evading phagocytosis, as an enabling approach for myeloid cell hitchhiking.<sup>119–123</sup> While promising, these approaches often lack modularity, are difficult to scale, and may not be adaptable for cells with varying properties including phagocytosis and material sensitivity.

One of the major advantages of drug delivery systems incorporating TA is the capacity to form supramolecular assemblies using substrates ranging in size from the nanoscale to macroscale. Based upon this property, researchers in our lab theorized that metal phenolic networks containing TA could be used as a particle-free toolkit for cellular engineering with biomolecules. TA has many theoretical advantages for cell-mediated drug delivery platforms including biocompatibility, modularity, and scalability. Zhao et al first showed that MPNs containing TA and Fe<sup>3+</sup> could be formed upon the membranes of living cells with various cargoes including antibodies, proteins, and RNA.<sup>100</sup> In this and subsequent work, red blood cells functionalized with MPNs were explored as biological carriers for proteins and adenoviral vectors for targeted delivery to the lungs.<sup>124</sup> Macrophages were also explored as carriers of checkpoint antibodies to solid tumors, and an optimized MPN/antibody formulation was found to control tumor growth without adversely affecting macrophage viability or migration. This work provides a fundamental proof of concept for TA-mediated supramolecular assembly of drug cargo on the cell membrane as a viable hitchhiking approach. However, much remains to be understood about the compatibility of different cell types with this approach from the standpoint of viability, phenotype, and payload longevity. Most importantly, existing approaches have utilized injected cells for targeted delivery to physiologic sites of interest, yet have not investigated the impacts of incorporated biological cargo on cell functionality.

## **1.6. Aims and scope of thesis**

Vaccines are perhaps the most successful public health intervention, as evidenced by their efficacy against infectious disease. Despite this success, much additional work is needed to harness the potential of vaccination to treat cancer and autoimmune diseases, and to produce effective, accessible vaccines at scale to confront emerging infectious threats. This thesis explores diverse applications of the polyphenol tannic acid (TA) as a vaccine delivery agent by harnessing the capacity of TA for supramolecular interactions with proteins, cells, and tissues.

We demonstrate that TA can be used for productive modulation of immune responses in different contexts by exploring **(i)** a cellular hitchhiking system for phenotypic control of DC vaccines, and **(ii)** a subunit vaccine delivery platform that enhances humoral immunity via prolonged injection site retention. Overall, we leverage TA to develop modular, scalable, “one-pot” systems for protein drug delivery to enhance the efficacy of vaccines across a variety of potential applications.

In Chapter 2, we sought to enable DC cellular hitchhiking for the first time by expanding upon previous work employing TA-containing MPNs as a modular toolkit for cell surface engineering. DC vaccines hold great potential for a spectrum of diseases, and combination drug delivery is an attractive strategy to manipulate their function and overcome *in vivo* plasticity. However, DCs are not compatible with current hitchhiking approaches due to their broad phagocytic capacity. Although MPNs represent a potential solution due to their particle-free nature, we found that the transition metal component is highly cytotoxic to DCs. In this work, we developed and validated META (**M**embrane **E**ngineering using **T**annic **A**cid) as an approach that employs tannic acid (TA) alone to facilitate supramolecular assembly of protein drug cargoes upon the DC membrane. We optimized META formulations to incorporate and release protein cargoes with varying physical properties alone and in combination, and to preserve DC viability and critical functions such as migration. Then, we showed that META carrying either pro- or anti-inflammatory cargo could influence the carrier cell phenotype accordingly, demonstrating the flexibility of the approach for applications from cancer to autoimmune disease. Overall, META enabled the creation of a new platform for the local control of phagocytic immune cells in a next step to advance DC therapies in the clinic.

In Chapter 3, we hypothesized that TA could facilitate prolonged injection site residence of protein subunit vaccines via supramolecular interactions with tissue. In doing so, we aimed to show that simple admixture of TA into subunit vaccine formulations could function as an inexpensive and scalable method to improve the efficacy of subunit vaccines. We demonstrated that TA associates with protein antigens in solution and facilitates extended antigen residence at the subcutaneous injection site for over one week. We then investigated the impact of various TA concentrations on lymph node cellular activation and antigen accumulation, identifying monocyte-derived dendritic cells (moDCs) as critical mediators of immunity. Finally, we dissected humoral immune responses to the receptor-binding domain (RBD) of SARS-CoV-2 and variants of concern and identified a formulation that improves antibody titers by over 100-fold. This system, termed TAPER (**T**issue-**A**dhesive **P**olyphenol-mediated **E**nhanced **R**etention) provides various translational advantages including one-pot synthesis, scalability, low cost, and modularity, towards realization of effective and accessible subunit vaccines.

## 2. Chapter 2: Dendritic cell immune modulation via polyphenol membrane coatings

Note: This chapter is adapted from a research article with the same title that has been submitted to ACS Applied Materials and Interfaces: **M.E. Janes**, K.S. Park, A.P. Gottlieb *et al.* (2024). Dendritic cell immune modulation via polyphenol membrane coatings. *ACS Applied Materials and Interfaces* (submitted).

### 2.1. Abstract

Cellular hitchhiking is an emerging strategy for the *in vivo* control of adoptively transferred immune cells. Hitchhiking approaches are primarily mediated by adhesion of nano and micro-particles to the cell membrane, which conveys an ability to modulate transferred cells via local drug delivery. Although T cell therapies employing this strategy have progressed into the clinic, phagocytic cells including dendritic cells (DCs) are much more challenging to engineer. DC vaccines hold great potential for a spectrum of diseases, and combination drug delivery is an attractive strategy to manipulate their function and overcome *in vivo* plasticity. However, DCs are not compatible with current hitchhiking approaches due to their broad phagocytic capacity. In this work, we developed and validated META (**M**embrane **E**ngineering using **T**annic **A**cid) to enable DC cellular hitchhiking for the first time. META employs the polyphenol tannic acid (TA) to facilitate supramolecular assembly of protein drug cargoes upon the cell membrane, enabling the creation of cell surface-bound formulations for local drug delivery to carrier DCs. We optimized META formulations to incorporate and release protein cargoes with varying physical properties alone and in combination, and to preserve DC viability and critical functions such as migration. Then, we showed that META carrying either pro- or anti-inflammatory cargo could influence the carrier cell phenotype accordingly, demonstrating the flexibility of the approach for applications from cancer to autoimmune disease. Overall, this approach illustrates a new platform for the local control of phagocytic immune cells in a next step to advance DC therapies in the clinic.

### 2.2. Introduction

Cell therapy represents a significant therapeutic advance that has shown promise for the treatment of immune-related diseases, especially cancer.<sup>125</sup> Chimeric antigen receptor (CAR) T cell therapy has led to functional cures in multiple blood cancers, and several additional cell types including natural killer (NK) cells, stem cells, macrophages, and dendritic cells (DCs), are being explored in preclinical and clinical studies.<sup>126,127</sup> DC-based therapies, especially DC vaccines, have the potential to treat a variety of conditions including cancer and inflammatory diseases.<sup>17,35,46</sup> The primary focus of DC vaccines to date has been on cancer, in which DCs primed *ex vivo* with tumor antigens and a maturation stimulus initiate an anti-tumor T cell response upon infusion.<sup>126,128</sup> DC vaccines are also being investigated for the treatment of autoimmune diseases such as rheumatoid arthritis and multiple sclerosis.<sup>37,129,130</sup> Although theoretically promising, DCs, like many other cell types, face the challenge of limited viability and inherent plasticity *in vivo*.<sup>17,131–134</sup>

The administration of supporting therapies, such as cytokines, is a widely used strategy to address phenotypic plasticity of injected cells. However, systemic administration is associated with many challenges including poor pharmacokinetics, toxicity, and off-target effects due to pleiotropy.<sup>135-137</sup> A variety of materials-based drug delivery strategies are being investigated to modulate the phenotype of injected cells in a more targeted manner. Several approaches have been proposed to accomplish this goal, including loading the cell surface with supportive therapies *ex vivo*.<sup>138,139</sup> For example, membrane-bound nanogels encapsulating IL-15 superagonist have been shown to induce T cell proliferation *in vitro* by more than 10-fold, promote the specific expansion of T cells in tumors, and decrease tumor burden in absence of systemic toxicity.<sup>140</sup> Polymeric discoidal microparticles, also known as backpacks, have been used to maintain pro-inflammatory polarization of macrophages and natural killer cells and have shown efficacy for the treatment of solid tumors.<sup>121,122</sup> While these approaches offer possible means to decorate various cell types, none of them can be used to modify DCs due to their exceedingly high phagocytic ability. DCs internalize most membrane-bound particles, including large (>1  $\mu\text{m}$ ) particles and those with high aspect ratios<sup>141-144</sup>, thus rendering particle-based strategies ineffective.

Recently, iron-containing metal phenolic networks (MPNs) have been used to decorate the surfaces of red blood cells with adeno-associated viruses for gene therapy and macrophages with PD-L1 antibodies for cancer treatment.<sup>100,124</sup> These constructs consist of a polyphenol, usually tannic acid (TA), which forms supramolecular nanocomplexes with biomolecular cargo to promote direct adhesion to the cell membrane. Inclusion of a transition metal ion facilitates stable complexation by producing metal coordination bonds among phenolic moieties, and is historically a critical component of materials-based approaches for thin film engineering using polyphenols. Iron-based MPNs, though compatible with RBCs and macrophages, can be potentially toxic to DCs due to high local concentrations of iron. Overall, existing strategies are insufficient to enable cell surface engineering of DCs, and novel particle-free strategies are needed to facilitate targeted administration of supporting therapeutics with DC therapies.

Here, we report for the first time the control of DC phenotype by engineering the cell surface with supporting therapies in a strategy referred to as **Membrane Engineering using Tannic Acid (META)**. Inspired by MPNs, META incorporates a polyphenol and biomolecule cargo in absence of an ion component to facilitate adsorption of therapeutic proteins to the DC membrane while preserving cell viability. META supports the incorporation of multiple distinct cargoes, and enables both drug release to the environment and interaction with the carrier cell. Importantly, optimized META formulations do not disrupt essential functions such as phagocytosis and migration. Finally, META has the ability to control DC phenotype in a cargo-specific manner. Overall, META provides a means to modulate DC function for a variety of potential therapeutic applications, including cancer and autoimmune diseases (**Fig. 2-1**).

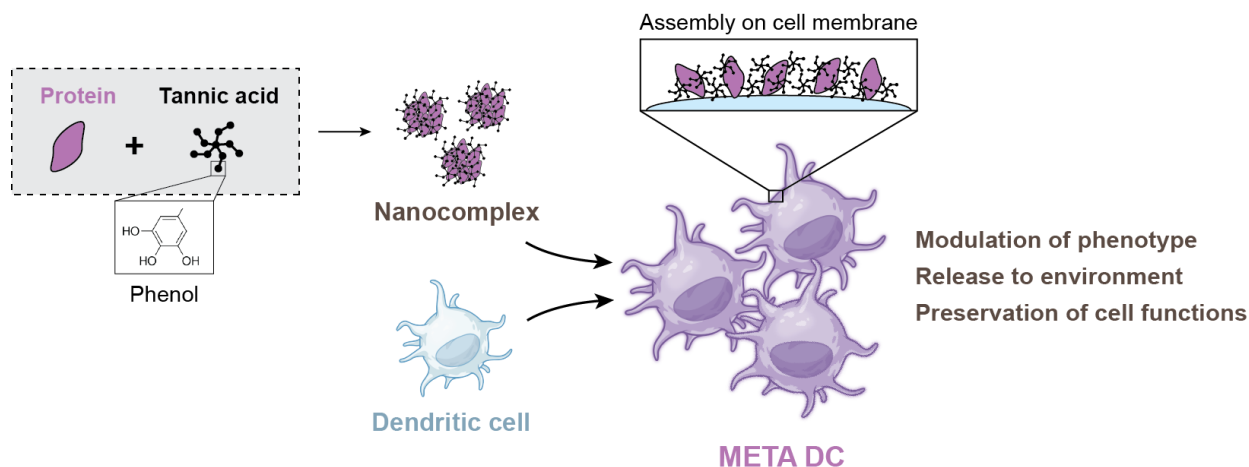


**Fig. 2-1. Formation of META DCs.**

TA associates non-specifically with protein via supramolecular interactions. When cells are added to the mixture, TA initiates adsorption of protein cargo to the membrane to produce META DCs.

## 2.3. Results

### 2.3.1. Formulation development and biocompatibility of protein networks

META was formed by incubating proteins with varying concentrations of TA in phosphate-buffered saline (PBS), then adding DCs and gently washing. The optimum TA concentration for designing META was determined by coating DCs with networks consisting of TA and the model protein BSA across a range of TA concentrations. We investigated the compatibility of these networks with both immature and LPS-matured DCs to elucidate the effects of cell phenotype on network tolerability. In mature DCs, cell viability was preserved at a TA concentration of 4  $\mu\text{M}$  and cell death increased non-linearly with increasing TA concentration (**Fig. 2-2A**). The effect of TA on immature cells was quite different (**Fig. 2-2B**). These experiments were performed in the presence as well as absence of GM-CSF, which plays a key role in DC survival. Baseline DC viability was poor in absence of GM-CSF, and increasing network TA concentrations improved viability. In contrast, no toxicity was observed at any TA concentration in the presence of GM-CSF. The effect of TA on apoptosis was also assessed. In mature as well as immature DCs, increasing TA induced increases in apoptotic cells (**Fig. 2-2C,D**). Based on these results, a TA concentration of 4  $\mu\text{M}$  was chosen for META in the case of mature DCs and 75  $\mu\text{M}$  in case of immature DCs in the presence of GM-CSF.

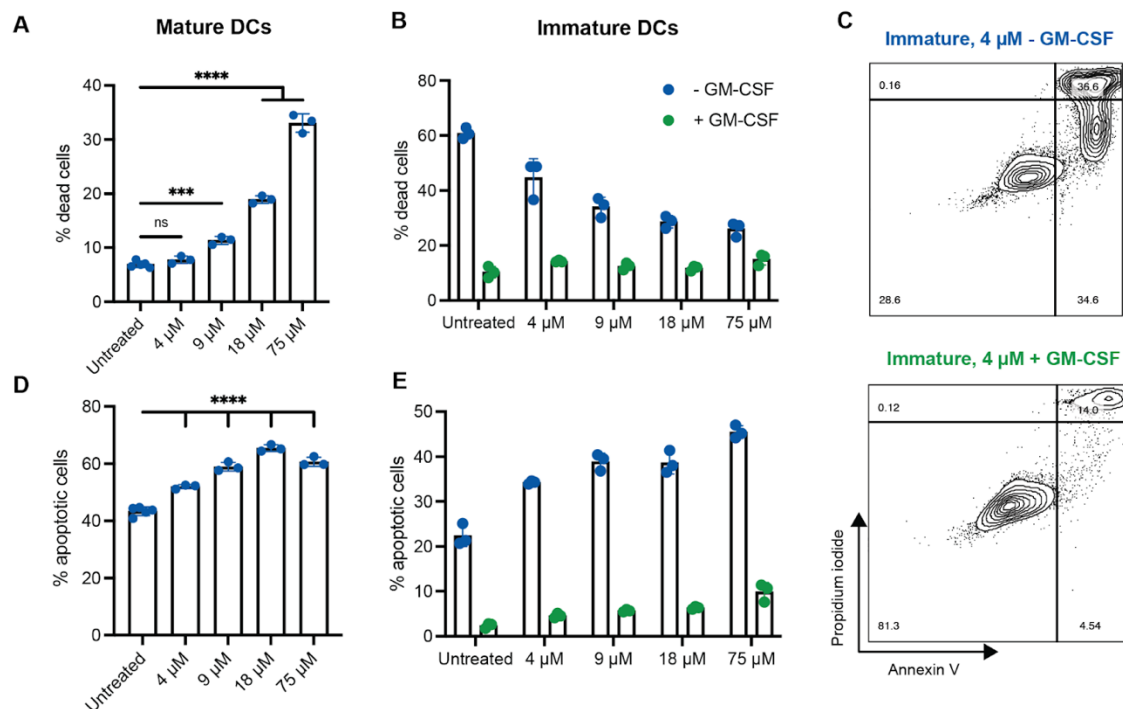


**Fig. 2-2. Effect of TA concentration on viability of coated cells.**

(A,B) Induction of cell death in mature (A) and immature (B) DCs as measured by Annexin V+/PI+ staining after 24 hours of culture, with or without GM-CSF as indicated. (C) Representative flow plots of Annexin V/PI staining. (D, E) Induction of early apoptosis in mature (D) and immature (E) DCs as measured by Annexin V+/PI- staining after 24 hours of culture, with or without GM-CSF as indicated. Data represented as mean  $\pm$  standard deviation. P-values were determined by ordinary one-way ANOVA followed by Tukey's multiple comparison test (\*\*\* $p$ <0.001; \*\*\*\* $p$ <0.0001; ns, not significant,  $p$ >0.05).

META coated DCs with proteins as assessed using Alexa Fluor 647-labeled BSA as a model cargo. BSA uniformly covered the DC surface as confirmed by confocal microscopy (**Fig. 3**). Network formation on the membrane was visible, with some evidence of uptake noted as punctate regions within putative endosomes or diffuse staining throughout the cell body. Dynamic light scattering (DLS) analysis of solutions consisting of TA (4  $\mu$ M) and BSA revealed no change in the average size of the constituents (**Appendix Fig. 1**), thus suggesting that individual protein molecules do not aggregate; instead, it is likely that proteins associate independently with multiple molecules of TA and subsequently bind to the cell membrane.

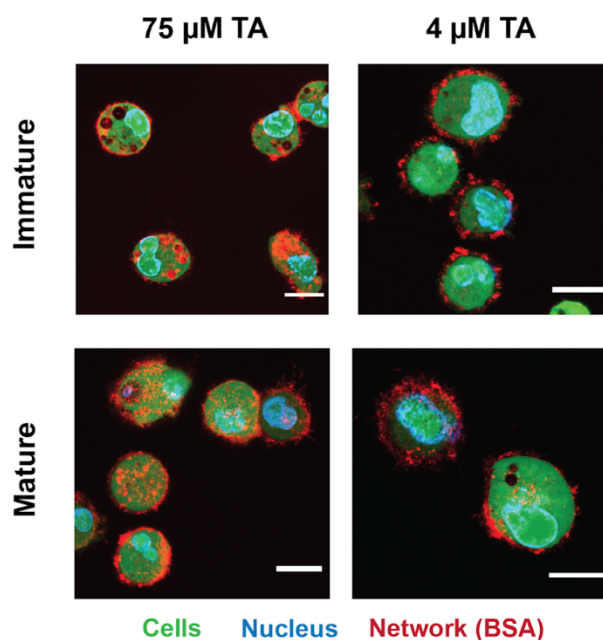


**Fig. 2-3. Confocal imaging of fluorescently labeled protein networks.**

Immature and mature cells were stained with CellTracker Green and Hoechst and coated at the indicated TA concentrations with 48  $\mu\text{g}/\text{mL}$  Alexa Fluor 647-labeled BSA. Live cells were visualized immediately after staining. Scale bar is 10  $\mu\text{m}$ .

META is a distinct, particle-free approach that is differentiated from alternative drug delivery approaches including nanoparticles, backpacks, and MPNs, all of which have been previously used to decorate other cell membranes. DCs are known to internalize nano and micro-particles with diverse material properties.<sup>145–148</sup> Specifically, we found that even mature DCs readily internalized 8  $\mu\text{m}$ -diameter disk-shaped backpacks, which possess a high aspect ratio (**Appendix Fig. 2**). Less than 10% of the cells demonstrated stable backpack attachment, which is quite distinct from that reported for macrophages,<sup>121</sup> thus attesting to the superior phagocytic ability of DCs. Metal phenolic networks could also not be used for DCs owing to their susceptibility to iron-induced toxicity (**Appendix Fig. 3**). While iron induced dose-dependent toxicity to DCs in both MPN and soluble form, TA alone was well-tolerated (**Appendix Fig. 4**).

### 2.3.2. Cargo loading, release, and characterization

The ability of META to load therapeutically relevant proteins on DCs was tested using several candidates including anti-CD40 antibody, GM-CSF, IL-15, and IL-12. CD40 agonism is an emerging therapeutic intervention that mimics endogenous signaling between DCs and helper T cells to promote DC survival, costimulatory molecule expression, and IL-12 secretion.<sup>149,150</sup> GM-CSF promotes DC survival, while IL-15 and IL-12 are of interest due to their ability to stimulate T cells. Anti-CD40 antibody loading increased non-linearly with its concentration in the incubating solution (**Fig. 2-4A**). 48  $\mu\text{g}/\text{mL}$  was chosen as an optimal concentration to maximize loading efficiency, which yielded an average loading of 2.11  $\mu\text{g}$  per million cells, for a loading efficiency of 4.1%. Similar behavior was noted for other cargos. The ultimate loading of the cargo could be modulated by maintaining the incubation concentration at 48  $\mu\text{g}/\text{mL}$  and “doping in” BSA as a

model inert protein. The loading of GM-CSF varied across orders of magnitude at feed percentages from 1% to 100% with BSA as the other constituent, demonstrating the flexibility of the approach to incorporate highly potent and/or expensive reagents (**Fig. 2-4B**). META also enabled loading of multiple cargos. For example, IL-15 and anti-CD40 were co-loaded on DCs (**Fig. 2-4C**). Loading of both cargos could be controlled independently (**Fig. 2-4C, Appendix Fig. 5**). Protein loading was rather independent of the TA concentration in META. A 16-fold increase in TA concentration (75  $\mu\text{M}$  vs 4  $\mu\text{M}$ ) yielded a minimal change in protein loading (**Appendix Fig. 6**).

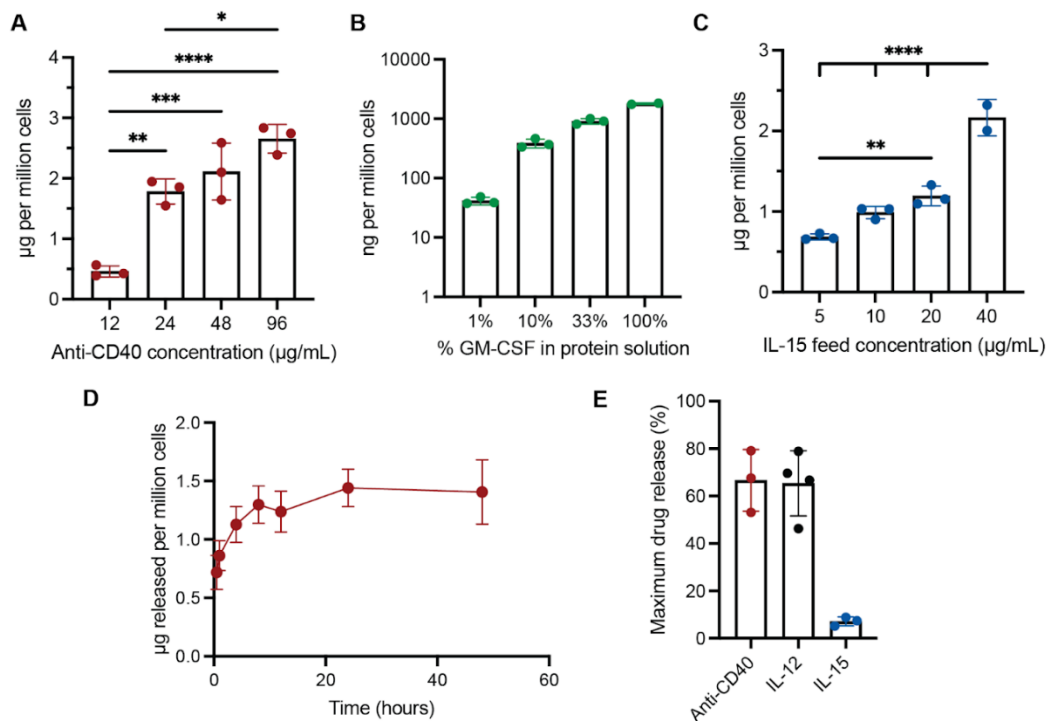


**Fig. 2-4. Loading and release of model protein cargo from networks. All assessments of loading and release were conducted using ELISA.**

(A) Loading of anti-CD40 at various protein feed concentrations. (B) Loading of GM-CSF at indicated percentages of 48  $\mu\text{g/mL}$  protein feed solution, with the remainder constituted by BSA. (C) Loading of IL-15 in networks containing a consistent feed concentration of 96  $\mu\text{g/mL}$  anti-CD40. Total protein feed concentration varied according to the amount of IL-15 added. (D) Release of anti-CD40 from immature DCs over time. Cells were plated at 100,000 per 200  $\mu\text{L}$  volume, and values were normalized to reflect the amount of drug release per million cells. (E) Maximum percentage (%) of loaded drugs released over the 48-hour analysis period. Data represented as mean  $\pm$  standard deviation. P-values were determined by ordinary one-way ANOVA followed by Tukey's multiple comparison test (\* $p < 0.05$ ; \*\* $p < 0.01$ ; \*\*\* $p < 0.001$ ; \*\*\*\* $p < 0.0001$ ).

Anti-CD40 demonstrated a release profile from the coating consisting of distinct burst and extended-release phases, with detectable release up to 24 hours (**Fig. 2-4D**). However, the cytokines IL-15 and IL-12 demonstrated highly rapid, yet incomplete release. About two-thirds of the IL-12 cargo, but less than 10% of the IL-15 cargo, were released within one hour, while the remainder was not released up to the final time point of 48 hours (**Fig. 2-4E**). Previous work has shown that protein properties including molecular weight, isoelectric point, and hydrophobicity can influence network disassembly, which may explain the differential behavior of these proteins.<sup>151</sup>

Overall, the platform allowed for flexible incorporation of a variety of cargoes with the potential to stimulate carrier cells or be released to the environment. However, the ultimate release (and potential internalization) was highly cargo-dependent, suggesting the need for careful validation of each cargo.

### 2.3.3. Bioactivity of loaded cargo

The bioactivity of cargoes captured in the network must be maintained to ensure their therapeutic efficacy. The functionality of the cytokine IL-15, a potent stimulator of T cell proliferation, was investigated after incorporation in the networks. IL-15 is highly susceptible to degradation *in vivo*, with a half-life of about 70 minutes.<sup>152</sup> The EC<sub>50</sub> of IL-15, assessed using a cell reporter assay, increased from 49.6 in the case of unmodified IL-15 to 90.5 pg/mL (48 µg/mL condition), indicating a ~1.8-fold loss in bioactivity that does not preclude its use in therapeutic applications (**Fig. 2-5A, Appendix Fig. 7**).<sup>153</sup> Interestingly, decreasing the protein feed concentration resulted in better preservation of bioactivity despite an increased molar ratio of TA to protein. To further elucidate the effects of networking on protein structure, circular dichroism spectroscopy (CD) was conducted on BSA complexed with TA. CD measurements revealed that the alpha helical secondary structure of BSA was preserved at various TA to protein ratios even after 24 hours of incubation (**Fig. 2-5B**). These results confirm the biological compatibility of network formation with a variety of proteins.

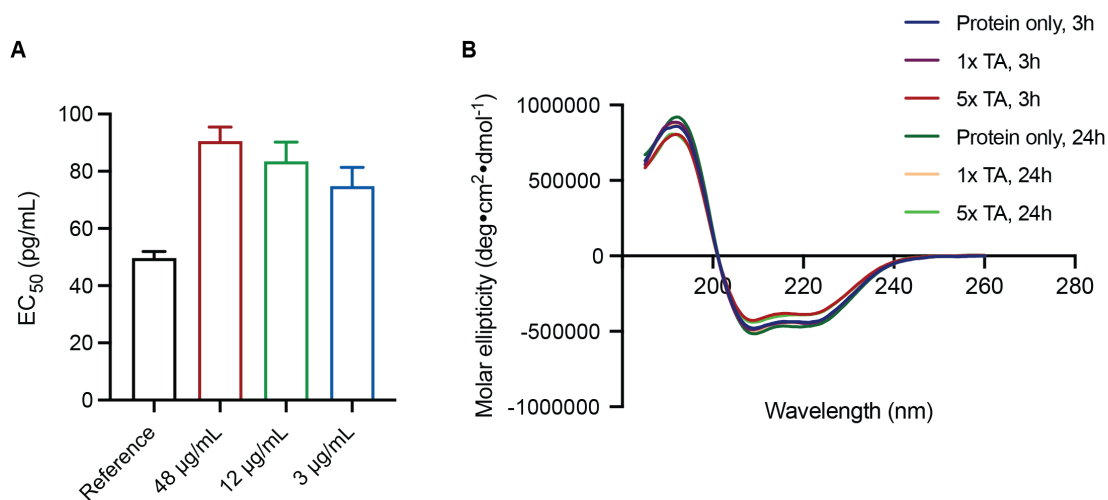


**Fig. 2-5. Bioactivity of networked proteins.**

(A) EC<sub>50</sub> of human IL-15 in networks at various protein feed concentrations. Immature cells were coated with IL-15 networks, cultured for 24 hours, and the released media was collected for a reporter assay. (B) Circular dichroism spectroscopy of BSA complexed with TA. Data in (A) represented as mean ± standard error.

### 2.3.4. Cellular uptake of network components

The cellular uptake of loaded cargo was assessed using DQ-albumin, a BODIPY dye-tagged ovalbumin (OVA) that fluoresces upon endosomal uptake (**Fig. 2-6**). Immature cells coated with DQ-OVA showed reduced uptake of their protein cargo (19.5%) compared controls (soluble DQ-OVA, up to 54.2%). Although some fluorescence was noted at early time points, little additional fluorescence was seen over 24 hours. The same trends were observed for mature DCs, which internalized DQ-OVA (19.7% internalization with META compared to 68.6% for soluble protein).

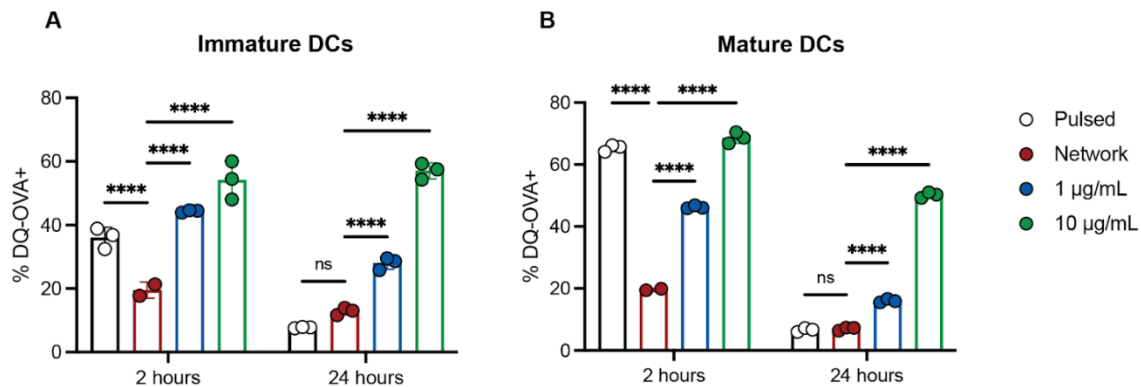


**Fig. 2-6. Uptake of proteins networked in META.**

DQ-OVA was incorporated into networks or cultured in soluble form with immature (A) and mature (B) DCs for 2 and 24 hours. Uptake of protein was assessed via DQ-OVA fluorescence, which only occurs upon exposure to proteases in the endosome/lysosome. “Pulsed” indicates cells exposed to coating solution in absence of TA, while 1 µg/mL and 10 µg/mL indicate culture with soluble DQ-OVA for the indicated time. Data represented as mean ± standard deviation. P-values were determined by ordinary one-way ANOVA followed by Tukey’s multiple comparison test (\*\*\*\*p<0.0001; ns, not significant, p>0.05).

### 2.3.5. Networked cells maintain capacity for migration and phagocytosis

For protein networks to serve as a hitchhiking system *in vivo*, DCs must maintain their ability to execute critical functions including directed migration and phagocytosis. When employed as vaccines, subcutaneously injected DCs must migrate to the lymph nodes to encounter T cells and initiate an immune response. Therefore, an ideal network formulation must preserve the capacity for directed migration. The ability of mature DCs to migrate in response to the chemokine CCL19, a key driver of immune cell homing to lymphoid tissue,<sup>154,155</sup> was assessed in the presence or absence of META in a Transwell culture system (**Fig. 2-7A**). At a TA concentration twice as high as the standard (9 µM vs. 4 µM), migration was reduced by 70.2% for cells carrying BSA, even though viability decreased by less than 10%. Interestingly, while DCs in the BSA 4 µM TA condition migrated as efficiently as untreated control cells, DCs carrying anti-CD40 migrated significantly less efficiently, indicating that the structure and/or function of the cargo has implications for DC trafficking behavior. We assessed the phagocytosis capacity of META-coated DCs by measuring uptake of polystyrene beads. META-coated immature DCs displayed slightly reduced bead uptake (43% vs. 35.7%) after two hours of incubation, while uptake by mature cells was not significantly different compared to an untreated control (**Fig. 2-7B**). Overall, these results suggest that phagocytic ability is maintained. The META coating was stable against shear stresses associated with delivery conditions. Passage of META DCs containing Alexa Fluor 647-labeled BSA through 27- and 30-gauge needles led to only a minor reduction in fluorescent intensity (**Appendix Fig. 8**).

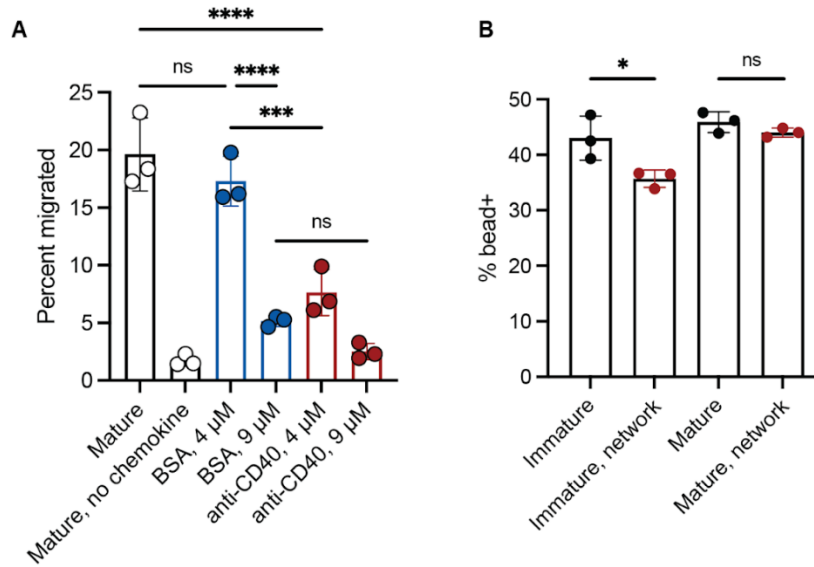


**Fig. 2-7. Migration and phagocytosis capacity of META DCs.**

(A) Migration of mature DCs in response to a CCL19 chemokine gradient in a 5 µm pore Transwell system lacking an endothelial monolayer, which mimics lymphatic capillaries encountered upon subcutaneous administration. Groups with listed concentrations represent cells with protein networks, consisting of the listed cargo and indicated TA feed concentration. (B) Uptake of polystyrene beads by immature and mature cells with and without BSA networks. Data represented as mean ± standard deviation. P-values in (A) were determined by ordinary one-way ANOVA followed by Tukey's multiple comparison test (\*p<0.05; \*\*p<0.01; \*\*\*p<0.001; \*\*\*\*p<0.0001, ns, not significant, p>0.05). P-values in (B) were determined by an unpaired t-test for each condition, immature and mature (\*p<0.05; ns, not significant).

### 2.3.6. Networks promote cell viability and maturation of carrier DCs

We theorized that the surface residence of the coatings could enable “pseudo-autocrine” stimulation of the carrier cells, conferring an ability to modulate the phenotype of DCs used as vaccines *in vivo*. To begin, we studied the effect of network-loaded GM-CSF on cell viability. DCs require GM-CSF for optimal survival, proliferation, and migration, yet systemic administration of GM-CSF can expand and support cell populations that drive resistance to therapy.<sup>132,156</sup> We coated immature DCs with networks consisting of 10% GM-CSF and 90% BSA, and assessed their viability after 24 hours in culture. The viability of coated DCs was not significantly different from that of cells cultured in GM-CSF, while DCs deprived of GM-CSF diminished in viability to 69.3% (**Appendix Fig. 9**).

The ability of META to activate DCs was assessed using CD40 ligand (CD40L), an endogenous CD40 agonist. Potent signaling by CD40L is triggered via clustering of the CD40 receptor, which is achieved by sustained display of CD40L molecules in close proximity to one another on the cell surface.<sup>157</sup> We hypothesized that the incorporation of CD40L in cell surface-associated networks would increase both the local concentration and extent of receptor clustering, leading to more potent DC activation than exposure to soluble CD40L alone. While up to 5 µg/mL of soluble CD40L trimer did not affect DC phenotype, CD40L cell coatings significantly enhanced the surface expression of CD80 and MHCII (**Fig. 2-8A,B**). Coatings containing BSA did not alter expression compared to untreated controls, indicating that TA-driven assembly does not possess an intrinsic stimulatory effect and the observed activation is cargo-driven.

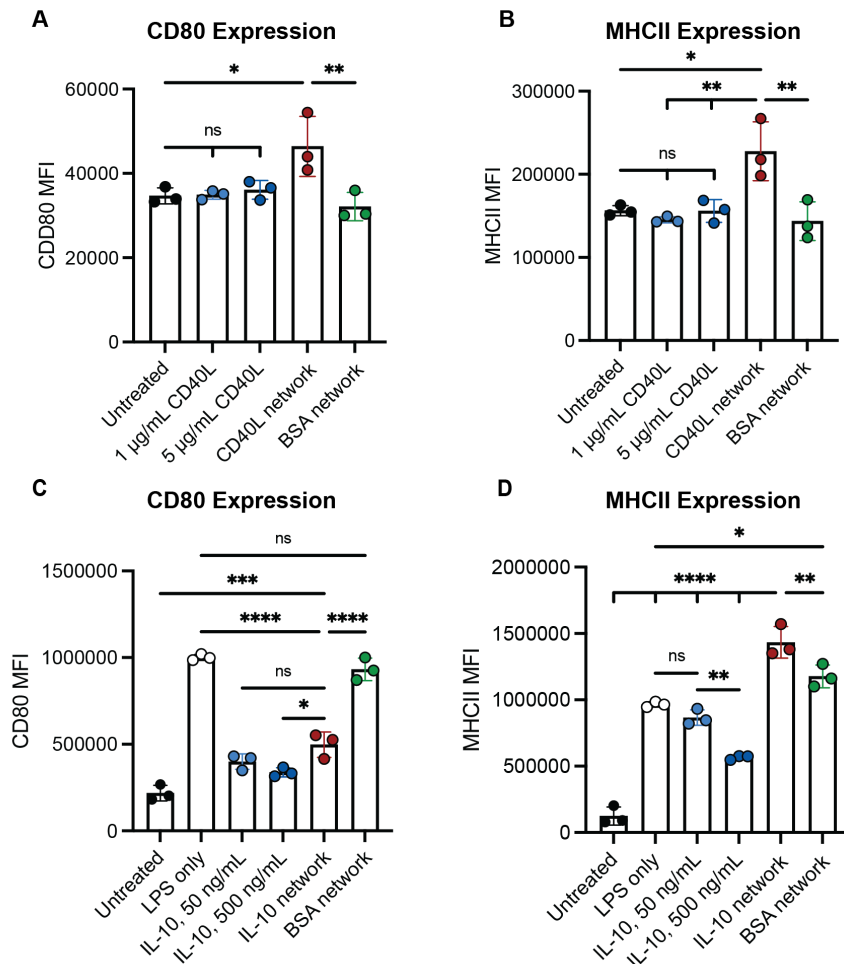


**Fig. 2-8. Response of immature DCs to the activating stimulus CD40L or tolerogenic stimulus IL-10 in cell networks.**

(A, B) Immature DCs were coated with networks containing CD40L or BSA, or cultured with soluble CD40L at indicated concentrations for 24 hours. (A) Quantification of CD80 expression. (B) Quantification of MHCII expression. (C, D) Immature DCs were coated with networks containing IL-10 or BSA, or cultured with soluble IL-10 at indicated concentrations for 24 hours in the presence of 100 ng/mL LPS. (C) Quantification of CD80 expression. (D) Quantification of MHCII expression. Data represented as mean  $\pm$  standard deviation. P-values were determined by ordinary one-way ANOVA followed by Tukey's multiple comparison test (\* $p < 0.05$ ; \*\* $p < 0.01$ ; \*\*\* $p < 0.001$ ; \*\*\*\* $p < 0.0001$ ; ns, not significant).

As another example, the ability of META to sustain an anti-inflammatory DC phenotype was assessed using IL-10 as the chosen cargo. IL-10 META immature DCs were challenged with LPS and the changes in maturation and antigen presentation machinery were assessed. IL-10 coatings reduced CD80 expression as efficiently as 50 ng/mL and 500 ng/mL soluble IL-10 (**Fig. 2-8C,D**). Interestingly, while soluble IL-10 reduced MHCII expression in a dose-dependent manner, both IL-10 and BSA in network significantly increased MHCII expression. This result suggests a combined effect of TA and protein cargo, with some contribution from cargo identity, on induction of MHCII expression.

## 2.4. Discussion

To begin, we assessed the compatibility of TA/Fe<sup>3+</sup> networks containing the model protein bovine serum albumin (BSA) with immature DCs at a variety of protein concentrations. This previously-reported formulation induced substantial cell death (~90%) within 24 hours of culture, and cells coated with these networks showed hallmark signs of ferroptosis (**Appendix Fig. 3**).<sup>158</sup> As a result, we suspected that the high local concentration of iron in the networks rapidly induced cell death. We investigated the effects of the soluble network components TA and Fe<sup>3+</sup> individually and combined in complete media. We found that while TA alone had little effect, Fe<sup>3+</sup> and combined TA/Fe<sup>3+</sup> induced cell death in a concentration-dependent manner (**Appendix Fig. 4**). While macrophages and red blood cells were shown to tolerate Fe<sup>3+</sup> concentrations within this range in previous works, DCs were more susceptible to cell death. These results suggest that differential tolerance of high local concentrations of Fe<sup>3+</sup> amongst immune cell types necessitates the development of a more broadly biocompatible approach.

Given the potential of transition metal ions to impact cell viability and alter crucial biological processes,<sup>158,159</sup> we investigated an ion-free approach for polyphenol hitchhiking with the goal of preserving DC viability and function. To accomplish this, we relied on intermolecular interactions amongst TA molecules and between TA and cargo to facilitate membrane adhesion. This strategy has been previously applied to form ion-free networks using nanoparticle substrates, but has yet to be investigated using cellular substrates.<sup>151</sup> We found that META formation induced cell death in a TA concentration-dependent manner in mature DCs, yet enhanced cell viability of immature DCs. The inclusion of GM-CSF in the culture media abolished all effects of network complexation on immature DC viability. These results suggest a striking influence of cell state on tolerance of network formation. One potential explanation is that direct TA complexation to the cell membrane may drive changes in metabolic activity that are detrimental to mature cells, which already exhibit indicators of apoptosis in absence of GM-CSF, yet protect immature cells from metabolic stress. These results underscore the importance of accounting for cellular phenotype in developing an optimal hitchhiking system.

In addition to adequate viability, therapeutic cells must maintain their ability to execute critical functions. In the case of DCs, these include directed migration and phagocytosis. When employed as vaccines, subcutaneously injected DCs must migrate to the lymph nodes to encounter T cells and initiate an immune response. Therefore, an ideal network formulation must preserve the capacity for directed migration. We found that both protein cargo identity and TA concentration had an impact on DC migration capacity. Interestingly, while DCs in the BSA 4  $\mu$ M TA condition migrated as efficiently as untreated control cells, DCs carrying anti-CD40 migrated significantly less efficiently, indicating that the structure and/or function of the cargo has implications for DC trafficking behavior. Increasing the TA concentration to 9  $\mu$ M reduced migration by over 3-fold, suggesting a direct impact of TA on chemotaxis. DCs coated with META preserved their capacity to phagocytose particles, suggesting that META does not disrupt contact between particles and the cell membrane.

Another key consideration in the development of META is the potential uptake of cargo by the carrier cell. Due to DCs ability to constitutively sample the extracellular environment via

macropinocytosis, uptake of cargo both during and after the complexation process is an important consideration for network longevity.<sup>160</sup> Incubation with DQ-OVA in soluble or META form showed that while cargo uptake does occur, the proportion of cells taking in cargo is lesser than that associated with soluble incubation. These data may also explain the lack of complete extracellular release observed with multiple cargoes, as some proportion of cargo is internalized.

Finally, we demonstrated the ability of META to modulate cell phenotype in a cargo-dependent manner. Only CD40L META increased expression of the activation marker CD80, while soluble CD40L and BSA META had no effect. This may be a result of CD40L proximity induced by encapsulation in META, which has the ability to promote CD40 crosslinking and amplify downstream signaling. Importantly, BSA META did not alter the expression of CD80 or MHCII, suggesting that TA does not itself have an immunomodulatory effect. In a pro-inflammatory environment, IL-10 META reduced CD80 expression as effectively as soluble IL-10. However, IL-10 META increased MHCII, suggesting a potential synergy of TA and IL-10 in generating this effect. Overall, the cargo-dependent nature of META provides a distinct benefit over particle-based hitchhiking approaches, in which the constituent biomaterials often have substantial effects on cell phenotype in absence of therapeutic cargo.<sup>161</sup> The use of a carrier such as TA opens the door to finely tune DC phenotype for both pro- and anti-inflammatory applications. Overall, these results suggest that MPNs are a suitable approach for the modulation of cell phenotype across therapeutic contexts.

## 2.5. Conclusions

Herein, DC hitchhiking was demonstrated for the first time by leveraging an ion-free polyphenol network for direct complexation of drug cargo to the DC membrane. An existing MPN formulation was adapted for biocompatibility with DCs by eliminating the ion component and reducing the TA concentration, indicating that cell tolerance of MPNs varies widely depending on cell type and state. The loading and release of a variety of protein cargoes was characterized in-depth, demonstrating the modular nature of the platform to support combinations of proteins with varying sizes and properties. DCs maintained their ability to migrate in response to a chemokine gradient and phagocytose particles, showing that the formulation maintains critical DC behaviors. Finally, protein cargo was shown to have functional effects on DC viability and phenotype, further bolstering the use case of MPNs for *in vivo* control of DC vaccines. To our knowledge, this is the first investigation of MPNs and their derivatives with an ultimate purpose of drug delivery to immune carrier cells. The facile, modular approach presented here lays the groundwork for a repertoire of strategies to better control phagocytic myeloid cells and further their use as transformative cell therapies.

## 2.6. Materials and Methods

### Reagents

Tannic acid, iron chloride hexahydrate, BSA, Alexa Fluor 647-labeled BSA, CellTracker Green CMFDA, and DQ-OVA were obtained from Thermo Fisher Scientific. Flow cytometry compensation beads and stain buffer were obtained from eBioscience. All recombinant murine proteins (IL-12, IL-15, GM-CSF, CD40L, and CCL19) and recombinant human IL-15 were

obtained from Peprotech. CD40 agonist antibody (anti-CD40) was obtained from Bio X Cell. ELISA kits for human and murine IL-15, murine IL-12, and murine GM-CSF were obtained from R&D Systems. A rat IgG ELISA kit was obtained from Abcam and used to quantify the concentration of CD40 agonist antibody.

### **Animals**

Female C57BL/6 mice (Charles River Labs) and C57BL/6J mice (Jackson Laboratory) aged 5 weeks were used for the generation of all bone marrow cell cultures.

### **Bone marrow DC (BMDC) culture**

Bone marrow mononuclear cells were isolated from the femurs and tibias of mice as described previously.<sup>121</sup> Cells were centrifuged at 350 g for 5 minutes after isolation and washed twice with PBS, then cultured in RPMI-1640 containing L-glutamine (Gibco) and supplemented with 1% penicillin/streptomycin (Gibco), 2-mercaptoethanol (Gibco), and 20 ng/mL recombinant murine GM-CSF (Peprotech). Cells were divided and plated at 10 mL per dish in non-tissue culture-treated dishes (Corning) and cultured at 37 °C in a humidified incubator under 5% CO<sub>2</sub>. Media addition (10 mL) was performed on day 3 of culture. On day 6 and every other day thereafter, a media exchange was performed by isolating 10 mL media from each dish, centrifuging the contents at 250 g for 5 minutes to collect cells, and resuspending in 10 mL fresh media to reconstitute the dish. Cells were used between days 8 and 12 of culture for all experiments.

### **BMDC harvesting and maturation**

BMDCs were isolated by collecting the non-adherent and loosely adherent cellular fractions via gentle aspiration with a serological pipette. Dishes were gently washed once with 5 mL of room temperature PBS, pH 7.4 (Gibco). Cells were centrifuged at 200 g for 5 min and washed twice with PBS before being manually counted with a hemocytometer for downstream applications. For experiments requiring mature DCs, cells were harvested as described above, resuspended in media supplemented with 1 µg/mL lipopolysaccharide (LPS) (eBioscience), and added to new culture dishes. Cells were incubated overnight for use the following day.

### **Preparation and assembly of networks**

Network precursor solutions consisting of tannic acid (TA) and proteins were prepared in low-binding 1.5 mL Eppendorf tubes (Pierce) using PBS, pH 7.4 (Gibco). The solution volume was scaled according to the total number of cells in the reaction, such that the final cell concentration was 1 M/mL. All cell stock solutions had a concentration of 10 M/mL. To begin, protein was added to a stock solution of PBS such that the final concentration upon cell addition would total 48 µg/mL. TA was added to the protein solution and thoroughly mixed to enable complexation. Protein/TA solutions were incubated at RT for at least 15 minutes. Next, cells were added and gently mixed to facilitate TA-mediated protein binding. Cells were incubated for ~3 minutes, followed by the addition of an equal volume of PBS. Cells were centrifuged at 150 g for 4 minutes in a centrifuge with a swinging bucket rotor. The TA solution was thoroughly aspirated, and cells were gently resuspended in 1 mL PBS. After a second wash, the solution was again carefully aspirated, and cells were resuspended in complete medium for downstream applications. All experiments were conducted in biological triplicate.

### **Protein loading in networks**

The loading of protein cargo was assessed by ELISA. After the second washing step, cells were resuspended in RIPA buffer (G Biosciences) containing Halt protease inhibitor cocktail (Pierce) to facilitate cell lysis and network disassembly. Cell solutions were incubated on ice for 30 minutes with periodic vortexing. Lysed solutions were stored at -80 °C for later analysis by ELISA. All ELISAs were conducted according to the manufacturer's instructions.

### **Release of proteins from networks**

Following coating, cells were resuspended in complete medium to a concentration of 0.5M/mL and plated into non-tissue culture-treated U-bottom 96 well plates. Cells from the same tube (technical replicates) were added to separate plates for each time point, such that each plate was only spun one time. At each time point, the corresponding plate was centrifuged at 150g for 4 minutes, and the media was carefully aspirated. Samples were stored at -80 °C for later analysis by ELISA. Samples were taken up to 48 hours after initial resuspension in media.

### **Flow cytometry**

Cells were washed at least once in stain buffer prior to staining. Cells were resuspended in anti-CD16/CD32 antibody (clone 93, eBioscience) at a dilution of 1:30 and incubated on ice for 5-10 minutes to block Fc receptors. Staining antibodies were then added at a final antibody dilution of 1:100. Cells were stained for CD11c (FITC, clone N418, BioLegend), CD86 (APC-eFluor 780, clone GL1, eBioscience), CD80 (Super Bright 600, clone 16-10A1, eBioscience), CD40 (PE, clone 1C10, eBioscience), and MHC Class II I-A/I-E (Alexa Fluor 700, clone M5/114.15.12, eBioscience). Cells were incubated on ice in the dark for 25 minutes and washed three times prior to resuspension in DAPI (Thermo Fisher Scientific) at a 1:1000 dilution in stain buffer. Samples were run on a Cytex Aurora and analyzed using FlowJo software (v 10.8.1).

For viability studies, cells were assessed using an Annexin V/Propidium Iodide (PI) staining kit (BioLegend). Cells were washed twice in stain buffer and resuspended in Annexin binding buffer. Annexin V and PI were added sequentially according to the manufacturer's instructions, and samples were collected immediately for flow analysis.

### **Cell viability assays**

Cells were added to a flat-bottom 96 well plate in 100 µL of media at 10,000 or 50,000 cells per well. Plain media or media containing soluble factors (iron chloride, TA) were then added to a total volume of 200 µL. Cytotoxicity was assessed at multiple time points using a Cell Counting Kit-8 (CCK8) assay (Dojindo) on a BioTek Neo2 plate reader. To correct for background absorbance effects of the soluble components, identical plates lacking cells were prepared. Measurements from the control plates were subtracted from those of the cell plates prior to analysis.

### **Backpack incubation and imaging studies**

Cellular backpacks composed of PLGA were synthesized as described previously.<sup>121</sup> PLGA tagged with rhodamine (Akina) was incorporated into PLGA 502H (Sigma) for particle tracking.

After microcontact printing, backpacks were washed, counted, and resuspended in complete media. Backpacks were added to cells at a ratio of 6:1 and incubated for 24 hours. At the end of the incubation, cells were stained with CellTracker Green (Thermo Fisher Scientific) for 20 minutes and washed thoroughly before analysis. For image analyses, cells were resuspended in stain buffer and added to a glass-bottom confocal dish (Thermo Fisher Scientific). Cells were imaged on an LSM 900 confocal scanning microscope (Zeiss). To assess backpack internalization and uptake, four fields of view from two distinct biological samples were analyzed for a total of ~300 cells assessed. Backpack association with cells and uptake status were observed and counted manually.

### **Nanoparticle uptake**

For nanoparticle uptake studies, cells were cultured with Fluoresbrite™ YG 500 nm beads (Polysciences) at a final bead concentration of 10 µg/mL for 3 hours. Cells were washed thoroughly in stain buffer to eliminate residual particles and resuspended in DAPI solution at a 1:1000 dilution in stain buffer. Samples were run on a Cytex Aurora and analyzed using FlowJo software (v10.8.1).

### **Network**

### **imaging**

After conducting the coating procedure with Alexa Fluor 647-labeled BSA cargo, cells were resuspended to 0.5 M/mL in phenol red-free complete RPMI. Cells were added to glass-bottom confocal dishes and imaged on an LSM 900 confocal scanning microscope (Zeiss) immediately under standard incubation conditions.

### **Bioactivity assay**

Mature DCs were coated with human IL-15 at multiple protein feed concentrations and cultured under standard conditions. Control IL-15 was cultured under the same conditions in the absence of cells or network components. After 24 hours, cells were centrifuged and the media containing released IL-15 was collected and frozen at -80 °C for further analysis. First, a human IL-15 ELISA (R&D Systems) was conducted to determine the concentration in the media. An IL-15 Bioassay (Promega) using reporter cells was then carried out according to the manufacturer's instructions. Curve fitting was conducted in Graphpad Prism (v9.4.1) to determine the EC<sub>50</sub>.

### **Circular dichroism spectroscopy (CD)**

Protein precursor solutions were prepared as described at a final BSA concentration of 300 µg/mL, and TA was added at multiple concentrations. In this experiment, the 1x condition corresponded to the TA:protein molar ratio associated with the selected condition for cell studies. Samples were incubated at RT for 4 or 24 hours prior to being filtered and buffer exchanged into 10 mM sodium phosphate buffer using 40K MWCO, 0.5 mL Zeba spin columns (Pierce). Samples were run on a Jasco J-815 spectropolarimeter. The CD spectra were collected at 25 °C from 185 to 280 nm using quartz cuvettes (Starna Cells) with a 1 mm path length. The ellipticity of the buffer was subtracted from all measurements. Data were smoothed using a second order smoothing polynomial in Graphpad Prism for plotting.

### **Dynamic light scattering (DLS)**

Protein/TA precursor solutions were prepared as described at a final BSA concentration of 48 µg/mL and TA concentration of 4 µM. Samples were incubated for at least 15 minutes at RT prior to being run on a ZetaSizer Pro (Malvern) with an equilibration time of 120 seconds.

### **Transwell studies**

Prior to network coating, DCs were stained with CellTracker Green and washed thoroughly with PBS. After coating, 100K DCs were seeded in 100 µL of serum-free RPMI 1640 in the upper chamber of a Transwell apparatus (Corning) consisting of 5 µm pores. The lower chamber contained 600 µL of 100 ng/mL recombinant murine CCL19 (Peprotech) in serum-free RPMI. Cells were allowed to migrate for 3 hours under standard incubation conditions. Afterwards, the cells were carefully collected from the bottom chamber, added to stain buffer, and washed once. After carefully aspirating the media, cells were resuspended in stain buffer containing CountBright absolute counting beads (Thermo Fisher Scientific) and the number of cells per well was analyzed using flow cytometry.

### **Statistics**

Statistical analyses were performed using GraphPad Prism (v9.4.1). Details are listed in all figure legends.

### 3. Chapter 3: Controlling Vaccine Kinetics Using Polyphenols for Enhanced Humoral Immunity

Note: Part of this chapter is adapted from a manuscript with the same title that is currently in preparation.

#### 3.1. Abstract

Despite the success of global vaccination campaigns, vaccine access in low-resource settings is an ongoing challenge. Subunit vaccines are a well-established and clinically scalable intervention, yet they have achieved limited success for weak or rapidly-evolving antigens such as those associated with SARS-CoV-2. Delivery strategies that promote gradual release of subunit vaccines from the injection site offer the potential to improve humoral immunity by enhancing lymph node exposure, however, clinical implementation of this strategy is challenging due to poor scalability and high costs. Here, we propose an approach that uses polyphenols as a simple and inexpensive strategy to enhance tissue residence of vaccines and subsequent humoral immunity. We show that tannic acid (TA), a representative polyphenol, mediates supramolecular interactions between vaccine components and tissue at the subcutaneous injection site to promote extended retention of protein antigens for over one week. In addition to enhancing the magnitude and duration of vaccine drainage to the lymph nodes, inclusion of TA improved accumulation of activated, antigen-laden monocyte-derived dendritic cells (moDCs), promoting long-lasting humoral immunity against the receptor-binding domain (RBD) of SARS-CoV-2 and variants of concern. This system, termed TAPER (Tissue-Adhesive Polyphenol-mediated Enhanced Retention) provides various translational advantages including one-pot synthesis, scalability, low cost, and modularity, towards realization of effective and accessible subunit vaccines.

#### 3.2. Introduction

Vaccines are a critical public health tool for protection against infectious diseases, as exemplified by the COVID-19 pandemic.<sup>1-3</sup> However, vaccine access in low-resource settings is an ongoing challenge.<sup>162,163</sup> Subunit vaccines, which consist of a protein antigen and an adjuvant, remain important candidates for global vaccination efforts due to favorable properties including low cost, stability, scalability, and ease of transport.<sup>1,50,164,165</sup> However, subunit vaccines that employ weak and/or rapidly-evolving antigens such as those associated with HIV and SARS-CoV-2 have generally been met with limited success.<sup>61,62</sup> This is a result of multiple contributing factors including poor immunogenicity, ineffective adjuvant selection and dosing regimen, and inefficient transport to the lymph nodes.

The inherent immunogenicity of protein antigens is a major driver governing the immune response. However, the manner of vaccine delivery to the lymph nodes also has a significant impact, as both the magnitude and duration of antigen availability have significant implications for the resulting immune response.<sup>56,63,64</sup> During a natural infection, highly immunogenic pathogens may persist on the order of weeks, and such prolonged exposure plays a major role in the resulting immune response.<sup>66</sup> In contrast, standard subunit vaccine formulations offer little control over kinetics, and are rapidly cleared from the injection site and lymphatics.<sup>65</sup> Extending the duration

of antigen delivery to the lymph nodes offers an opportunity to enhance the magnitude and diversity of the humoral immune response.

Several efforts have been made to develop drug delivery systems that prolong antigen residence at the injection site, which can both facilitate interactions with migratory immune cells and prolong soluble antigen drainage to the lymph nodes. Repeat daily administration and implantable osmotic pumps have demonstrated the positive impact of prolonged antigen exposure, however, the use of these techniques in the clinic is not practical.<sup>67</sup> Biomaterial-based approaches including polymer microparticles, scaffolds, and microneedle patches have improved vaccine efficacy in animal models.<sup>84,85,166–168</sup> While polymeric particles can be tuned to facilitate long-term antigen release over weeks to months, poor antigen stability and unscalable manufacturing processes have limited their translation.<sup>54,169</sup> Scaffolds and hydrogels offer some advantages including tunable cargo loading and release, self-assembly, and formation of an immune-stimulatory niche.<sup>170</sup> In addition, scaffolds including chemokines or cytokines can recruit and reprogram monocytes and dendritic cells, facilitating vaccine uptake and cellular infiltration into lymph nodes.<sup>171,172</sup> However, complex and lengthy fabrication processes and unfavorable material degradation profiles have limited clinical use.<sup>55</sup> To aid vaccination at scale, new technologies must possess scalable manufacturing processes, exhibit minimal batch-to-batch variation, and be cost-effective.<sup>64,77,82,173</sup>

To address this challenge, we hypothesized that simple addition of a supramolecular compound<sup>87</sup> to subunit vaccines could extend vaccine residence at the injection site to enhance humoral immunity. We focused on polyphenols, a class of multidentate molecules with phenolic groups that facilitate both hydrophilic and hydrophobic intermolecular interactions.<sup>88–90</sup> This unique structure endows polyphenols with strong cohesive and adhesive properties and lends them an ability to associate with diverse biomolecules including proteins and nucleic acids.<sup>97–100</sup> In particular, the polyphenol tannic acid (TA) has been shown to facilitate stable interactions between biomolecular cargoes and proteins of the extracellular matrix (ECM).<sup>112,113</sup> Therefore, we hypothesized that incorporation of TA in subunit vaccine formulations could promote transient adsorption of the vaccines to tissue, thereby extending antigen retention to improve vaccine efficacy, in a strategy we refer to as Tissue-Adhesive Polyphenol-mediated Enhanced Retention of Vaccines (TAPER vaccines). TAPER is the first demonstration of the use of polyphenols to increase vaccine residence in tissue and amplify the resulting immune response.

We formulated subunit vaccines with TA as a model polyphenol via simple admixture and demonstrated prolonged subcutaneous retention of two model protein antigens. Our results show that TAPER vaccines enhance accumulation of vaccine components in the lymph nodes and elicit antigen uptake and activation of key immune cells. In particular, we identified monocyte-derived dendritic cells (moDC) as critical mediators of immunity, and characterized the impact of TA on the viability and phenotype of this subset. Finally, we showed that TAPER vaccines containing the adjuvant CpG led to a marked improvement in humoral responses against the receptor-binding domain (RBD) of SARS-CoV-2. These results demonstrate that TAPER vaccines have the potential to positively improve vaccine delivery kinetics and boost antibody responses. Importantly, this system provides multiple various translational advantages

over more complex drug delivery approaches, including one-pot synthesis, scalability, low cost, and modularity.

### **3.3. Results**

#### **3.3.1. TA associates with protein antigens and nucleic acid adjuvants in vitro**

The association of TA with vaccine components, and subsequently with the ECM at the injection site, are central to the design of the TAPER vaccine. Therefore, we assessed interactions of TA with ovalbumin (OVA) as a model antigen or CpG ODN 1826 as a model molecular adjuvant in solution (**Fig. 3-1A**). TA was mixed with OVA or CpG at molar ratios across multiple orders of magnitude, and solution turbidity was assessed by measuring the absorbance at 600 nm (**Fig. 3-1B,C**). Turbidity serves as an indicator of colloidal stability, wherein the complexation of proteins which are otherwise stable in solution leads to increased absorbance.<sup>174</sup> Above a critical TA:OVA or TA:CpG ratio, the turbidity of both OVA and CpG solutions increased, indicating aggregate formation. A higher relative abundance of TA was required to induce aggregation with CpG than that for OVA. Fluorescent imaging of TA complexes confirmed the formation of larger complexes at higher TA ratios (**Fig. 3-1D**). To further validate association, TA was mixed with fluorescent OVA or CpG. Since TA is a potent fluorescence quencher, loss of fluorescent signal was used as an indicator of binding. The signals from Alexa Fluor 647-labeled OVA and FITC-labeled CpG both decreased inversely in proportion to TA:target ratio, indicating binding even in conditions that did not increase the turbidity (**Fig. 3-1E,F**).

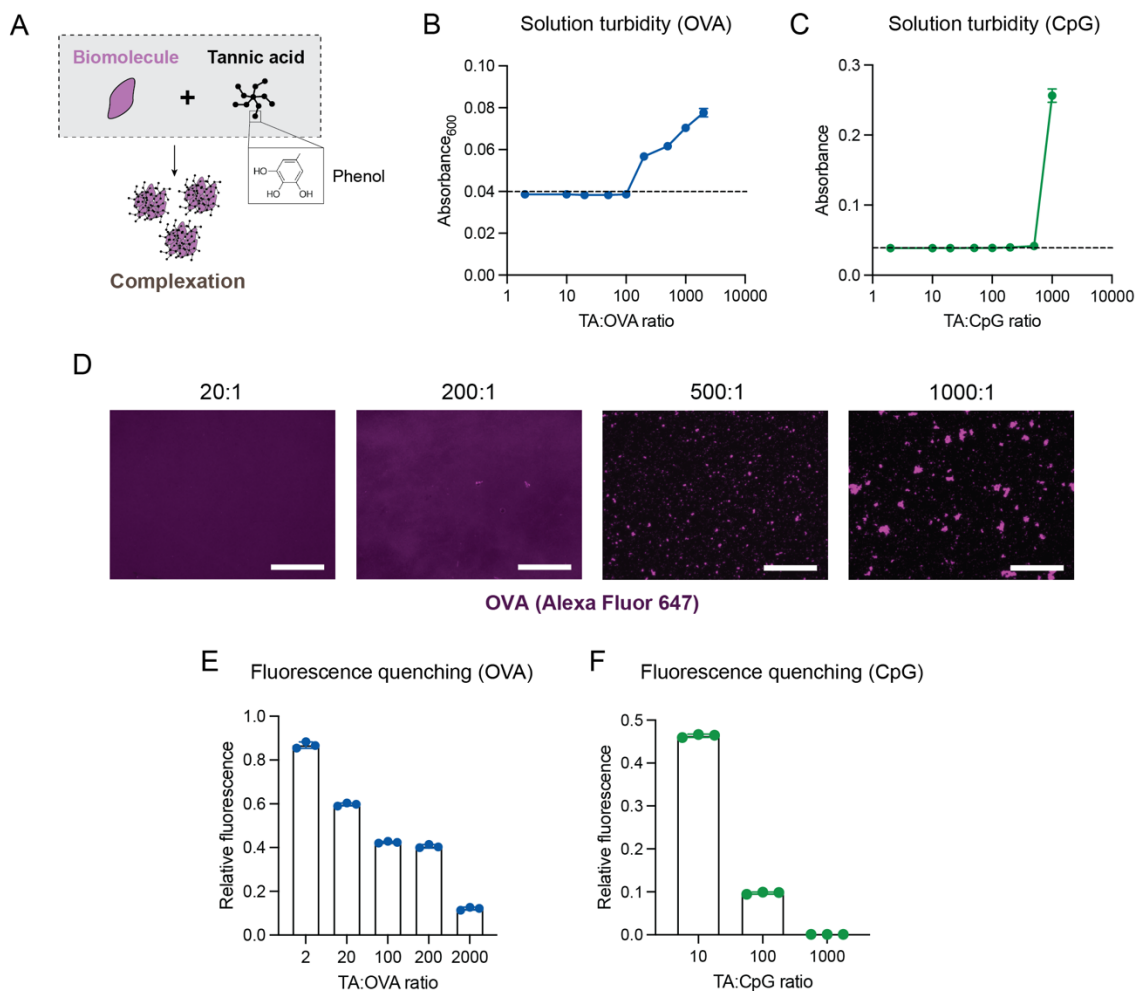


**Fig. 3-1. Complexation of OVA and CpG with TA.**

(A) Schematic of biomolecule association with TA. (B) Absorbance at 600 nm of OVA mixed with various molar ratios of TA at a final OVA concentration of 50 μg/mL. The dashed line indicates the absorbance of free OVA in absence of TA. (C) Absorbance at 600 nm of CpG mixed with various molar ratios of TA at a final CpG concentration of 50 μg/mL. The dashed line indicates the absorbance of free CpG in absence of TA. (D) Representative images of fluorescent OVA mixed with TA at indicated ratios. All scale bars are 150 μm. (E) Fluorescence of Alexa Fluor 647-labeled OVA with different ratios of TA relative to fluorescence in absence of TA. (F) Fluorescence of FITC-labeled CpG with different ratios of TA relative to fluorescence in absence of TA.

Upon confirming complexation of TA with OVA and CpG separately, we investigated TA complexation with a vaccine formulation containing OVA and CpG together (50 μg/mL each) at various TA concentrations (**Fig. 3-2A**). Solution turbidity increased above a TA:OVA ratio of 900:1 (**Fig. 3-2B**). When vaccine components were labeled with fluorescent tags and mixed with TA, the fluorescence of FITC-CpG decreased consistently with increasing TA (**Fig. 3-2C**). However, the signal from Alexa Fluor 647-OVA decreased before increasing at the 5625:1 ratio, potentially indicating preferential association with CpG under this condition.

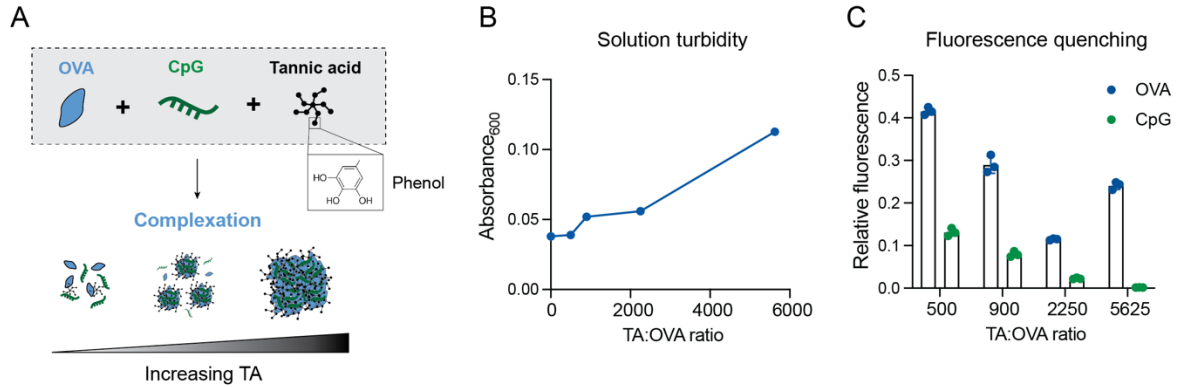


**Fig. 3-2. TA associates with model antigen OVA.**

(A) Schematic of vaccine formulation with OVA and CpG and complex state at equilibrium as a factor of TA concentration. (B) Turbidity of vaccine solutions at different OVA:TA ratios. (C) Fluorescence of OVA (Alexa Fluor 647) and CpG (FITC) relative to that of soluble solution without TA.

Dynamic light scattering (DLS) confirmed that the complex size increased with increasing TA; a ratio of 500:1 yielded ~100 nm complexes, while 5625:1 produced ~4  $\mu\text{m}$  complexes. These conditions were explored further along with two intermediate ratios (900:1, 2250:1) (**Fig. 3-3A**). The polydispersity index of these formulations ranged from ~0.2-0.5 across tested concentrations, and generally decreased with increasing TA (**Fig. 3-3B**). The complexes were observed using fluorescence microscopy and transmission electron microscopy (TEM), which showed that complex size increased with increasing TA (**Fig. 3-3C,D**). These results indicate that TA can associate with both OVA and CpG together in solution to form heterogeneous complexes.

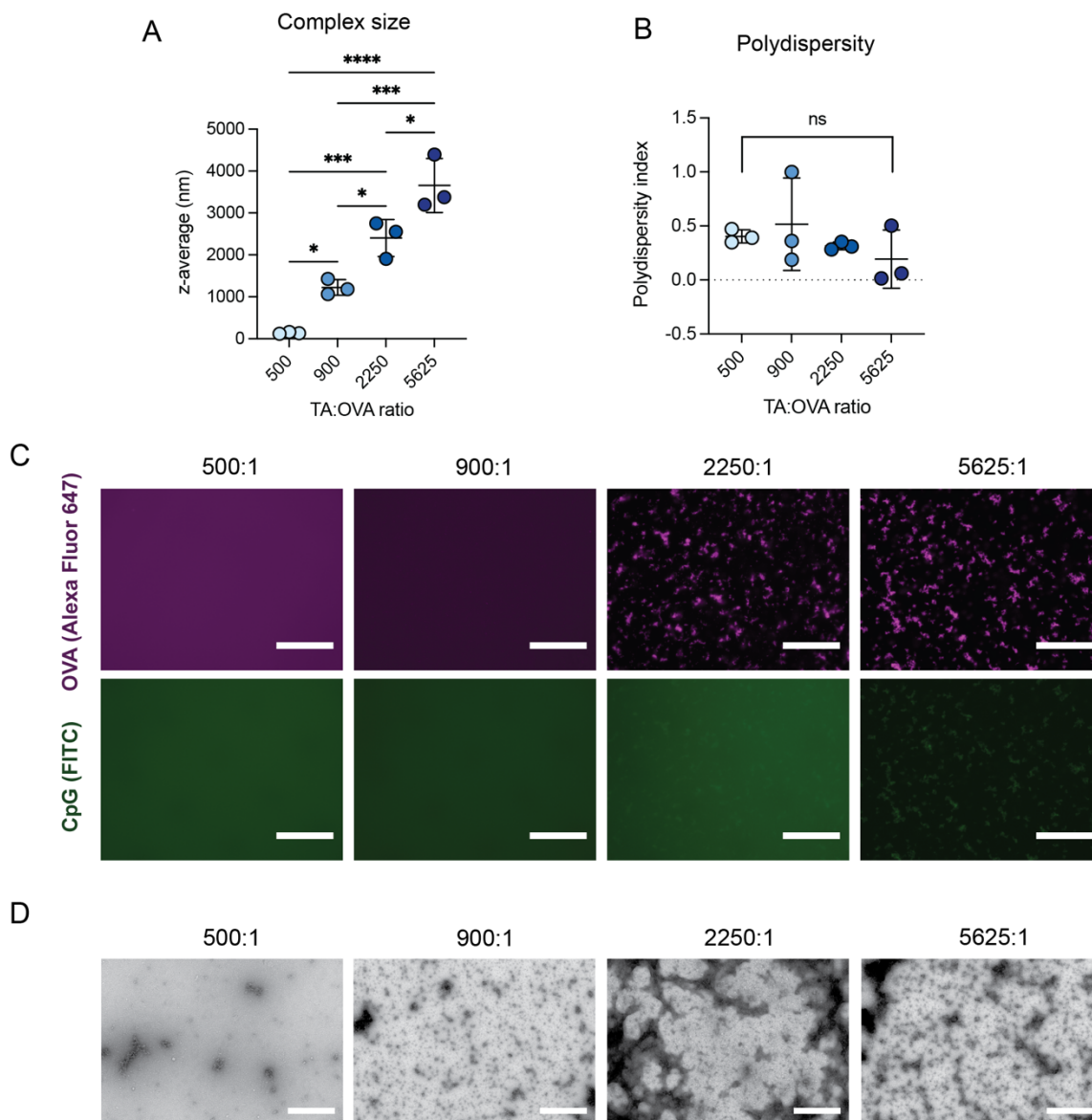


**Fig. 3-3. Complexation of OVA and CpG together with TA.**

(A) Complex size (z-average) and (B) polydispersity index of indicated formulations assessed by DLS. (C) Representative images of Alexa Fluor 647-labeled OVA and FITC-labeled CpG mixed with TA at indicated TA:OVA molar ratios. All scale bars are 150  $\mu$ m. (D) Representative TEM images of OVA and CpG mixed with TA at indicated TA:OVA molar ratios. All scale bars are 500 nm.

### 3.3.2. TAPER vaccines extend antigen retention in vivo at the injection site

Given the ability of TA to associate with the vaccine components in solution, we hypothesized that it could facilitate vaccine retention by associating with tissue at the site of injection. We compared tissue retention of a microscale formulation (900:1 ratio), nanoscale formulation (520:1 ratio), and soluble formulation each consisting of Alexa Fluor 647-labeled OVA and unlabeled CpG (Fig. 3-4A,B). Both TAPER formulations significantly increased the retention of OVA out to 7 days. While only 20% of the antigen in the soluble formulation remained at the injection site after 24 hours, nearly 70% of TA-formulated antigens were retained. The TAPER

formulation state (nanoscale at 520 vs. microscale at 900) did not significantly impact the residence time, suggesting that the presence of a sufficient amount of TA is more important for retention than the nature of complexation in solution.

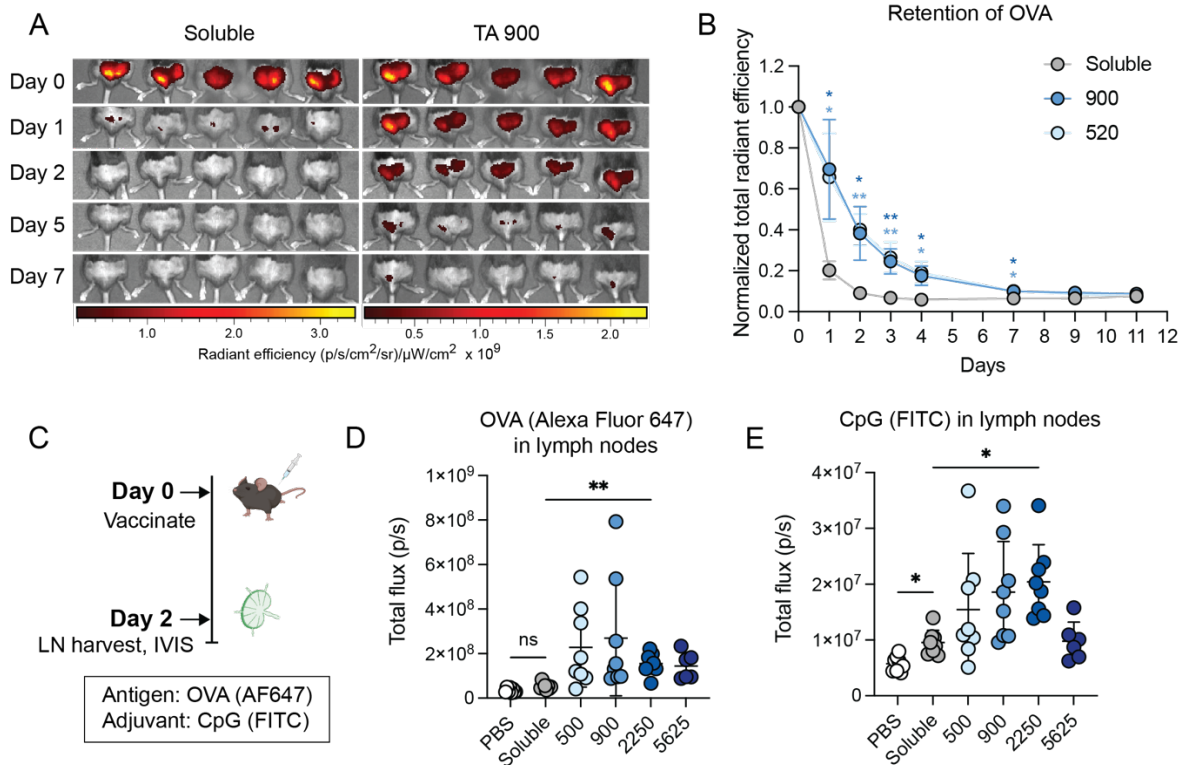


**Fig. 3-4. TA facilitates injection site retention and enhances lymph node accumulation of a model subunit vaccine.**

(A, B) Fluorophore-labeled OVA (Alexa Fluor 647) (10  $\mu$ g) and unlabeled CpG (10  $\mu$ g) were mixed with different ratios of TA and injected subcutaneously at the tail base of C57BL/6J mice ( $n=4$ ). Injection sites were tracked longitudinally by in vivo imaging system (IVIS) imaging. Shown are representative images of the injection site (A) and quantification of total radiant efficiency at the injection site (B), normalized to the signal on Day 0 for each group. \*\* $p<0.01$ , \* $p<0.05$ , as determined by two-way ANOVA followed by Tukey's post-hoc test. Displayed statistics indicate comparison between the group with the labeled color and the soluble group at each indicated time point. (C, D, E) C57BL/6J mice ( $n=4$ ) were immunized subcutaneously at the tail base with fluorophore-labeled OVA (AF647) (10  $\mu$ g) and CpG (FITC) (10  $\mu$ g) with different ratios of TA. After 48 hours, lymph nodes were extracted and arranged for IVIS imaging of fluorescence. (C) Timescale of the experiment. Shown are accumulation of OVA (D) and CpG (E), wherein each point represents a single lymph node. Data in (D, E) were analyzed by one-way ANOVA followed by Tukey's post-hoc test. ns, not significant, \*\* $p<0.01$ , \* $p<0.05$ . Center lines and error bars represent mean and standard deviation, respectively.

### 3.3.3. TAPER vaccines enhance lymph node accumulation of antigen and adjuvant

The gradual release of antigen imparted by retention at the injection site may extend the duration of vaccine exposure in the lymph nodes, which has been shown to enhance the humoral immune response.<sup>63,175</sup> Therefore, we investigated whether TAPER vaccines can improve vaccine delivery to the lymph nodes. Mice were vaccinated with Alexa Fluor 647-OVA and FITC-CpG at various TA ratios and the lymph nodes were extracted and imaged after 48

hours (**Fig. 3-4, Appendix Fig. 10**). While OVA signal from the soluble vaccine did not exceed background levels (PBS control), detectable lymph node accumulation was observed in the TAPER groups across multiple TA concentrations. On average, the OVA signal was increased over the soluble vaccine across all TAPER groups, by 4.3-fold, 5.1-fold, 2.9-fold, and 2.7-fold in the 500, 900, 2250, and 5625 groups, respectively (**Fig. 3-4D**). In an earlier pilot study, a ratio of 280:1 significantly increased accumulation by over 10-fold, suggesting that within the concentration range tested, TA concentration is not predictive of accumulation (**Appendix Fig. 11**). CpG accumulation followed a similar trend but with a lesser magnitude, with respective increases of 1.6-fold, 2.0-fold, and 2.1-fold. Curiously, CpG signal did not increase in the 5625 group (**Fig. 3-4E**). Detection in the 5625 group may have been impeded by fluorescence quenching, given the near-complete loss of CpG fluorescence in this group in vitro. These results indicate that antigen tissue retention imparted by TAPER vaccines may enhance and extend lymph node exposure of both OVA and CpG.

Next, we examined the potential impact of TAPER formulation on antigen structure. We found that association with TA did not adversely impact the structure of OVA. Following incubation for 24 hours at 37 °C to mimic in vivo conditions, robust detection was maintained in the TA groups by ELISA, with a slight reduction at 2 mg/mL TA (TA:OVA ratio ~800:1) (**Fig. 3-5A,B**). The secondary structure of OVA following TA incubation was investigated directly using circular dichroism spectroscopy (**Fig. 3-5C**). The alpha helical structure of the protein was maintained at both investigated TA concentrations, although the magnitude of the signal decreased with increasing TA. Association of TA with OVA was reversible, as assessed by the fluorescence of Alexa Fluor 647-OVA following filtration through a desalting column to remove excess TA. We found that fluorescent signal did not differ from that of a free control, suggesting minimal residual association of TA (**Fig. 3-5D**). These results suggest that structurally intact antigens may be released from the injection site with minimal retention of TA binding.

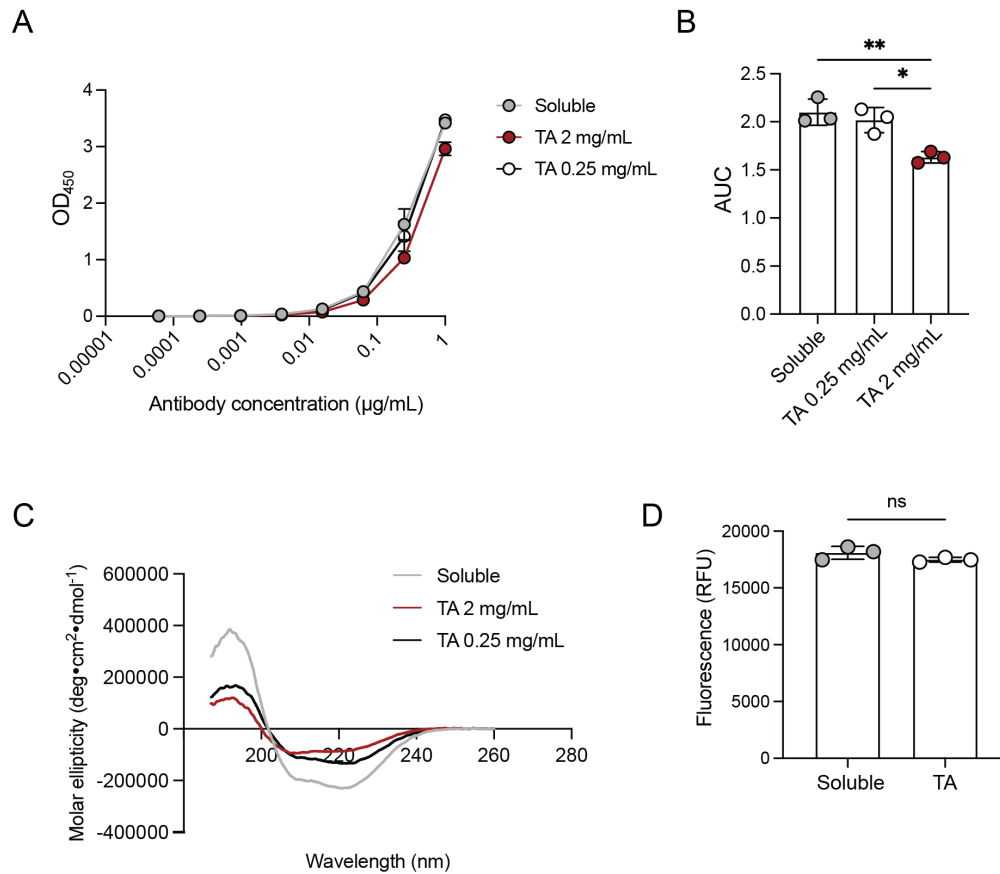


**Fig. 3-5. Key structural features of OVA are maintained upon TA binding.**

In (A) through (C), OVA was incubated alone (soluble condition) or with TA at the indicated concentrations for 24 hours at 37 °C and filtered to remove excess TA. (A) Binding of an HRP-tagged anti-OVA polyclonal antibody at multiple antibody dilutions. (B) Area under the curve (AUC) of the binding curves in (A). Data were analyzed by one-way ANOVA followed by Tukey's post-hoc test. \*\* $p < 0.01$ , \* $p < 0.05$ . (C) Circular dichroism spectra of OVA. (D) Fluorescence of Alexa Fluor 647-labeled OVA post-filtration. Data were analyzed by unpaired two-tailed Student's t test. ns, not significant.

### 3.3.4. TAPER vaccines promote antigen acquisition and activation in multiple cell types in the lymph nodes

Given the improvements in lymph node delivery observed with TAPER vaccines, we investigated how TAPER vaccination alters antigen uptake and activation in key immune cells including B cells, macrophages, and various DC subsets (**Fig. 3-6A**). We vaccinated mice with TAPER vaccines consisting of Alexa Fluor 647-labeled OVA and FITC-labeled CpG and extracted them after 48 hours for flow cytometric analysis. Strikingly, inclusion of TA had a substantial influence on the average frequency of moDC within the overall DC compartment (**Fig. 3-6B**). MoDCs comprised less than 2% of lymph node DCs in control mice, while vaccination with TA increased the frequency to as high as 30% in the TAPER 500 group. The relative abundance of moDC then decreased in inverse proportion to TA concentration, from an average of 21.8% in the TA 500 group to 1.8% in the TA 5625 group. Multiple TA vaccine groups increased the moDC frequency compared to PBS controls, while the soluble vaccine did not.

Activation and antigen uptake of moDCs and other cell types were then examined. CD86 expression on moDC, which is indicative of activation and costimulatory potential, increased up to 1.9-fold compared to the soluble vaccine and 5.8-fold compared to the PBS control (**Fig. 3-6C,D**). Further, the uptake of OVA by moDCs was significantly increased in all TA groups, while uptake in the soluble group did not exceed the baseline (**Fig. 3-6C,E**). While we did not observe detectable OVA accumulation in B cells, inclusion of TA increased CD86 expression on B cells up to 2-fold compared to the soluble vaccine (**Fig. 3-6F**). Conversely, macrophage activation was unaffected by TA, however, OVA accumulation in macrophages was increased up to 1.7-fold compared to the soluble vaccine (**Fig. 3-6G**). Among other DC subsets, resident cDC1 exhibited significant upregulation of CD86 expression in TA groups (**Appendix Fig. 12A**). Compared to the soluble vaccine, cDC2 and migratory cDC1 did not show any changes (**Appendix Fig. 12B,C**). Across all cell types analyzed, no significant changes in CpG uptake were detected as a result of TA (**Appendix Fig. 12D**). Together, these results indicate that TAPER formulations improve antigen accumulation and enhance activation of relevant antigen-presenting cell subsets in the lymph nodes.

### **3.3.5. TAPER vaccination improves humoral immune responses to OVA**

We then studied the effect of TAPER vaccines on the humoral immune response by immunizing C57BL/6J mice with vaccines consisting of OVA and CpG and measuring the antibody response over time. Robust total IgG titers were observed in all vaccine groups (**Fig. 3-6H**). Notably, multiple TAPER formulations induced statistically significant increases in antibody titers compared to the soluble vaccine at different time points (**Fig. 3-6I**). At week 8, TAPER 500, 900, and 2250 vaccination produced titers between 8 and 11-fold greater on average than soluble vaccination. Over 3 months following the last immunization (week 17), titers remained significantly elevated in the 500 and 2250 groups by factors of 6.3 and 4.4, respectively, with a similar trend in the 900 group (**Fig. 3-6J**). TAPER vaccines with a TA:OVA ratio of up to 2250 amplified the humoral immune response, while a further increase to 5625 failed to improve the titer compared to soluble vaccination.

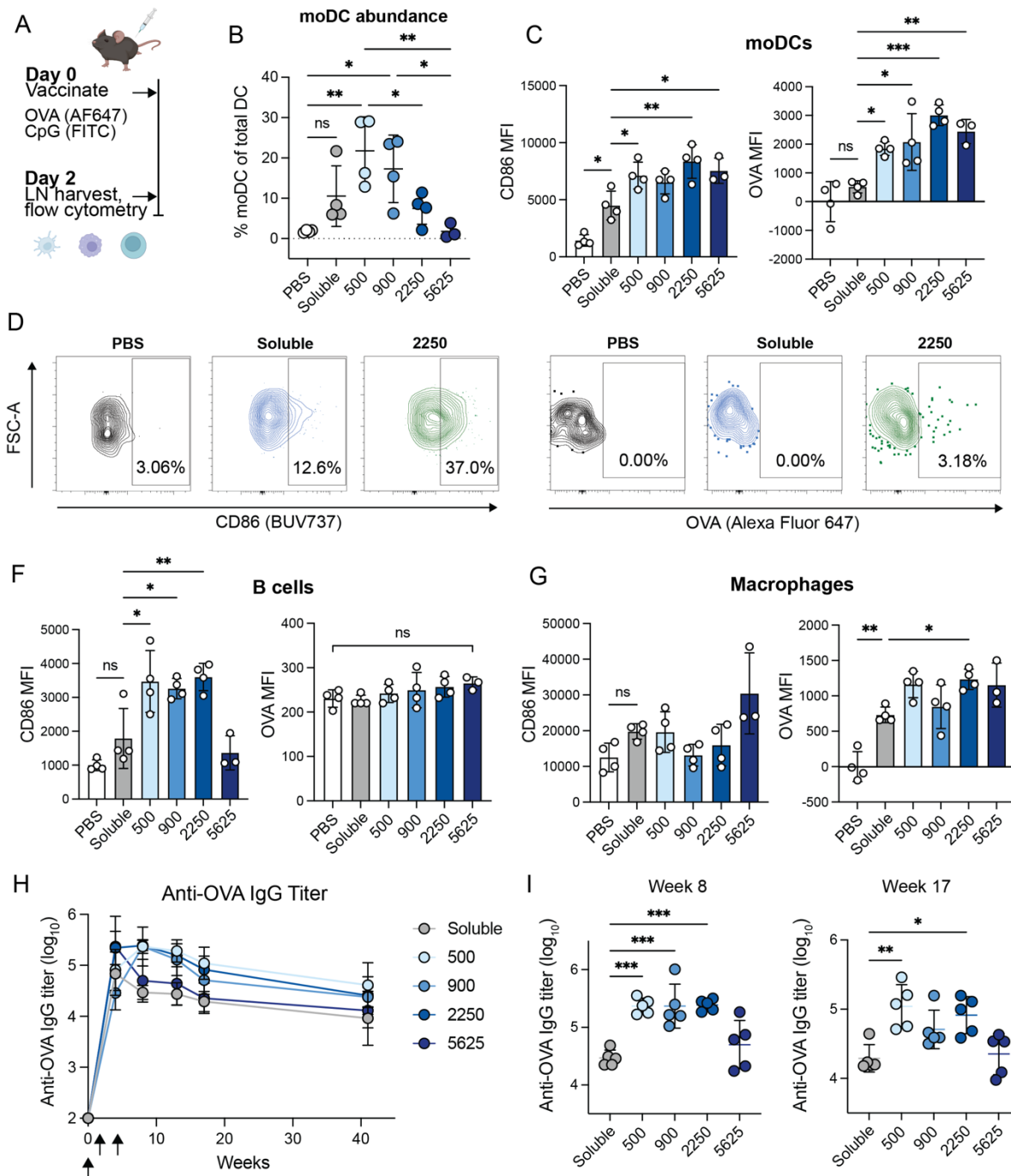


**Fig. 3-6. TA modulates immune cell activation and composition in the LNs.**

(A through G) C57BL/6J mice ( $n=5$ ) were immunized subcutaneously at the tail base with fluorophore-labeled OVA (Alexa Fluor 647) (10  $\mu$ g) and CpG (FITC) (10  $\mu$ g) with different ratios of TA. After 48 hours, lymph nodes were removed and processed into a single-cell suspension for flow cytometry. (A) Timeline of the experiment. (B) Relative frequency of moDCs among all DCs in the lymph node. (C) MFI of CD86 expression and OVA accumulation in moDCs. (D) Representative flow cytometry plots of CD86 expression among moDCs. (E) Representative flow cytometry plots of OVA signal among moDCs. (F) Phenotype of B cells. (G) Phenotype of macrophages. (H, I) C57BL/6J mice ( $n=5$ ) were immunized subcutaneously at the tail base with OVA (10  $\mu$ g) and CpG (10  $\mu$ g) with various ratios of TA. Serum antibody titers were monitored longitudinally. (H) Total anti-OVA IgG titers over time. Arrows denote immunization time points (days 0, 14,

and 28). (I) Total IgG titers at weeks 8 and 17. For C, F, G, and I, data were analyzed by one-way ANOVA followed by Tukey's post-hoc test. ns, not significant, \*\*\* $p < 0.001$ , \*\* $p < 0.01$ , \* $p < 0.05$ . Center lines and error bars represent mean and standard deviation, respectively.

### **3.3.6. TA induces moDC apoptosis and modulates responses to CpG in a concentration-dependent manner**

The lymph node studies showed that the TAPER 5625 group failed to achieve B cell activation beyond that of the soluble vaccine, and the moDC frequency in this group was similar to that of PBS controls. Given that this formulation also failed to improve vaccine immunogenicity, we hypothesized that high concentrations of TA could have a direct effect on the viability or phenotype of moDC infiltrating the injection site, which could shape the subsequent immune response in the lymph nodes. To elucidate the effects of TA on moDCs, we cultured bone marrow-derived DCs (BMDCs) with OVA/CpG complexes at different TA ratios with and without GM-CSF, since this cytokine is required for DC survival, and examined viability. TA exhibited a concentration-dependent effect on both necrosis and apoptosis, although the magnitude of these effects was reduced in part by GM-CSF (**Fig. 3-7A-C**). Lower TA ratios (250 through 900) induced minimal changes. However, increasing the ratio to 2250 substantially increased the frequency of necrotic and apoptotic cells in absence of GM-CSF (**Fig. 3-7B,C**). Equivalent TA alone induced similar effects. These results suggest that the observed alterations in moDC abundance in vivo could be a byproduct of TA-induced cell death at the injection site.

We also assessed IL-6 secretion by BMDCs to understand potential impacts of TA on DC responses to the CpG adjuvant. Treatment with free CpG and OVA produced high levels of IL-6 after 24 hours of incubation. IL-6 secretion was not impacted by TA up to a TA:OVA ratio of 900, but was nearly eliminated in the 2250 group and above, suggesting a suppressive effect of TA on the biological processes underlying the response to CpG (**Fig. 3-7D**). We then conducted a separate experiment in which BMDCs were either incubated with pre-complexed TAPER formulations as before, or equivalent vaccine components and TA added separately to the culture media. Spiking in TA separately induced the same response, suggesting that the observed effects are not a result of complex formation and can be attributed to TA directly (**Appendix Fig. 13A**). TA also showed an inhibitory effect on expression of co-stimulatory markers; relative to the soluble vaccine, the CD86 median fluorescence intensity (MFI) of CD86-expressing cells decreased consistently in response to increasing TA (**Fig. 3-7E**). CD80 expression followed a similar trend (**Appendix Fig. 13B**). Expression of the chemokine receptor CCR7, which facilitates chemotactic cellular migration to the lymph nodes from peripheral tissue, was increased by the free vaccine components, dampened slightly by low-concentration formulations, and unaffected by high-concentration formulations, suggesting that live cells at high TA concentrations do retain an ability to migrate (**Appendix Fig. 13C**).

Altogether, these results suggest that TA concentrations corresponding to the 900:1 ratio and below can promote injection site retention and increase the lymph node frequency of moDCs with minimal effects on cell viability and responses to the CpG adjuvant. Therefore, a range of concentrations below this ratio were selected for further study.

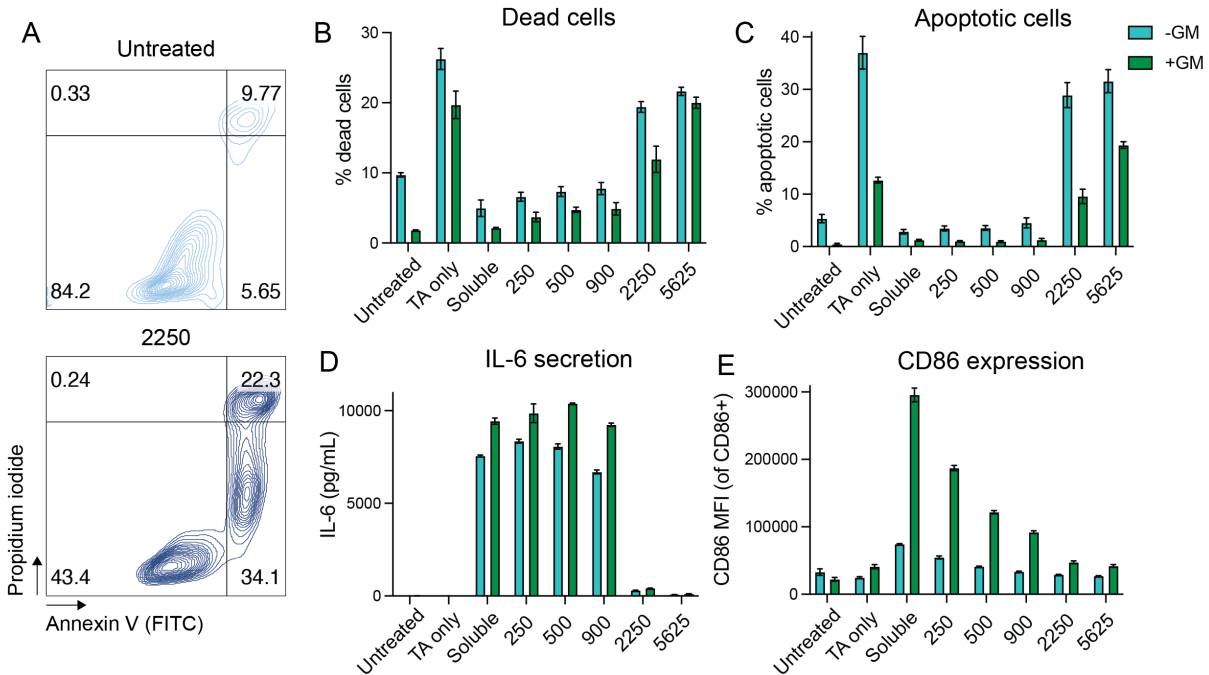


**Fig. 3-7. The presence of TA modifies BMDC viability and phenotype.**

BMDCs were cultured with vaccine formulations at a 1:50 dilution in complete media with or without GM-CSF for 24 hours. (A) Representative flow cytometry plots of cell viability as assessed by Annexin V/propidium iodide (PI) staining. Numbers indicate the percentage of cells in each quadrant. (B) Percentage of dead (necrotic) cells (AV+PI+). (C) Percentage of apoptotic cells (AV+PI-). (D) IL-6 secretion by BMDCs. (E) Median fluorescence intensity (MFI) of CD86 among CD86-positive cells. Center lines and error bars represent mean and standard deviation, respectively. GM, GM-CSF.

### 3.3.7. TAPER vaccination enhances multiple aspects of the humoral immune response to the SARS-CoV-2 RBD antigen

Next, we sought to determine if TAPER vaccination could enhance immune responses to a minimally immunogenic and clinically relevant antigen. We selected the receptor-binding domain (RBD) of SARS-CoV-2 for further study, since it is relatively small (~25 kDa) and a weakly immunogenic antigen both on its own and in combination with alum or CpG.<sup>165,176,177</sup> We formulated TAPER vaccines consisting of 5 µg RBD and 10 µg CpG with a range of TA ratios from 73 to 1176 based on the outcome of the studies with OVA. BALB/cJ mice were vaccinated in a prime-boost regimen on days 0 and 14, and serum antibody titers were monitored over time. The soluble RBD vaccine only transiently increased titers above the background at 2 weeks (**Fig. 3-8A**). However, TAPER 147 demonstrated a 21.6-fold increase in average titer compared to the soluble group at 6 weeks (**Fig. 3-8B**). At TA ratios above 173, the titer trended lower with increasing TA.

To better understand the nature of the immune response, we investigated IgG isotypes IgG1 and IgG2a at early (6 week) and late (15 week) time points. TAPER 147 vaccination significantly elevated the IgG1 titer at 6 weeks by 124-fold on average compared to the soluble group, which exhibited titers close to the baseline. Three out of four mice in the TAPER group maintained robust IgG1 titers out to week 15. While IgG2a was not detected in the soluble group, two mice

in the TAPER group produced a weak yet detectable titer at week 6, one of which was sustained at week 15 (**Fig. 3-8C**). We also quantified the total IgG titer to RBD antigens associated with SARS-CoV-2 variants of concern Beta (B.1.351) and Omicron (B.1.1.529) to determine the breadth of protection. TAPER 147 vaccination induced statistically significant increases in total titers to the Beta variant protein at both time points, including a >9-fold enhancement at week 15, while the soluble vaccine largely failed to increase titers over the baseline (**Fig. 3-8D**). Titers against the Omicron variant exhibited a similar trend, though the differences were not statistically significant.

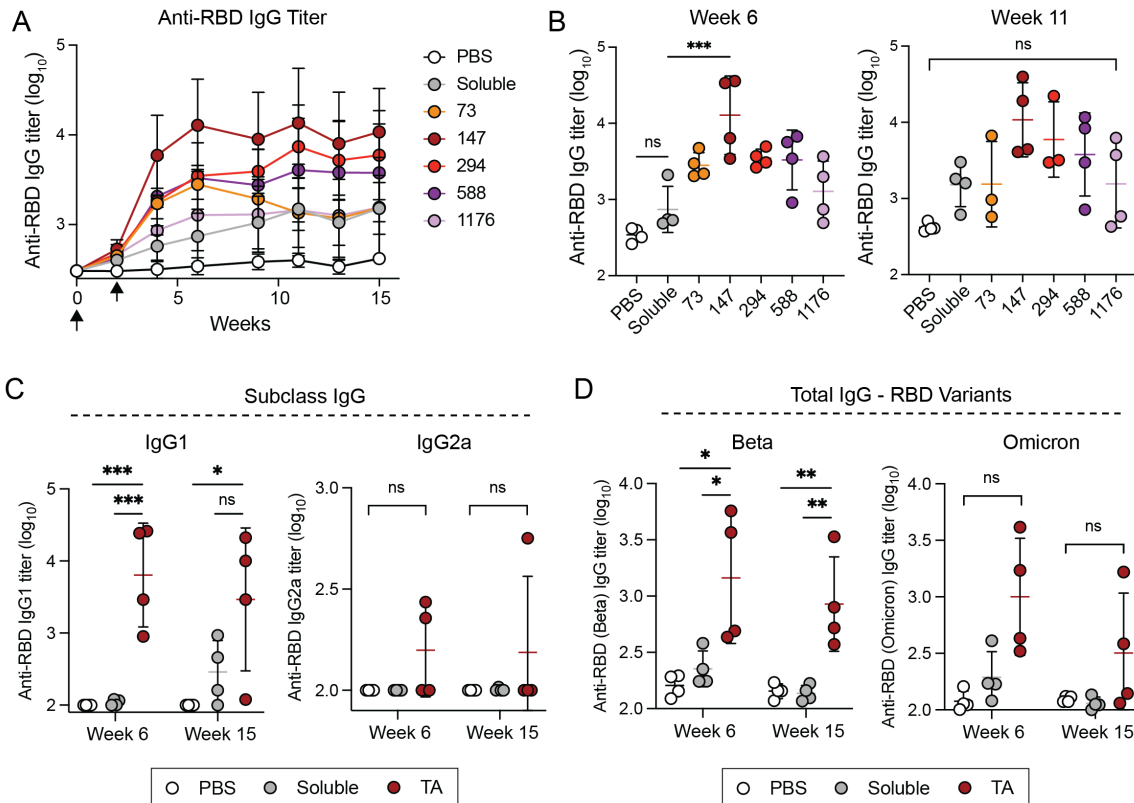


**Fig. 3-8. TA enhances humoral immunity to RBD vaccines.**

BALB/cJ mice ( $n=4$ ) were immunized subcutaneously at the tail base with RBD ( $5 \mu\text{g}$ ) and CpG ( $10 \mu\text{g}$ ) with different concentrations of TA. Group labels indicate the molar ratio of TA to RBD. Serum antibody titers were monitored longitudinally. (A) Total anti-RBD IgG titers over time. Arrows denote immunization time points (days 0 and 14). (B) Total IgG titers at weeks 6 and 11. (C) IgG1 and IgG2a titers to RBD at weeks 6 and 15. (D) Total IgG titers to RBD variants of concern B.1.351 (Beta) and B.1.1.529 (Omicron) at weeks 6 and 15. Data in (B, C) were analyzed by one-way ANOVA followed by Tukey's post-hoc test. ns, not significant, \*\*\* $p<0.01$ , \*\* $p<0.01$ , \* $p<0.05$ . Data for the Beta variant in (D) were analyzed by one-way ANOVA followed by Tukey's post-hoc test. \*\* $p<0.01$ , \* $p<0.05$ . Data for the Omicron variant in (D) were analyzed by Brown-Forsythe ANOVA followed by Dunnett's multiple comparisons test. ns, not significant. Bars with brackets indicate the result of the one-way ANOVA. Bars without brackets indicate the result of multiple comparisons. Center lines and error bars represent mean and standard deviation, respectively.

The ability of the TAPER 147 vaccine to retain the vaccine at the injection site was assessed. RBD was significantly retained at the injection site by TA out to 10 days (**Fig. 3-9A**). After 24 hours, 28.1% of protein remained in the soluble formulation, while 52.5% was retained with the

inclusion of TA, a 1.9-fold improvement. While RBD was retained by TA, the retention profile of CpG was unaltered (**Fig. 3-9B**).

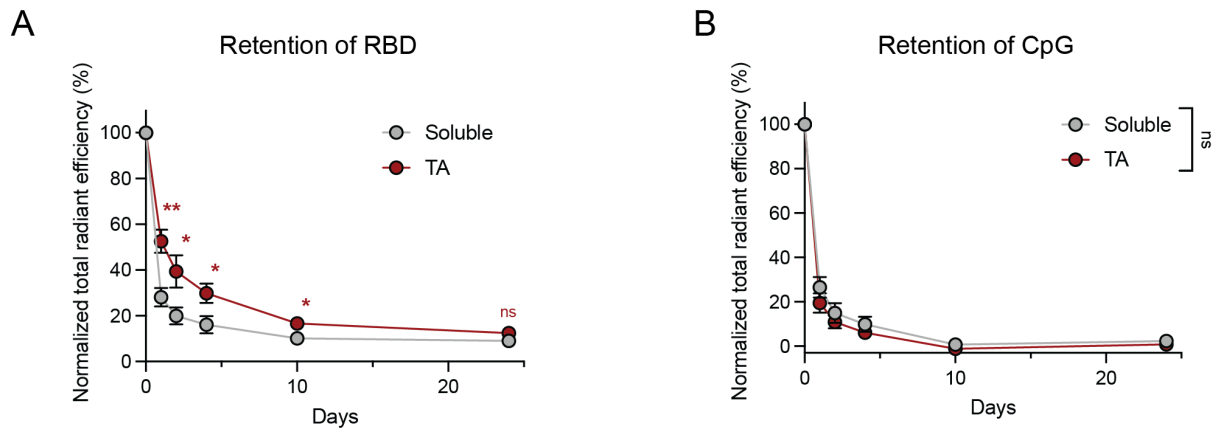


**Fig. 3-9. Retention of RBD and CpG at the injection site.**

BALB/cJ mice ( $n=4$ ) were immunized subcutaneously at the tail base with fluorophore-labeled RBD (Alexa Fluor 647) (10  $\mu$ g) and fluorophore-labeled CpG (FITC) (10  $\mu$ g) either in soluble form or with TA (0.25 mg/mL, 73:1 TA:RBD ratio). Injection sites were tracked longitudinally by in vivo imaging system (IVIS) imaging. Shown are quantification of total radiant efficiency at the injection site for (A) RBD and (B) CpG, normalized to the signal on Day 0 for each group. Data were analyzed by two-way ANOVA followed by Tukey's post-hoc test. ns, not significant,  $**p<0.01$ ,  $*p<0.05$ . Displayed statistics in (A) indicate the comparison between the group with the labeled color and the soluble group at each indicated time point. The displayed statistic in (B) indicates the result of the two-way ANOVA.

Because the improvements in antibody titers could be a byproduct of increased germinal center (GC) activity, we evaluated the GC response to a single TAPER vaccination out to 4 weeks. The absolute number of GC B cells in the soluble RBD + CpG group peaked at 2-3 weeks and declined to nearly half that level by 4 weeks (54%). In contrast, GC B cells in the TA group continued to increase throughout the duration of the study (**Fig. 3-10A-C**). At 4 weeks, the number of GC B cells in the TA group was 3.5-fold greater than in the soluble group on average, though the difference was not significant. T follicular helper ( $T_{FH}$ ) cell counts were slightly elevated in the TA group at weeks 2 through 4 (**Fig. 3-10D,E**). Taken together, TAPER formulation sustained the emerging GC B cell population out to at least 4 weeks, which may underlie the observed improvements in humoral immunity.

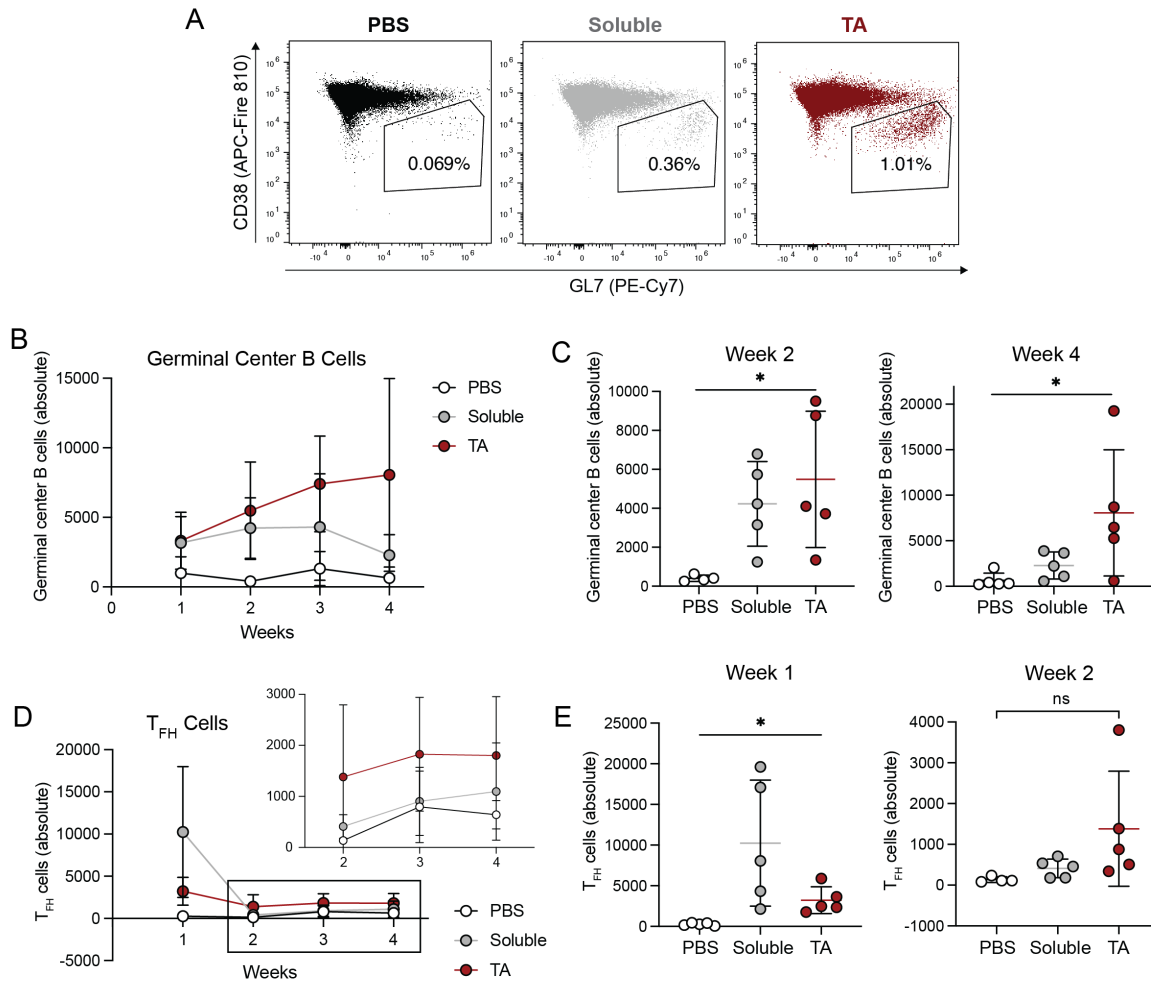


**Fig. 3-10. Retention of RBD modulates kinetics of the germinal center (GC) response.**

BALB/cJ mice ( $n=5$ ) were immunized subcutaneously at the tail base with RBD ( $5 \mu\text{g}$ ) and CpG ( $10 \mu\text{g}$ ) either in soluble form or with TA ( $0.25 \text{ mg/mL}$ ,  $147:1$  TA:RBD ratio). Lymph nodes were extracted at indicated time points and GC and  $T_{FH}$  responses were assessed by flow cytometry. Shown are (A) representative flow cytometry gating of GC B cells, (B) absolute GC B cell counts over time and (C) GC B cell counts at 2 and 4 weeks, (D) absolute  $T_{FH}$  cell counts over time and (E)  $T_{FH}$  cell counts at weeks 1 and 2. Data in (C) were analyzed by one-way ANOVA followed by Tukey's post-hoc test.  $*p<0.05$ . Week 1 data in (E) were analyzed by Brown-Forsythe ANOVA followed by Dunnett's multiple comparisons test.  $*p<0.05$ . Week 2 data in (E) were analyzed by one-way ANOVA followed by Tukey's post-hoc test. ns, not significant. Bars with brackets indicate the result of the ANOVA. Bars without brackets indicate the result of multiple comparisons.

Effective vaccination against SARS-CoV-2 necessitates cooperation between the humoral and cellular arms of the immune system. After confirming the improvements in the magnitude and breadth of the humoral immune response, we sought to understand whether TAPER vaccination could improve RBD-specific T cell responses. Mice were vaccinated with three doses of the indicated vaccines consisting of  $5 \mu\text{g}$  RBD and  $10 \mu\text{g}$  CpG, and IFN $\gamma$ -secreting splenocytes were analyzed two weeks following the last booster (**Fig. 3-11A**). Mice vaccinated with TAPER 147 produced a higher proportion of IFN $\gamma$  spot-forming cells (SFC) than mice in the PBS or soluble vaccine groups. TAPER vaccination resulted in a statistically significant increase in SFC compared to the PBS control, while the soluble vaccine did not (**Fig. 3-11B**). As a preliminary

indicator of safety, the three-dose TAPER regimen did not result in any significant changes to mouse body weight for the duration of the study, suggesting the absence of severe systemic toxicity (**Appendix Fig. 14**).

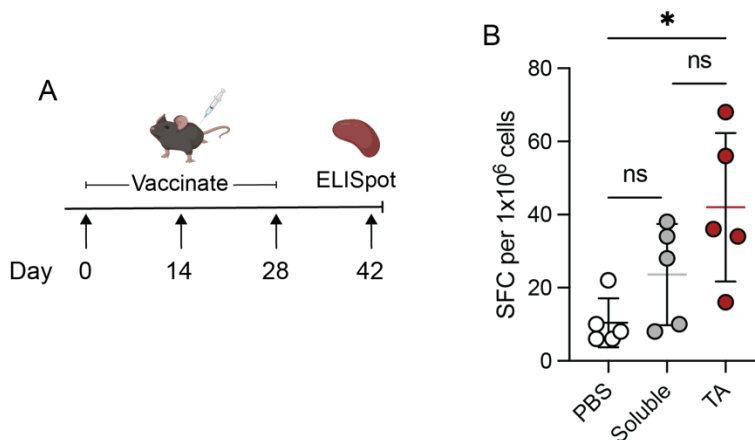


**Fig. 3-11. Impact of TA on cellular immunity.**

C57BL/6J mice ( $n=5$ ) were immunized subcutaneously at the tail base with RBD (5  $\mu\text{g}$ ) and CpG (10  $\mu\text{g}$ ) either in soluble form or with TA (0.25 mg/mL, 147:1 TA:RBD ratio) for a total of three doses according to the scheme shown in (A). (B) Splenocytes were restimulated with an overlapping SARS-CoV-2 spike protein peptide pool and assessed for IFN $\gamma$  production via an ELISpot assay. Shown are the number IFN $\gamma$  spot-forming cells (SFC) per million splenocytes. Data in (B) were analyzed by one-way ANOVA followed by Tukey's post-hoc test. ns, not significant,  $*p<0.05$ . Center lines and error bars represent mean and standard deviation, respectively.

### 3.4. Discussion

Improving the efficacy of subunit vaccines is an important endeavor to broaden global vaccine coverage. One established method to enhance immunity is to prolong retention of the vaccine at the injection site, which promotes gradual drainage to the lymph nodes and enhances interactions with APCs.<sup>75,83</sup> While preclinical technologies including scaffolds and microneedle patches have shown efficacy in animal models, they often have stringent and complex manufacturing processes, are costly, and/or lack modularity. Here, we show that simply incorporating the polyphenol tannic acid (TA) into a subunit vaccine solution facilitates antigen retention at the injection site via supramolecular association. Vaccines containing TA (TAPER vaccines) showed enhanced antigen and adjuvant accumulation in the lymph nodes and improved activation and vaccine uptake by antigen-presenting cells to drive improvements in humoral immunity.

We demonstrated that TA was able to retain both OVA (MW ~45 kDa, pI ~5.2) and RBD (MW ~25 kDa, pI ~9.0) at the subcutaneous injection site. Significant increases in injection site retention compared to the soluble vaccine were observed up to 10 days for OVA and 7 days for RBD. These results show that retention driven by TAPER vaccines is robust and modular, evidenced by its conserved effect on protein antigens with varying molecular weights and net charges at physiologic pH. While protein antigens were retained at the injection site by TA, CpG was not. Given that a very high concentration of TA was required to induce aggregation with CpG *in vitro*, it is possible that intermolecular interactions between TA and CpG are less

favorable than those between TA and RBD. Molecular weight and charge distribution may play a role in stability of TA complexation and subsequent retention. CpG has a low MW (6.1 kDa), which may not offer a sufficient contact area with TA for long-term retention. Because CpG is a single-stranded DNA, it possesses a uniform negative charge that may repel TA, which is also negatively charged at pH 7.4.

The TAPER 147 vaccine against RBD produced significant increases in total IgG titers over time, while the soluble vaccine failed to induce an immune response compared to the PBS control. TAPER 147 formulation increased total IgG titers by over 30-fold and amplified the IgG1 titer over 100-fold on average at 6 weeks. Importantly, the immune response was durable out to at least 15 weeks. TAPER vaccination did not promote robust switching to IgG2a, suggesting that TA serves to amplify the existing humoral response. TAPER vaccines induced humoral responses against the Beta variant of RBD which were also sustained for over 3 months, while the soluble vaccine did not. This result may suggest that TA improves the diversity of epitopes targeted by the antibody repertoire. The differential effects of the various TA formulations in this study indicate that antigen and dose-specific optimization are likely required to achieve maximal efficacy. The experiments with OVA suggest that the size of TAPER complexes at equilibrium does not have a substantial effect on retention, nor on the activation of cells in the lymph node. Therefore, it is more likely that the total amount or concentration of TA governs the response. The *in vitro* experiments suggest that TA itself does not have an adjuvant effect, as it did not activate BMDCs. Therefore, the changes in immunogenicity likely result from a complex interplay of effects arising from antigen retention, including vaccine uptake and lymph node transport by migratory DCs. In conditions with high TA, infiltrating mDCs could be derived from a smaller population of surviving cells that become activated.

Overall, this work shows that incorporation of TA in subunit vaccine formulations promotes subcutaneous site retention of protein antigens to enhance humoral immunity. We demonstrate for the first time the utility of supramolecular, tissue-adsorptive compounds as effective vaccine delivery agents. These findings have multiple implications for further development and translation of subunit vaccines. Current clinical vaccines have limited design considerations for delivery kinetics. While the significance of this factor has been recognized in pre-clinical research, its translation is restricted by design complexity and cost, especially in resource-limited settings. A formulation-based approach to control delivery kinetics has the potential to provide both performance and scalability. In the clinical landscape, the primary consideration for formulation engineering is adjuvant selection, of which alum is a leading example.<sup>52,72</sup> However, studies have shown that alum exhibits limited efficacy with many antigens including RBD, motivating the exploration of adjuvant combinations.<sup>51,73,165,178</sup> Combinations of alum and CpG have shown promising pre-clinical and clinical successes as a vaccination strategy against RBD.<sup>73,165,178–181</sup> In contrast, TAPER provides an additional means of formulation engineering that is based upon improvement of delivery kinetics. TA alone does not function as a molecular adjuvant, but its ability to extend vaccine site residence produces a marked impact on the immune response. The TAPER 147 vaccine enhanced IgG1 titers against RBD by over 100-fold in a low-dose prime/boost regimen comprising 3-5x less CpG than in other reports,

demonstrating that TAPER offers a compelling addition to the repertoire of subunit vaccine formulations.

TAPER vaccines also offer many translational advantages to overcome barriers including scalability and cost. Because TA and other polyphenols are abundant, naturally-occurring compounds, TAPER vaccines are amenable to large-scale production at low cost. In addition, they can be produced rapidly in a “one-pot” synthesis scheme that does not require specialized equipment or purification steps. TA is also generally recognized as safe (GRAS) by the Food and Drug Administration (FDA) for oral administration (Food and Drugs, 21 C.F.R. § 184.1097), which provides a foundation for safety, although further evaluation is needed. Overall, the results presented here show that TAPER approach is a diverse and modular platform for enhancement of subunit vaccine immunogenicity and a potential enabling approach for subunit vaccine delivery.

### **3.5. Materials and Methods**

#### **Materials**

All reagents were purchased and used as received. Ovalbumin (OVA) was purchased from Invivogen (Cat# vac-pova) and RBD (His tag) (Cat# Z03479) and all other variants were purchased from Genscript. CpG was purchased from Invivogen (Cat# tlr-1826). OVA labeled with Alexa Fluor 647 was purchased from Invitrogen (Cat# O34784), and CpG labeled with FITC was purchased from Invivogen (Cat# tlr-1826f). RBD was fluorescently labeled using an Alexa Fluor 647 Microscale Protein Labeling Kit from Invitrogen (Cat# A30009). Tannic acid (TA) was purchased from Sigma Aldrich (Cat #16-201). Cell staining buffer was obtained from Invitrogen (Cat# 00-4222-26). All other reagents were purchased from the suppliers listed.

#### **Animals**

All animal experiments were conducted following federal, state, and local guidelines under approved Institutional Animal Care and Use Committee (IACUC) protocols of the Faculty of Arts and Sciences at Harvard University. Female C57BL/6J and BALB/cJ mice (5 to 10 weeks old) were purchased from the Jackson Laboratory for use in these studies.

#### **Vaccine Preparation**

Mice were immunized with 10 µg of OVA and 10 µg of CpG ODN 1826, or 5 µg of RBD and 10 µg of CpG ODN 1826. Antigen and CpG were mixed together in sterile PBS pH 7.4 (Gibco) at 2x the target vaccine concentration. Solutions of tannic acid (TA) were prepared separately in sterile PBS. Vaccine solution and TA were then combined at a 1:1 volume ratio and the solution was pipetted gently to mix. Soluble vaccine solutions were combined with PBS only. For all studies, samples were incubated for at least 15 minutes at RT prior to injection, and mice were injected bilaterally at the tail base with 100 µL on each side. For experiments involving monitoring of antibody titers, mice were vaccinated with three doses for the OVA vaccine, two weeks apart, and two doses for the RBD vaccine, two weeks apart.

#### **In Vitro Characterization of Vaccine Complexes**

Vaccine solutions containing antigen and adjuvant were prepared in PBS and 50  $\mu$ L was added to a 96 well-plate. In a separate plate, TA was prepared at different concentrations in PBS via serial dilution. TA dilutions were added to the vaccine solution at a 1:1 volume ratio and gently pipetted up and down. Samples were incubated for 15 minutes prior to reading the absorbance at 600 nm. For fluorescence quenching, vaccines were prepared using fluorescent components and added to black-walled plates, and the signals were assessed using a plate reader (FITC ex/em 490/520, Alexa Fluor 647 ex/em 640/670). Signals were normalized to the fluorescence exhibited by complexes without TA. To assess the stability of TA binding to OVA, excess TA was removed using a desalting column (Invitrogen) and the fluorescence was measured. Imaging of fluorescent vaccines was conducted by adding 10  $\mu$ L of vaccine solution to a hemocytometer and visualizing using an EVOS M5000 microscope (Thermo Fisher Scientific). Vaccine complex size was assessed using DLS. Vaccine solution was added to a 40  $\mu$ L cuvette, equilibrated at 25 °C for 120 seconds, and read on a Zetasizer Pro (Malvern Panalytical).

### **Transmission Electron Microscopy (TEM)**

TEM grids consisting of a 200 carbon hex mesh on copper (Electron Microscopy Sciences) were glow discharge cleaned using a PELCO easiGlow™. The grids were then exposed to samples, which were allowed to adsorb for 1 minute. Grids were washed with 5 drops of 2% uranyl acetate and the edges were blotted using Whatman® grade 50 filter paper. Samples were imaged on a Hitachi 7800 TEM at 100 kV accelerating voltage.

### **Imaging of Injection Sites**

Alexa Fluor 647-labeled OVA was purchased from Invitrogen and FITC-labeled CpG was purchased from Invivogen. RBD was labeled using an Alexa Fluor 647 Microscale Labeling Kit (Invitrogen) according to the manufacturer's instructions. Briefly, RBD was incubated with AF647 succinimidyl (NHS) ester at a 10:1 molar ratio at room temperature (RT) for 15 minutes and purified. The degree of labeling was 3.75. For studies with OVA, C57BL/6J mice were vaccinated with 10  $\mu$ g labeled OVA and 10  $\mu$ g unlabeled CpG at indicated TA:OVA ratios. For studies with RBD, BALB/cJ mice were vaccinated with 10  $\mu$ g labeled RBD (2x vaccine concentration) and 10  $\mu$ g labeled CpG. Longitudinal imaging was conducted using IVIS (Perkin Elmer) and the total radiant efficiency at the injection site was computed using Living Image software. For accurate quantification of FITC-CpG, background signals from mice injected with PBS were subtracted from all measurements.

### **Lymph Node Imaging**

C57BL/6J mice were vaccinated with AF647-labeled OVA and FITC-labeled CpG at the indicated TA to OVA ratios. Both inguinal lymph nodes were extracted after 48 hours and arranged on black paper for IVIS imaging of fluorescence. The total flux was calculated using Living Image software.

### **Circular Dichroism Spectroscopy**

OVA was prepared at a final concentration of 0.1 mg/mL (2x in vivo concentration) with TA at the indicated TA concentrations. Complexes were incubated either for 1 hour at RT or 24 hours at 37 °C. Samples were passed through a pre-equilibrated desalting column (Invitrogen, Cat#

87766) to remove excess TA and perform buffer exchange into 10 mM sodium phosphate buffer. The protein concentration of the filtered solution was assessed using a Nanodrop One spectrophotometer (Thermo Scientific). Samples were run on a Jasco J-815 spectropolarimeter. The 25 °C CD spectra were collected from 200 to 290 nm using quartz cuvettes (Starna Cells) with a 1 mm path length. The ellipticity of the buffer was subtracted from all measurements. Data were smoothed for plotting using a second order smoothing polynomial in Graphpad Prism.

### **Structural Analysis via ELISA**

OVA was mixed with TA at the indicated concentration and incubated for 24 hours at 37 °C. Excess TA was filtered using a desalting column, and the samples were diluted in PBS and added to a high-binding 96-well plate at 2 µg/mL for coating overnight at 4 °C. The next day, plates were washed and blocked for 1 hour in reagent diluent. To detect OVA, a polyclonal anti-OVA tagged with HRP was added at 1 µg/mL with 1:4 serial dilutions and incubated for 2 hours. Plates were developed using TMB and read at 450 nm with background correction at 540 nm.

### **Flow Cytometry of Lymph Nodes**

For flow cytometry analysis, both lymph nodes were suspended together in 100 µL serum-free RPMI in a 1.5 mL centrifuge tube and mechanically digested using a handheld homogenizer and pestle. The suspension was added to a pre-wetted 20 µm strainer and rinsed with RPMI, then centrifuged and resuspended in PBS. The cells were washed and then resuspended in LIVE/Dead™ Fixable Blue Stain (Invitrogen) at a 1:1000 dilution in PBS for 30 minutes on ice. Cells were washed again in stain buffer and blocked with anti-CD16/CD32 (Thermo Fisher) for 5-10 minutes on ice. Then, 25 µL of antibody staining cocktail was added for a final volume of 50 µL (antibodies listed in **SI Appendix, Table S1** for lymph node analysis and **SI Appendix, Table S2** for germinal center studies) and cells were stained for 25 minutes on ice. Finally, cells were washed two times and resuspended in 200 µL stain buffer for acquisition on a Cytex Aurora. For the germinal center study, CountBright™ Absolute Counting Beads (Invitrogen) were included to enumerate cells. Data were analyzed using FlowJo software. In some groups, the mean OVA (Alexa Fluor 647) signal was below zero in the PBS group. Therefore, data points in all groups were scaled such that the mean of the PBS group was equal to zero. Gating of relevant cell types is illustrated in **Appendix Fig. 15**.

### **Antibody ELISA (OVA)**

Blood was collected from mice at indicated time points via submandibular blood draw into serum gel tubes (Sarstedt). Serum was separated by centrifugation for 5 minutes at 10,000g and stored at -80 °C until analysis. High-binding Microlon plates (Greiner) were coated with OVA at 10 µg/mL overnight at 4 °C. The following day, plates were washed with 0.05% Tween-20 in PBS and blocked in reagent diluent for 1 hour. Serum was added to the plate at a 1:10 dilution followed by further 1:10 serial dilutions (up to 10<sup>7</sup>) and incubated for 2 hours. Plates were washed and incubated with biotin anti-mouse IgG detection antibody (Biolegend) at a 1:100 dilution. Plates were washed again and incubated with streptavidin-HRP (Biolegend) at a 1:1000 dilution for 20 minutes. Finally, plates were washed and incubated with tetramethylbenzidine (TMB) Reagent A and Reagent B (Biolegend). The reaction was stopped and plates were read

at 450 nm with 540 nm background correction on a Biotek Neo2 plate reader. Titers were defined as the reciprocal serum dilution that produced an OD of 0.5.

### **Bone Marrow Dendritic Cell (BMDC) Culture**

Bone marrow mononuclear cells were isolated by flushing the marrow from the femurs and tibias of C57BL/6J mice. Cells were filtered through a 40 µm strainer and centrifuged at 350 g for 5 minutes, then washed twice with PBS. Next, cells were resuspended in complete RPMI-1640 containing L-glutamine (Gibco) and supplemented with 1% penicillin/streptomycin (Gibco), 2-mercaptoethanol (Gibco), and 20 ng/mL recombinant murine GM-CSF (Peprotech). The cell solution was plated at 10 mL per dish in non-tissue culture-treated dishes (Corning) and cultured at 37 °C in a humidified incubator under 5% CO<sub>2</sub>. Media addition (10 mL) was performed on day 3 of culture. On day 6 and every other day thereafter, a media exchange was performed by isolating 10 mL media from each dish, centrifuging the contents at 250 g for 5 minutes to collect cells, and resuspending in 10 mL fresh media to reconstitute the dish. Cells were used between days 8 and 12 of culture for all experiments.

### **Viability and Phenotype of BMDCs**

Vaccine complexes containing OVA and CpG were prepared at the indicated TA to OVA ratios at the same concentration used for injections in vivo. BMDCs were harvested from the culture dishes via gentle pipetting to collect suspended and loosely adherent cells from the dish. The cells were washed twice in PBS and resuspended in complete BMDC media with or without GM-CSF at a concentration of 1M cells/mL. 100K cells were added to each well of a U-bottom 96-well plate. Vaccine complexes were diluted 1:25 into complete media, and 100 µL was added to the cells for a final dilution of 1:50 (corresponding to a final CpG concentration of 1 µg/mL). For indicated conditions, the vaccine solution and TA were added to the media separately. Cells were incubated for 24 hours at 37 °C.

Cell viability was assessed using a FITC Annexin V Apoptosis Detection Kit with PI (Biolegend Cat# 640914). Cells were washed twice in stain buffer and resuspended in 50 µL Annexin binding buffer. Annexin V and propidium iodide (PI) were added at the manufacturer-indicated concentrations and incubated for 15 minutes in the dark. Then, 200 µL of Annexin binding buffer was added, and the cells were run on a Cytex Aurora. Data were analyzed using FlowJo software.

To assess IL-6 release, cells were centrifuged and the culture media was extracted and frozen at -80 °C for further analysis. The samples were run using an IL-6 ELISA kit (R&D Systems, Cat# DY406). To assess surface marker expression via flow cytometry, cells were washed in stain buffer and stained with LIVE/Dead™ Blue (Invitrogen), then fixed using Fluorofix buffer (Biolegend). The next day, cells were resuspended in 20 µL of Fc block solution on ice for 5-10 minutes. Next, 20 µL of antibody staining cocktail was added for a final volume of 40 µL, and cells were stained for 25 minutes on ice. Cells were stained for CD11c-BV421 (Biolegend), CD86-APC-eFluor 780 (Invitrogen), CD80-BV711 (Biolegend), MHCII-BV605 (Biolegend), and CCR7-PE (Biolegend). Cells were washed twice and resuspended in 200 µL stain buffer for

analysis on a Cytex Aurora. Data were analyzed in FlowJo, and BMDCs were defined as CD11c-positive.

### **Antibody ELISA (RBD)**

Blood was collected from mice at indicated time points via submandibular blood draw into serum gel tubes (Sarstedt). Serum was separated by centrifugation for 5 minutes at 10,000g and stored at -80 °C until analysis. High-binding Costar plates (Corning) were coated with RBD at 1.5 µg/mL overnight at 4 °C. The following day, plates were washed with 0.05% Tween-20 in PBS and blocked in reagent diluent for 1 hour. Serum was added to the plate at a 1:50 dilution followed by a 1:100 and then 1:10 serial dilutions (up to 10<sup>7</sup>) and incubated for 2 hours. Plates were washed and incubated with biotin anti-mouse IgG detection antibody at a 1:100 dilution. Plates were washed again and incubated with streptavidin-HRP at a 1:1000 dilution for 20 minutes. Finally, plates were washed and incubated with TMB (Biolegend). The reaction was stopped (Biolegend stop solution) and plates were read at 450 nm with 540 nm background on a Biotek Neo2 plate reader. Titers were defined as the reciprocal serum dilution that produced an OD of 0.5.

For isotype ELISAs against RBD, serum samples were incubated as previously described. Plates were washed and incubated with either HRP-conjugated goat anti-mouse IgG1 (Invitrogen, Cat# A10551) or HRP-conjugated goat anti-mouse IgG2a (Invitrogen, Cat# M32207) at a 1:2000 dilution for 1 hour. Plates were washed and incubated with TMB, the reaction was stopped, and plates were read at 450 nm with 540 nm background on a Biotek Neo2 plate reader. Due to the lower background exhibited in this assay, titers were defined as the reciprocal serum dilution that produced an OD of 0.1. Samples below the limit of detection were assigned a value of 100.

For ELISAs against RBD variants, high-binding plates were coated with RBD variants beta (B.1.351) (Genscript, Cat# Z03596) or omicron (B.1.1.529) (Genscript, Cat# Z03728) at 1.5 µg/mL overnight at 4C. The assay was then conducted as described above for total IgG.

### **Statistical Analysis**

Data were analyzed and plotted using Graphpad Prism (v9). All statistical methods and sample sizes are indicated in figure captions. All values shown in graphs include the mean plus or minus the standard deviation. Flow cytometry data was analyzed using FlowJo (v10).

## 4. Chapter 4: Conclusions and Outlook

### 4.1. Overview

In this thesis I demonstrate the utility of the polyphenol tannic acid (TA) for engineering of vaccine delivery systems employing supramolecular chemistry for their assembly. In particular, I leverage the capacity of TA to bind proteins with a wide swath of molecular properties to solve distinct clinical challenges faced by cellular vaccines and subunit vaccines.

In Chapter 2, I engineer a cellular hitchhiking system for local delivery of immunomodulatory protein therapeutics to dendritic cells (DCs). I adapt a previous approach employing metal phenolic networks for compatibility with DCs by eliminating the cytotoxic transition metal ion component and scaling the concentration of TA. This system, termed META, preserved DC viability, migration, phagocytosis, and responsiveness to stimuli. I also elucidate the impact of cell maturation on compatibility with META. META enabled loading of various protein drugs including antibodies, cytokines, and growth factors on the order of micrograms. The extent of total release was variable depending on the payload from as low as 10% up to 60%, indicating either stable complexation or cellular uptake of the payload. Importantly, therapeutics loaded in META could directly influence the carrier cell phenotype, including in the presence of oppositional stimuli. To our knowledge, this is the first demonstration of DC hitchhiking, opening the door for new approaches to modulate the phenotype of phagocytic cells.

### 4.2. Future Directions

#### 4.2.1. META Platform

In Chapter 2, we establish META for hitchhiking of protein drugs on the DC membrane. The data presented in this thesis show that TA mediates adhesion of proteins to the cell membrane, and that the payloads can be released into the environment. In addition, the studies with DQ-OVA show that while endolysosomal uptake of proteins networked in META does occur, the rate of uptake is lower than that of cells incubated with soluble protein in absence of TA. Future work focused elucidating the fate of proteins in META in a more granular manner in terms of both location (external, complexed, intracellular) and time would facilitate an improved understanding of the potential restrictions on therapeutic efficacy and optimal contexts for application. For example, the duration of drug availability on the cell surface should be considered in the context of in vivo migration patterns. While cells injected intravenously may reach a target organ or tumor on the order of minutes to hours, cells injected subcutaneously may require more than 24 hours to reach sites of interest including the lymph nodes. While the studies outlined here clearly demonstrate the ability of META payloads to influence cell phenotype, the insights that can be derived in vitro are inherently limited by the close proximity of cells in culture, in which therapeutics released from the cell membrane may act upon neighboring cells. Evaluating the cell phenotype over time in vivo would provide a more complete picture of the specific capacity of META to influence the carrier cell. Although DC vaccines have been most heavily investigated for treatment of cancer, META may hold the most potential as an enabling approach for DC vaccines against autoimmune disease. Phenotypic plasticity of DCs in the context of systemic inflammation has the potential to render such vaccines ineffective or potentially disease-exacerbating. More

research is needed to understand the phenotypic course of injected DCs in autoimmune disease states to more completely understand the efficacy and potential pitfalls of current tolerogenic preconditioning regimens.

#### **4.2.2. TAPER Platform**

In Chapter 3, we introduce TAPER as a modular, facile platform for modulation of subunit vaccine delivery kinetics for enhanced humoral immunity. Here, we demonstrate that incorporation of TA into subunit vaccine formulations containing both OVA and RBD resulted in enhanced subcutaneous site retention for at least one week, and that these changes facilitated improvements in humoral immunity across a range of TA concentrations. The studies with OVA were conducted with final injected TA concentrations as high as 10 mg/mL, and RBD in the range of 0.125 to 2 mg/mL. In the studies with OVA, multiple formulations including the lowest dose of TA resulted in improvements to the antibody titer and other correlates of immunity, even though BMDC viability and adjuvant-responsiveness may have been partially impaired. In the studies with RBD, only the TAPER 147 group, the second lowest of five tested concentrations, produced statistically significant changes in the total IgG response. In the OVA study, the lack of efficacy of the highest concentration was likely related to direct TA-induced effects on moDC activation and migration to the lymph nodes. However, the factors underlying the lack of efficacy of other TA formulations in the RBD study is less clear, given that BMDC functionality is a less poignant concern at these low concentrations. The differences observed here could be RBD-specific, in that a fine balance is required to harness the benefits of site retention while also ensuring eventual detachment from TA to present crucial epitopes for initiation of B cell responses. For a highly immunogenic antigen like OVA, this constraint may be far more flexible, which could explain the efficacy observed across a wide range of TA concentrations. More detailed studies will be required to fully understand the nature of antigen binding to TA *in vivo*, especially upon presentation to B cells.

One major limitation of these studies overall is that while protein antigens were robustly retained at the injection site by TA, the CpG 1826 adjuvant was not. This may be a result of many factors including competition from the antigen, low molecular weight, and net negative charge. Co-delivery of the antigen and adjuvant in subunit vaccine formulations has great potential to improve immunogenicity. Future studies may focus on the identification of compatible adjuvants. Assuming molecular weight as a limiting factor, nanoparticles such as Matrix M or high molecular weight adjuvants such as poly(I:C) may be good choices. Given the compatibility of TAPER with protein antigens, cytokines such as IL-4 and IL-21 may also be good candidates to enhance immunogenicity or tune the bias of the immune response along the Th1-Th2 axis. Finally, though this approach entails greater complexity, conjugation of an adjuvant of choice to serum albumin would provide a more universal way to harness the tissue-adsorptive benefit of TA.

In terms of clinical translation, the approach presented here is well-poised to achieve success. The studies presented here suggest that multiple doses of TAPER vaccines are safe and well-tolerated, as evidenced by retention of mouse body weight and the absence of any serum markers of organ-specific damage. Although TA is GRAS as a food additive, very few clinical trials involving subcutaneous injection of TA have been conducted, and there is little information

available regarding the dosage. The accessibility of TAPER vaccines also hinges on their stability. Additional studies investigating the antigen stability and formulation solubility under different storage conditions are needed to understand this parameter.

### **4.3. Outlook**

This thesis investigates the polyphenol tannic acid as a supramolecular agent to create modular, simple, and scalable systems for vaccine engineering. The ability of TA to meaningfully improve immune outcomes via admixture into a standard vaccine formulation lays a strong foundation for clinical translation. Overall, the work presented here sets the stage for future investigation of formulation-compatible supramolecular materials in vaccine design, from tannic acid to the broader landscape of polyphenols and beyond.

## 5. Chapter 5: References

1. Pollard, A. J. & Bijker, E. M. A guide to vaccinology: from basic principles to new developments. *Nature Reviews Immunology* 2020 21:2 **21**, 83–100 (2020).
2. Watson, O. J. *et al.* Global impact of the first year of COVID-19 vaccination: a mathematical modelling study. *Lancet Infect Dis* **22**, 1293–1302 (2022).
3. Fitzpatrick, M. C., Moghadas, S. M., Pandey, A. & Galvani, A. P. Two Years of US COVID-19 Vaccines Have Prevented Millions of Hospitalizations and Deaths. *To the Point, Commonwealth Fund* <https://www.commonwealthfund.org/blog/2022/two-years-covid-vaccines-prevented-millions-deaths-hospitalizations> (2022).
4. Nabel, G. J. Designing Tomorrow's Vaccines. *New England Journal of Medicine* **368**, 551–560 (2013).
5. Lin, M. J. *et al.* Cancer vaccines: the next immunotherapy frontier. *Nature Cancer* 2022 3:8 **3**, 911–926 (2022).
6. Serra, P. & Santamaria, P. Antigen-specific therapeutic approaches for autoimmunity. *Nature Biotechnology* 2019 37:3 **37**, 238–251 (2019).
7. Janes, M. E., Gottlieb, A. P., Park, K. S., Zhao, Z. & Mitragotri, S. Cancer vaccines in the clinic. *Bioeng Transl Med* **9**, e10588 (2024).
8. Kenison, J. E., Stevens, N. A. & Quintana, F. J. Therapeutic induction of antigen-specific immune tolerance. *Nature Reviews Immunology* 2023 1–20 (2023) doi:10.1038/s41577-023-00970-x.
9. Mellman, I., Coukos, G. & Dranoff, G. Cancer immunotherapy comes of age. *Nature* 2011 480:7378 **480**, 480–489 (2011).
10. van der Burg, S. H. Correlates of immune and clinical activity of novel cancer vaccines. *Seminars in Immunology* vol. 39 119–136 Preprint at <https://doi.org/10.1016/j.smim.2018.04.001> (2018).
11. Fridman, W. H., Pagès, F., Sauts-Fridman, C. & Galon, J. The immune contexture in human tumours: impact on clinical outcome. *Nature Reviews Cancer* 2012 12:4 **12**, 298–306 (2012).
12. Van Der Burg, S. H., Arens, R., Ossendorp, F., Van Hall, T. & Melief, C. J. M. Vaccines for established cancer: overcoming the challenges posed by immune evasion. *Nature Reviews Cancer* 2016 16:4 **16**, 219–233 (2016).
13. McCarthy, E. F. The Toxins of William B. Coley and the Treatment of Bone and Soft-Tissue Sarcomas. *Iowa Orthop J* **26**, 154 (2006).
14. Morales, A., Eiding, D. & Bruce, A. W. Intracavitary Bacillus Calmette Guerin in the treatment of superficial bladder tumors. *Journal of Urology* **116**, 180–182 (1976).
15. Sabado, R. L., Balan, S. & Bhardwaj, N. Dendritic cell-based immunotherapy. *Cell Research* vol. 27 74–95 Preprint at <https://doi.org/10.1038/cr.2016.157> (2017).
16. Saxena, M., Balan, S., Roudko, V. & Bhardwaj, N. Towards superior dendritic-cell vaccines for cancer therapy. *Nature Biomedical Engineering* vol. 2 341–344 Preprint at <https://doi.org/10.1038/s41551-018-0250-x> (2018).
17. Wculek, S. K. *et al.* Dendritic cells in cancer immunology and immunotherapy. *Nature Reviews Immunology* vol. 20 7–24 Preprint at <https://doi.org/10.1038/s41577-019-0210-z> (2020).
18. Timmerman, J. M. & Levy, R. Dendritic cell vaccines for cancer immunotherapy. *Annu Rev Med* **50**, 507–529 (1999).
19. Nazarkina, Z. K., Zajakina, A. & Laktionov, P. P. Maturation and Antigen Loading Protocols Influence Activity of Anticancer Dendritic Cells. *Mol Biol* **52**, 222–231 (2018).

20. Perez, C. R. & De Palma, M. Engineering dendritic cell vaccines to improve cancer immunotherapy. *Nature Communications* vol. 10 Preprint at <https://doi.org/10.1038/s41467-019-13368-y> (2019).
21. Guo, Z. *et al.* Durable complete response to neoantigen-loaded dendritic-cell vaccine following anti-PD-1 therapy in metastatic gastric cancer. *npj Precision Oncology* 2022 **6**:1 **6**, 1–7 (2022).
22. Murphy, T. L. & Murphy, K. M. Dendritic cells in cancer immunology. *Cellular and Molecular Immunology* vol. 19 3–13 Preprint at <https://doi.org/10.1038/s41423-021-00741-5> (2022).
23. Saxena, M. & Bhardwaj, N. Re-Emergence of Dendritic Cell Vaccines for Cancer Treatment. *Trends in Cancer* vol. 4 119–137 Preprint at <https://doi.org/10.1016/j.trecan.2017.12.007> (2018).
24. Wculek, S. K. *et al.* Effective cancer immunotherapy by natural mouse conventional type-1 dendritic cells bearing dead tumor antigen. *J Immunother Cancer* **7**, (2019).
25. Hildner, K. *et al.* Batf3 deficiency reveals a critical role for CD8 $\alpha$ + dendritic cells in cytotoxic T cell immunity. *Science* (1979) **322**, 1097–1100 (2008).
26. Benteyn, D., Heirman, C., Bonehill, A., Thielemans, K. & Breckpot, K. mRNA-based dendritic cell vaccines. *Expert Review of Vaccines* vol. 14 161–176 Preprint at <https://doi.org/10.1586/14760584.2014.957684> (2014).
27. Kirkling, M. E. *et al.* Notch Signaling Facilitates In Vitro Generation of Cross-Presenting Classical Dendritic Cells. *Cell Rep* **23**, 3658-3672.e6 (2018).
28. Alspach, E. *et al.* MHC-II neoantigens shape tumour immunity and response to immunotherapy. *Nature* 2019 **574**:7780 **574**, 696–701 (2019).
29. Arrieta, V. A. *et al.* Immune checkpoint blockade in glioblastoma: from tumor heterogeneity to personalized treatment. *J Clin Invest* **133**, (2023).
30. Ghosh, A., Barba, P. & Perales, M. A. Checkpoint inhibitors in AML: are we there yet? *Br J Haematol* **188**, 159–167 (2020).
31. Bouneaud, C., Kourilsky, P. & Bousso, P. Impact of negative selection on the T cell repertoire reactive to a self-peptide: A large fraction of T cell clones escapes clonal deletion. *Immunity* **13**, 829–840 (2000).
32. Idoyaga, J. *et al.* Specialized role of migratory dendritic cells in peripheral tolerance induction. *J Clin Invest* **123**, 844–854 (2013).
33. Steinman, R. M., Hawiger, D. & Nussenzweig, M. C. Tolerogenic Dendritic Cells\*. <https://doi.org/10.1146/annurev.immunol.21.120601.141040> **21**, 685–711 (2003).
34. Schwartz, R. H. T Cell Anergy\*. <https://doi.org/10.1146/annurev.immunol.21.120601.141110> **21**, 305–334 (2003).
35. Van Brussel, I. *et al.* Tolerogenic dendritic cell vaccines to treat autoimmune diseases: Can the unattainable dream turn into reality? (2014) doi:10.1016/j.autrev.2013.09.008.
36. Bell, G. M. *et al.* Autologous tolerogenic dendritic cells for rheumatoid and inflammatory arthritis. *Ann Rheum Dis* **76**, 227–234 (2017).
37. Benham, H. *et al.* Citrullinated peptide dendritic cell immunotherapy in HLA risk genotype-positive rheumatoid arthritis patients. *Sci Transl Med* **7**, (2015).
38. Zubizarreta, I. *et al.* Immune tolerance in multiple sclerosis and neuromyelitis optica with peptide-loaded tolerogenic dendritic cells in a phase 1b trial. *Proc Natl Acad Sci U S A* **116**, 8463–8470 (2019).
39. Nikolic, T. *et al.* Safety and feasibility of intradermal injection with tolerogenic dendritic cells pulsed with proinsulin peptide—for type 1 diabetes. *Lancet Diabetes Endocrinol* **8**, 470–472 (2020).
40. Nikolic, T. *et al.* Tolerogenic dendritic cells pulsed with islet antigen induce long-term reduction in T-cell autoreactivity in type 1 diabetes patients. *Front Immunol* **13**, 1054968 (2022).

41. Phillips, B. E., Garciafigueroa, Y., Trucco, M. & Giannoukakis, N. Clinical tolerogenic dendritic cells: Exploring therapeutic impact on human autoimmune disease. *Front Immunol* **8**, 306740 (2017).
42. Mansilla, M. J., Hilkens, C. M. U. & Martínez-Cáceres, E. M. Challenges in tolerogenic dendritic cell therapy for autoimmune diseases: the route of administration. *Immunotherapy Advances* **3**, 1–14 (2023).
43. Hazini, A., Fisher, K. & Seymour, L. Deregulation of HLA-I in cancer and its central importance for immunotherapy. *J Immunother Cancer* **9**, e002899 (2021).
44. O'Donnell, J. S., Teng, M. W. L. & Smyth, M. J. Cancer immunoediting and resistance to T cell-based immunotherapy. *Nature Reviews Clinical Oncology* **16**:3 **16**, 151–167 (2018).
45. Sabado, R. L., Balan, S. & Bhardwaj, N. Dendritic cell-based immunotherapy. *Cell Research* vol. 27 74–95 Preprint at <https://doi.org/10.1038/cr.2016.157> (2017).
46. Saxena, M., Balan, S., Roudko, V. & Bhardwaj, N. Towards superior dendritic-cell vaccines for cancer therapy. *Nature Biomedical Engineering* vol. 2 341–344 Preprint at <https://doi.org/10.1038/s41551-018-0250-x> (2018).
47. Wculek, S. K. *et al.* Effective cancer immunotherapy by natural mouse conventional type-1 dendritic cells bearing dead tumor antigen. *J Immunother Cancer* **7**, (2019).
48. Zhou, Y. *et al.* Vaccine efficacy against primary and metastatic cancer with in vitro-generated CD103+ conventional dendritic cells. *J Immunother Cancer* **8**, 474 (2020).
49. Johnson, P., Rosendahl, N. & Radford, K. J. Conventional type 1 dendritic cells (cDC1) as cancer therapeutics: challenges and opportunities. *Expert Opin Biol Ther* **22**, 465–472 (2022).
50. Moyle, P. M. & Toth, I. Modern Subunit Vaccines: Development, Components, and Research Opportunities. *ChemMedChem* **8**, 360–376 (2013).
51. Reed, S. G., Orr, M. T. & Fox, C. B. Key roles of adjuvants in modern vaccines. *Nature Medicine* **19**:12 **19**, 1597–1608 (2013).
52. Pulendran, B., S. Arunachalam, P. & O'Hagan, D. T. Emerging concepts in the science of vaccine adjuvants. *Nature Reviews Drug Discovery* **20**:6 **20**, 454–475 (2021).
53. Abbas, A. K., Lichtman, A. H. & Pillai, S. *Cellular and Molecular Immunology*. (Elsevier, Philadelphia, 2018).
54. Irvine, D. J., Aung, A. & Silva, M. Controlling timing and location in vaccines. *Adv Drug Deliv Rev* **158**, 91–115 (2020).
55. Najibi, A. J. & Mooney, D. J. Cell and tissue engineering in lymph nodes for cancer immunotherapy. *Adv Drug Deliv Rev* **161–162**, 42 (2020).
56. Schudel, A., Francis, D. M. & Thomas, S. N. Material design for lymph node drug delivery. *Nature Reviews Materials* **4**:6 **4**, 415–428 (2019).
57. Gretz, J. E., Norbury, C. C., Anderson, A. O., Proudfoot, A. E. I. & Shaw, S. Lymph-Borne Chemokines and Other Low Molecular Weight Molecules Reach High Endothelial Venules via Specialized Conduits While a Functional Barrier Limits Access to the Lymphocyte Microenvironments in Lymph Node Cortex. *Journal of Experimental Medicine* **192**, 1425–1440 (2000).
58. Mesin, L., Ersching, J. & Victora, G. D. Germinal Center B Cell Dynamics. *Immunity* **45**, 471–482 (2016).
59. Eisen, H. N. Affinity Enhancement of Antibodies: How Low-Affinity Antibodies Produced Early in Immune Responses Are Followed by High-Affinity Antibodies Later and in Memory B-Cell Responses. *Cancer Immunol Res* **2**, 381–392 (2014).
60. Angeletti, D. *et al.* Defining B cell immunodominance to viruses. *Nature Immunology* **18**:4 **18**, 456–463 (2017).
61. Haynes, B. F. *et al.* Progress in HIV-1 vaccine development. *Journal of Allergy and Clinical Immunology* **134**, 3–10 (2014).

62. Cromer, D. *et al.* Neutralising antibody titres as predictors of protection against SARS-CoV-2 variants and the impact of boosting: a meta-analysis. *Lancet Microbe* **3**, e52–e61 (2022).
63. Cirelli, K. M. & Crotty, S. Germinal Center Enhancement by Extended Antigen Availability. *Curr Opin Immunol* **47**, 64 (2017).
64. Moyer, T. J., Zmolek, A. C. & Irvine, D. J. Beyond antigens and adjuvants: formulating future vaccines. *J Clin Invest* **126**, 799–808 (2016).
65. Pape, K. A., Catron, D. M., Itano, A. A. & Jenkins, M. K. The Humoral Immune Response Is Initiated in Lymph Nodes by B Cells that Acquire Soluble Antigen Directly in the Follicles. *Immunity* **26**, 491–502 (2007).
66. Lin, W. H. W., Kouyos, R. D., Adams, R. J., Grenfell, B. T. & Griffin, D. E. Prolonged persistence of measles virus RNA is characteristic of primary infection dynamics. *Proc Natl Acad Sci U S A* **109**, 14989–14994 (2012).
67. Cirelli, K. M. *et al.* Slow Delivery Immunization Enhances HIV Neutralizing Antibody and Germinal Center Responses via Modulation of Immunodominance. *Cell* **177**, 1153–1171.e28 (2019).
68. Hu, J. K. *et al.* Murine Antibody Responses to Cleaved Soluble HIV-1 Envelope Trimers Are Highly Restricted in Specificity. *J Virol* **89**, 10383–10398 (2015).
69. Tam, H. H. *et al.* Sustained antigen availability during germinal center initiation enhances antibody responses to vaccination. *Proc Natl Acad Sci U S A* **113**, E6639–E6648 (2016).
70. O'hagan, D. T., Ott, G. S., De Gregorio, E. & Seubert, A. The mechanism of action of MF59-An innately attractive adjuvant formulation. *Vaccine* **30**, 4341–4348 (2012).
71. Calabro, S. *et al.* Vaccine adjuvants alum and MF59 induce rapid recruitment of neutrophils and monocytes that participate in antigen transport to draining lymph nodes. *Vaccine* **29**, 1812–1823 (2011).
72. HogenEsch, H., O'Hagan, D. T. & Fox, C. B. Optimizing the utilization of aluminum adjuvants in vaccines: you might just get what you want. *npj Vaccines* **2018 3:1** **3**, 1–11 (2018).
73. Rodrigues, K. A. *et al.* Phosphate-mediated coanchoring of RBD immunogens and molecular adjuvants to alum potentiates humoral immunity against SARS-CoV-2. *Sci Adv* **7**, 6538 (2021).
74. Liu, H. *et al.* Structure-based programming of lymph-node targeting in molecular vaccines. *Nature* **2014 507:7493** **507**, 519–522 (2014).
75. Moyer, T. J. *et al.* Engineered immunogen binding to alum adjuvant enhances humoral immunity. *Nat Med* **26**, 430–440 (2020).
76. Chang, J. Y. H. *et al.* Co-Anchoring of Engineered Immunogen and Immunostimulatory Cytokines to Alum Promotes Enhanced-Humoral Immunity. *Adv Ther (Weinh)* **5**, 2100235 (2022).
77. Yousefpour, P., Ni, K. & Irvine, D. J. Targeted modulation of immune cells and tissues using engineered biomaterials. *Nature Reviews Bioengineering* **2023** 1–18 (2023) doi:10.1038/s44222-022-00016-2.
78. Singh, M., Chakrapani, A. & O'Hagan, D. Nanoparticles and microparticles as vaccine-delivery systems. <https://doi.org/10.1586/14760584.6.5.797> **6**, 797–808 (2014).
79. Chaudhary, N., Weissman, D. & Whitehead, K. A. mRNA vaccines for infectious diseases: principles, delivery and clinical translation. *Nature Reviews Drug Discovery* **2021 20:11** **20**, 817–838 (2021).
80. Anselmo, A. C., Mitragotri, | Samir, Mitragotri, S. & Paulson, J. A. Nanoparticles in the clinic: An update post COVID-19 vaccines. *Bioeng Transl Med* **6**, e10246 (2021).
81. Adu-Berchie, K. & Mooney, D. J. Biomaterials as local niches for immunomodulation. *Acc Chem Res* **53**, 1749–1760 (2020).

82. Roth, G. A. *et al.* Designing spatial and temporal control of vaccine responses. *Nature Reviews Materials* 2021 7:3 7, 174–195 (2021).
83. Najibi, A. J. *et al.* Scaffold Vaccines for Generating Robust and Tunable Antibody Responses. *Adv Funct Mater* 32, 2110905 (2022).
84. Dellacherie, M. O. *et al.* Single-Shot Mesoporous Silica Rods Scaffold for Induction of Humoral Responses Against Small Antigens. *Adv Funct Mater* 30, 2002448 (2020).
85. Gale, E. C. *et al.* Hydrogel-Based Slow Release of a Receptor-Binding Domain Subunit Vaccine Elicits Neutralizing Antibody Responses Against SARS-CoV-2. *Advanced Materials* 33, 2104362 (2021).
86. Roth, G. A. *et al.* Injectable hydrogels for sustained codelivery of subunit vaccines enhance humoral immunity. *ACS Cent Sci* 6, 1800–1812 (2020).
87. Webber, M. J., Appel, E. A., Meijer, E. W. & Langer, R. Supramolecular biomaterials. *Nature Materials* 2016 15:1 15, 13–26 (2015).
88. Lu, R. *et al.* Medical Applications Based on Supramolecular Self-Assembled Materials From Tannic Acid. *Front Chem* 8, 871 (2020).
89. Guo, J., Suma, T., Richardson, J. J. & Ejima, H. Modular Assembly of Biomaterials Using Polyphenols as Building Blocks. *ACS Biomater Sci Eng* 5, 5578–5596 (2019).
90. Zhou, J. *et al.* Polyphenol-Mediated Assembly for Particle Engineering. *Acc Chem Res* 53, 1269–1278 (2020).
91. Ejima, H., Richardson, J. J. & Caruso, F. Metal-phenolic networks as a versatile platform to engineer nanomaterials and biointerfaces. *Nano Today* 12, 136–148 (2017).
92. Ejima, H. *et al.* One-step assembly of coordination complexes for versatile film and particle engineering. *Science (1979)* 341, 154–157 (2013).
93. Guo, J. *et al.* Engineering Multifunctional Capsules through the Assembly of Metal–Phenolic Networks. *Angewandte Chemie International Edition* 53, 5546–5551 (2014).
94. Guo, J. *et al.* Modular assembly of superstructures from polyphenol-functionalized building blocks. *Nat Nanotechnol* 11, 1105–1111 (2016).
95. Taha, M. S. *et al.* Sustained Delivery of Carfilzomib by Tannic Acid-Based Nanocapsules Helps Develop Antitumor Immunity. *Nano Lett* 19, 8333–8341 (2019).
96. Chung, J. E. *et al.* Self-assembled micellar nanocomplexes comprising green tea catechin derivatives and protein drugs for cancer therapy. *Nature Nanotechnology* 2014 9:11 9, 907–912 (2014).
97. Fan, H., Wang, J., Zhang, Q. & Jin, Z. Tannic acid-based multifunctional hydrogels with facile adjustable adhesion and cohesion contributed by polyphenol supramolecular chemistry. *ACS Omega* 2, 6668–6676 (2017).
98. Han, Y. *et al.* Polyphenol-based nanoparticles for intracellular protein delivery via competing supramolecular interactions. *ACS Nano* 14, 12972–12981 (2020).
99. Chen, J. *et al.* Programmable Permeability of Metal–Phenolic Network Microcapsules. *Chemistry of Materials* 32, 6975–6982 (2020).
100. Zhao, Z. *et al.* Engineering of Living Cells with Polyphenol-Functionalized Biologically Active Nanocomplexes. *Advanced Materials* 32, 2003492 (2020).
101. Chen, J. *et al.* Metal-Phenolic Coatings as a Platform to Trigger Endosomal Escape of Nanoparticles. *ACS Nano* 13, 11653–11664 (2019).
102. Shukla, A., Fang, J. C., Puranam, S., Jensen, F. R. & Hammond, P. T. Hemostatic Multilayer Coatings. *Advanced Materials* 24, 492–496 (2012).
103. Guo, J. *et al.* Development of tannin-inspired antimicrobial bioadhesives. *Acta Biomater* 72, 35–44 (2018).
104. Zheng, L. Y., Shi, J. M. & Chi, Y. H. Tannic Acid Physically Cross-Linked Responsive Hydrogel. *Macromol Chem Phys* 219, 1800234 (2018).

105. Liu, S. *et al.* Injectable and Self-Healing Hydrogel Based on Chitosan-Tannic Acid and Oxidized Hyaluronic Acid for Wound Healing. *ACS Biomater Sci Eng* **8**, 3754–3764 (2022).
106. Fan, H. *et al.* Supramolecular Hydrogel Formation Based on Tannic Acid. *Macromolecules* **50**, 666–676 (2017).
107. Xu, J., Chen, T. Y., Tai, C. H. & Hsu, S. hui. Bioactive self-healing hydrogel based on tannic acid modified gold nano-crosslinker as an injectable brain implant for treating Parkinson's disease. *Biomater Res* **27**, 1–24 (2023).
108. Guo, J. *et al.* Influence of Ionic Strength on the Deposition of Metal–Phenolic Networks. *Langmuir* **33**, 10616–10622 (2017).
109. Siebert, K. J., Troukhanova, N. V. & Lynn, P. Y. Nature of Polyphenol–Protein Interactions. *J Agric Food Chem* **44**, 80–85 (1996).
110. Levit, S. L., Walker, R. C. & Tang, C. Rapid, Single-Step Protein Encapsulation via Flash NanoPrecipitation. *Polymers (Basel)* **11**, (2019).
111. Honda, Y. *et al.* Sequential Self-Assembly Using Tannic Acid and Phenylboronic Acid-Modified Copolymers for Potential Protein Delivery. *Biomacromolecules* **21**, 3826–3835 (2020).
112. Shin, M. *et al.* Targeting protein and peptide therapeutics to the heart via tannic acid modification. *Nature Biomedical Engineering* **2018 2:5 2**, 304–317 (2018).
113. Velmurugan, P., Singam, E. R. A., Jonnalagadda, R. R. & Subramanian, V. Investigation on interaction of tannic acid with type I collagen and its effect on thermal, enzymatic, and conformational stability for tissue engineering applications. *Biopolymers* **101**, 471–483 (2014).
114. Prakash, S., Kumbhojkar, N., Clegg, J. R. & Mitragotri, S. Cell-bound nanoparticles for tissue targeting and immunotherapy: Engineering of the particle–membrane interface. *Curr Opin Colloid Interface Sci* **52**, 101408 (2021).
115. Adebowale, K. *et al.* Materials for Cell Surface Engineering. *Advanced Materials* **2210059** (2023) doi:10.1002/ADMA.202210059.
116. Liu, Y. *et al.* Cytokine conjugation to enhance T cell therapy. *Proc Natl Acad Sci U S A* **120**, e2213222120 (2023).
117. Jones, D. S. *et al.* Cell surface–tethered IL-12 repolarizes the tumor immune microenvironment to enhance the efficacy of adoptive T cell therapy. *Sci Adv* **8**, 8075 (2022).
118. Stephan, M. T., Moon, J. J., Um, S. H., Bersthteyn, A. & Irvine, D. J. Therapeutic cell engineering with surface-conjugated synthetic nanoparticles. *Nat Med* **16**, 1035–1041 (2010).
119. Wang, L. L.-W. *et al.* Preclinical characterization of macrophage-adhering gadolinium micropatches for MRI contrast after traumatic brain injury in pigs. *Sci Transl Med* **16**, (2024).
120. Kapate, N. *et al.* Backpack-mediated anti-inflammatory macrophage cell therapy for the treatment of traumatic brain injury. *PNAS Nexus* **3**, (2024).
121. Wyatt Shields, C. *et al.* Cellular backpacks for macrophage immunotherapy. *Sci Adv* **6**, eaaz6579 (2020).
122. Prakash, S. *et al.* Polymer Micropatches as Natural Killer Cell Engagers for Tumor Therapy. *ACS Nano* **17**, 15918–15930 (2023).
123. Kapate, N. *et al.* A backpack-based myeloid cell therapy for multiple sclerosis. *Proc Natl Acad Sci U S A* **120**, e2221535120 (2023).
124. Zhao, Z. *et al.* Red Blood Cell Anchoring Enables Targeted Transduction and Re-Administration of AAV-Mediated Gene Therapy. *Advanced Science* **9**, 2201293 (2022).
125. El-Kadiry, A. E. H., Rafei, M. & Shammaa, R. Cell Therapy: Types, Regulation, and Clinical Benefits. *Front Med (Lausanne)* **8**, 2340 (2021).

126. Wang, L. L. *et al.* Cell therapies in the clinic. *Bioeng Transl Med* e10214 (2021) doi:10.1002/btm2.10214.
127. Klichinsky, M. *et al.* Human chimeric antigen receptor macrophages for cancer immunotherapy. *Nat Biotechnol* **38**, 947–953 (2020).
128. Carreno, B. M. *et al.* A dendritic cell vaccine increases the breadth and diversity of melanoma neoantigen-specific T cells. *Science* (1979) **348**, 803–808 (2015).
129. Ahmed, M. S. & Bae, Y. S. Dendritic Cell-based Immunotherapy for Rheumatoid Arthritis: from Bench to Bedside. *Immune Netw* **16**, 44 (2016).
130. Mansilla, M. J. *et al.* Paving the way towards an effective treatment for multiple sclerosis: advances in cell therapy. *Cellular & Molecular Immunology 2021 18:6* **18**, 1353–1374 (2021).
131. Perez, C. R. & de Palma, M. Engineering dendritic cell vaccines to improve cancer immunotherapy. *Nature Communications* vol. 10 1–10 Preprint at <https://doi.org/10.1038/s41467-019-13368-y> (2019).
132. Zhao, W., Zhao, G. & Wang, B. Revisiting GM-CSF as an adjuvant for therapeutic vaccines. *Cell Mol Immunol* **15**, 187–189 (2018).
133. Akkaya, B. *et al.* Regulatory T cells mediate specific suppression by depleting peptide–MHC class II from dendritic cells. *Nat Immunol* **20**, 218–231 (2019).
134. van der Burg, S. H. Correlates of immune and clinical activity of novel cancer vaccines. *Seminars in Immunology* vol. 39 119–136 Preprint at <https://doi.org/10.1016/j.smim.2018.04.001> (2018).
135. Milling, L., Zhang, Y. & Irvine, D. J. Delivering safer immunotherapies for cancer. *Adv Drug Deliv Rev* **114**, 79–101 (2017).
136. Larkin, J. *et al.* Combined Nivolumab and Ipilimumab or Monotherapy in Untreated Melanoma. *New England Journal of Medicine* **373**, 23–34 (2015).
137. Leonard, J. P. *et al.* Effects of Single-Dose Interleukin-12 Exposure on Interleukin-12–Associated Toxicity and Interferon- $\gamma$  Production. *Blood* **90**, 2541–2548 (1997).
138. Anselmo, A. C. & Mitragotri, S. Cell-Mediated Delivery of Nanoparticles: Taking Advantage of Circulatory Cells to Target Nanoparticles. *J Control Release* **0**, 531 (2014).
139. Zhao, Z., Ukidve, A., Kim, J. & Mitragotri, S. Targeting Strategies for Tissue-Specific Drug Delivery. *Cell* **181**, 151–167 (2020).
140. Tang, L. *et al.* Enhancing T cell therapy through TCR-signaling-responsive nanoparticle drug delivery. *Nat Biotechnol* **36**, 707 (2018).
141. Jia, J. *et al.* Interactions Between Nanoparticles and Dendritic Cells: From the Perspective of Cancer Immunotherapy. *Frontiers in Oncology* vol. 8 404 Preprint at <https://doi.org/10.3389/fonc.2018.00404> (2018).
142. Foged, C., Brodin, B., Frokjaer, S. & Sundblad, A. Particle size and surface charge affect particle uptake by human dendritic cells in an in vitro model. *Int J Pharm* **298**, 315–322 (2005).
143. Kumar, S., Anselmo, A. C., Banerjee, A., Zakrewsky, M. & Mitragotri, S. Shape and size-dependent immune response to antigen-carrying nanoparticles. *Journal of Controlled Release* **220**, 141–148 (2015).
144. Moore, K. M. *et al.* Injectable, Ribbon-Like Microconfetti Biopolymer Platform for Vaccine Applications. *ACS Appl Mater Interfaces* **12**, 38950–38961 (2020).
145. Jia, J. *et al.* Interactions Between Nanoparticles and Dendritic Cells: From the Perspective of Cancer Immunotherapy. *Front Oncol* **8**, 404 (2018).
146. Oyewumi, M. O., Kumar, A. & Cui, Z. Nano-microparticles as immune adjuvants: correlating particle sizes and the resultant immune responses. *Expert Rev Vaccines* **9**, 1095 (2010).
147. Sharp, F. A. *et al.* Uptake of particulate vaccine adjuvants by dendritic cells activates the NALP3 inflammasome. *Proc Natl Acad Sci U S A* **106**, 870–875 (2009).

148. Joshi, V. B., Geary, S. M. & Salem, A. K. Biodegradable Particles as Vaccine Delivery Systems: Size Matters. *AAPS J* **15**, 85 (2013).
149. Ma, D. Y. & Clark, E. A. The role of CD40 and CD154/CD40L in dendritic cells. *Seminars in Immunology* vol. 21 265–272 Preprint at <https://doi.org/10.1016/j.smim.2009.05.010> (2009).
150. Li, D. K. & Wang, W. Characteristics and clinical trial results of agonistic anti-CD40 antibodies in the treatment of malignancies (Review). *Oncology Letters* vol. 20 1–1 Preprint at <https://doi.org/10.3892/ol.2020.12037> (2020).
151. Han, Y. *et al.* Polyphenol-Mediated Assembly of Proteins for Engineering Functional Materials. *Angewandte Chemie International Edition* **59**, 15618–15625 (2020).
152. Bergamaschi, C. *et al.* Intracellular interaction of interleukin-15 with its receptor  $\alpha$  during production leads to mutual stabilization and increased bioactivity. *Journal of Biological Chemistry* **283**, 4189–4199 (2008).
153. Agarwal, Y. *et al.* Intratumorally injected alum-tethered cytokines elicit potent and safer local and systemic anticancer immunity. *Nature Biomedical Engineering* **2022 6:2 6**, 129–143 (2022).
154. Gunn, M. D. *et al.* A chemokine expressed in lymphoid high endothelial venules promotes the adhesion and chemotaxis of naive T lymphocytes. *Proc Natl Acad Sci U S A* **95**, 258–263 (1998).
155. Steen, A., Larsen, O., Thiele, S. & Rosenkilde, M. M. Biased and G protein-independent signaling of chemokine receptors. *Front Immunol* **5**, 277 (2014).
156. Serafini, P. *et al.* High-dose granulocyte-macrophage colony-stimulating factor-producing vaccines impair the immune response through the recruitment of myeloid suppressor cells. *Cancer Res* **64**, 6337–6343 (2004).
157. Elmetwali, T. *et al.* CD40L membrane retention enhances the immunostimulatory effects of CD40 ligation. *Sci Rep* **10**, 1–15 (2020).
158. Li, J. *et al.* Ferroptosis: past, present and future. *Cell Death & Disease* **2020 11:2 11**, 1–13 (2020).
159. Crans, D. C. & Kostenkova, K. Open questions on the biological roles of first-row transition metals. *Communications Chemistry* **2020 3:1 3**, 1–4 (2020).
160. Canton, J. Macropinocytosis: New insights into its underappreciated role in innate immune cell surveillance. *Front Immunol* **9**, 407505 (2018).
161. Yoshida, M., Mata, J. & Babensee, J. E. Effect of poly(lactic-co-glycolic acid) contact on maturation of murine bone marrow-derived dendritic cells. *J Biomed Mater Res A* **80A**, 7–12 (2007).
162. Covid World Vaccination Tracker - The New York Times. <https://www.nytimes.com/interactive/2021/world/covid-vaccinations-tracker.html>.
163. Koff, W. C. *et al.* Development and deployment of COVID-19 vaccines for those most vulnerable. *Sci Transl Med* **13**, 1525 (2021).
164. Dalvie, N. C. *et al.* Engineered SARS-CoV-2 receptor binding domain improves manufacturability in yeast and immunogenicity in mice. *Proc Natl Acad Sci U S A* **118**, e2106845118 (2021).
165. Nanishi, E. *et al.* An aluminum hydroxide:CpG adjuvant enhances protection elicited by a SARS-CoV-2 receptor binding domain vaccine in aged mice. *Sci Transl Med* **14**, 5305 (2022).
166. Langelotto, F. *et al.* A Modular Biomaterial Scaffold-Based Vaccine Elicits Durable Adaptive Immunity to Subunit SARS-CoV-2 Antigens. *Adv Healthc Mater* **10**, 2101370 (2021).
167. Kim, E. *et al.* Microneedle array delivered recombinant coronavirus vaccines: Immunogenicity and rapid translational development. *EBioMedicine* **55**, 102743 (2020).

168. Demuth, P. C., Min, Y., Irvine, D. J. & Hammond, P. T. Implantable silk composite microneedles for programmable vaccine release kinetics and enhanced immunogenicity in transcutaneous immunization. *Adv Healthc Mater* **3**, 47 (2014).
169. Bose, R. J. *et al.* Biodegradable polymers for modern vaccine development. *J Ind Eng Chem* **77**, 12 (2019).
170. Lei, L. *et al.* Hydrogel-guided strategies to stimulate an effective immune response for vaccine-based cancer immunotherapy. *Sci Adv* **8**, 8738 (2022).
171. Calmeiro, J. *et al.* Biomaterial-based platforms for in situ dendritic cell programming and their use in antitumor immunotherapy. *J Immunother Cancer* **7**, 238 (2019).
172. Kim, J. *et al.* Injectable, spontaneously assembling, inorganic scaffolds modulate immune cells in vivo and increase vaccine efficacy. *Nature Biotechnology* **2014 33:1** **33**, 64–72 (2014).
173. Singh, M., Chakrapani, A. & O'Hagan, D. Nanoparticles and microparticles as vaccine-delivery systems. <https://doi.org/10.1586/14760584.6.5.797> **6**, 797–808 (2014).
174. Hall, D. *et al.* Protein aggregate turbidity: Simulation of turbidity profiles for mixed-aggregation reactions. *Anal Biochem* **498**, 78–94 (2016).
175. Ding, Y., Li, Z., Jaklenec, A. & Hu, Q. Vaccine delivery systems toward lymph nodes. *Adv Drug Deliv Rev* **179**, 113914 (2021).
176. Dai, L. *et al.* A Universal Design of Betacoronavirus Vaccines against COVID-19, MERS, and SARS. *Cell* **182**, 722-733.e11 (2020).
177. Teplensky, M. H. *et al.* Spherical nucleic acids as an infectious disease vaccine platform. *Proc Natl Acad Sci U S A* **119**, e2119093119 (2022).
178. Pino, M. *et al.* A yeast expressed RBD-based SARS-CoV-2 vaccine formulated with 3M-052-alum adjuvant promotes protective efficacy in non-human primates. *Sci Immunol* **6**, (2021).
179. Brzuska, G. *et al.* The Influence of Adjuvant Type on the Immunogenicity of RBD/N Cocktail Antigens as a Vaccine Candidate against SARS-CoV-2 Virus. *Microbiol Spectr* **11**, (2023).
180. Kuo, T. Y. *et al.* Development of CpG-adjuvanted stable prefusion SARS-CoV-2 spike antigen as a subunit vaccine against COVID-19. *Scientific Reports* **2020 10:1** **10**, 1–10 (2020).
181. Thuluva, S. *et al.* Immunogenicity and safety of Biological E's CORBEVAX™ vaccine compared to COVISHIELD™ (ChAdOx1 nCoV-19) vaccine studied in a phase-3, single blind, multicentre, randomized clinical trial. *Hum Vaccin Immunother* **19**, (2023).

## 6. Chapter 6: Appendix

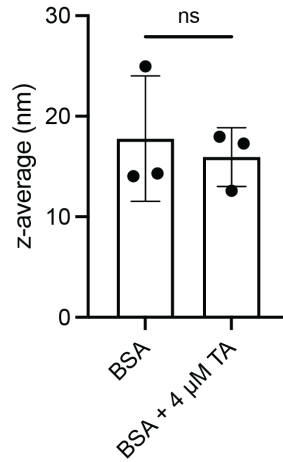
### 6.1. Appendix A: Methods

#### 6.1.1. Cancer vaccine trial analysis

We identified trials on clinicaltrials.gov using the following key words in the “Other terms” category: “cancer vaccine” (automatically searched for “tumor vaccine,” “cancer treatment vaccine,” “antineoplastic vaccine,” and “neoplasm vaccine”), “dendritic cell vaccine” (automatically searched for “antigen presenting cell”), “in situ vaccine,” “monocyte vaccine” (automatically searched for “monocytic”), and “PBMC vaccine” (automatically searched for “peripheral blood mononuclear cells”). In the recruitment status category, we selected trials designated as “not yet recruiting,” “recruiting,” “enrolling by invitation,” and “active/not recruiting.” The data reflect the trial space as of July 2022. From the initial pool of trials, we eliminated irrelevant listings, including: (i) those with indications other than cancer, (ii) those that had been active for 10+ years without release of expected results, and (iii) those that did not fit the definition of a vaccine. For the purpose of this study, cancer vaccines were defined as containing or encoding tumor antigens. The singular exception was *in situ* vaccines, which were searched for explicitly and were required to be designated as such in the trial listing. Vaccines designed to induce a response against non-cancer antigens, such as the influenza vaccine, were excluded unless combined with a tumor-specific vaccine. Prophylactic vaccines were included and analyzed separately from the major subcategories. Vaccines designed to prevent recurrence of cancers in remission were not designated as prophylactic and were included in the general analysis. Nonavalent, previously-approved human papillomavirus (HPV)-targeted vaccines for the prevention of HPV-associated cancers (i.e., Gardasil<sup>®</sup>) were excluded entirely, however, novel prophylactic HPV vaccines were included. Due to inconsistencies in terminology used for clinical reporting, it is unlikely that all cancer vaccine trials were captured in this analysis.

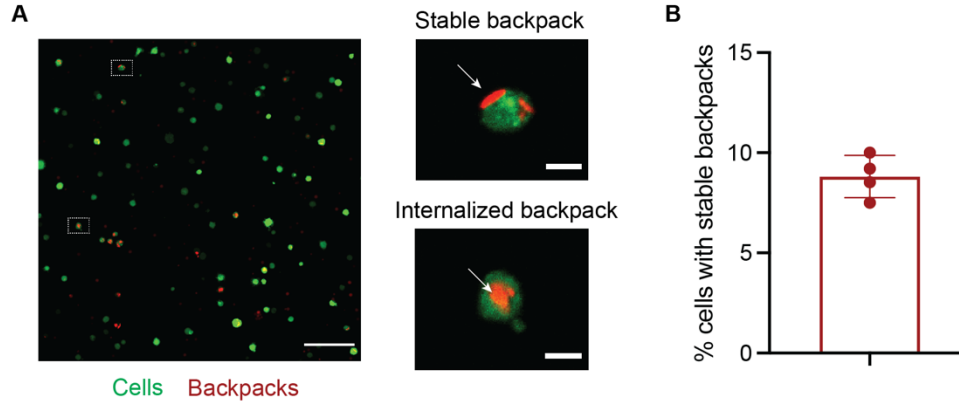
The trials were segmented according to the use of soluble or cellular materials to deliver the antigen(s). The major subcategories among the soluble vaccines include peptides, RNA, DNA, viral and heterologous, and other (**Fig. 1-2**). Because the vast majority of heterologous approaches employed at least one viral element, these categories were grouped together for downstream analysis. These trials are not counted twice in the subsection analyses of other categories such as RNA and DNA, unless explicitly stated. The major subcategories among the cellular vaccines are DC/PBMC, tumor cell, and other. The DC subcategory encompasses DC, PBMC, APC, and monocyte-based vaccines. Because various trials employ more than one intervention, **Fig. 1-2a** is represented as the total number of interventions identified by category.

## 6.2. Appendix B: Figures



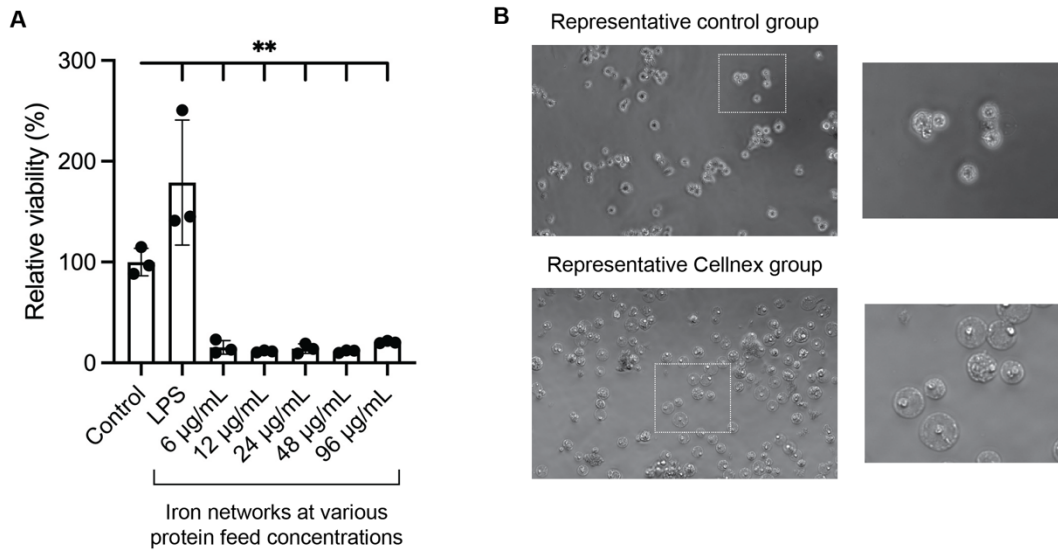
**Appendix Fig. 1. Hydrodynamic diameter of TA/BSA precursor solutions.**

The average diameter of BSA alone and BSA complexed with 4  $\mu$ M TA was assessed via dynamic light scattering (DLS). Data represented as mean  $\pm$  standard deviation. P-values were determined by an unpaired t-test (ns, not significant,  $p > 0.05$ ).

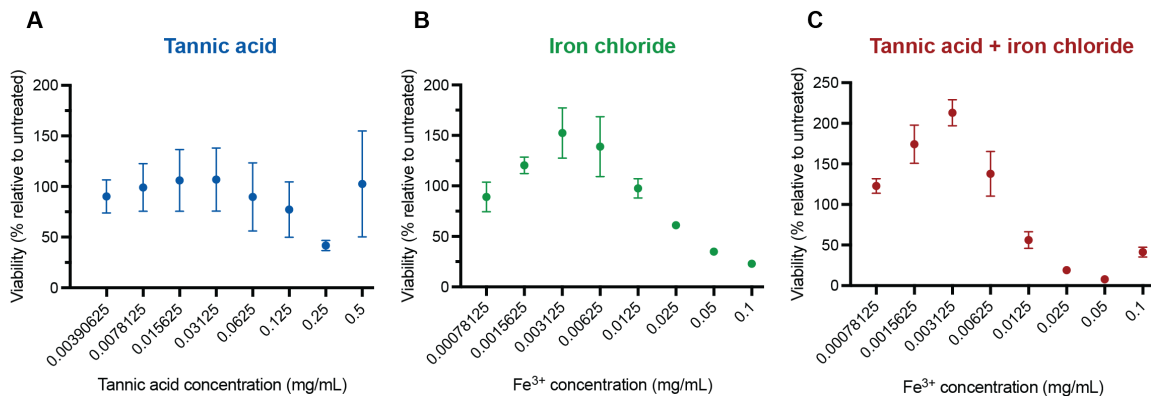


**Appendix Fig. 2. Confocal microscopy of backpack association with mature DCs after 24-hour incubation.**

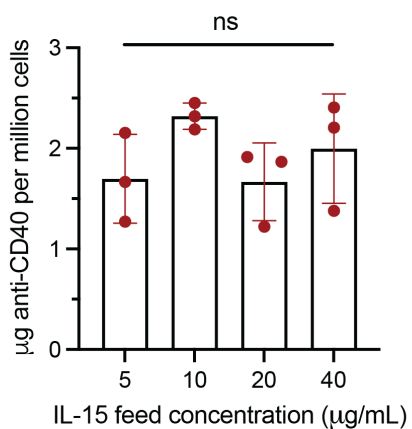
(A) Cells were stained with CellTracker Green and incubated with rhodamine-labeled PLGA backpacks. Scale bar is 100  $\mu$ m (left), 10  $\mu$ m (right). (B) Quantification of stable backpack association with cultured cells from four fields of view across two samples. Data represented as mean  $\pm$  standard deviation.



**Appendix Fig. 3. Effect of iron-containing metal phenolic networks on the viability of immature DCs.** (A) Cells coated with networks containing  $\text{Fe}^{3+}$  at various protein concentrations were cultured for 24 hours, and viability was assessed via a CCK8 metabolic activity assay. Percent viability was normalized to that of the untreated control, such that the control was on average 100% viable. (B) Representative images of untreated cells and network-coated cells. Network-coated cells display signs of ferroptosis, including loss of membrane integrity and ballooning of the cell contents. Data represented as mean  $\pm$  standard deviation. P-values were determined by ordinary one-way ANOVA followed by Tukey's multiple comparison test (\*\* $p < 0.001$ ).

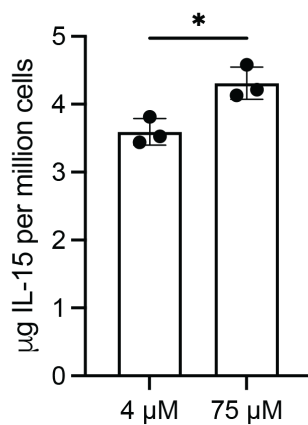


**Appendix Fig. 4. Effects of soluble network components on viability of immature DCs.** Cells were incubated with indicated concentrations of (A) TA, (B) Iron chloride, and (C) TA and iron chloride combined for 24 hours. Viability was assessed via a CCK8 metabolic activity assay. Percent viability was normalized to that of the untreated control, such that the control was on average 100% viable. In (C), both TA and  $\text{Fe}^{3+}$  were scaled together by a factor of 2, such that the rightmost condition contained 0.5 mg/mL TA. Data represented as mean  $\pm$  standard deviation.



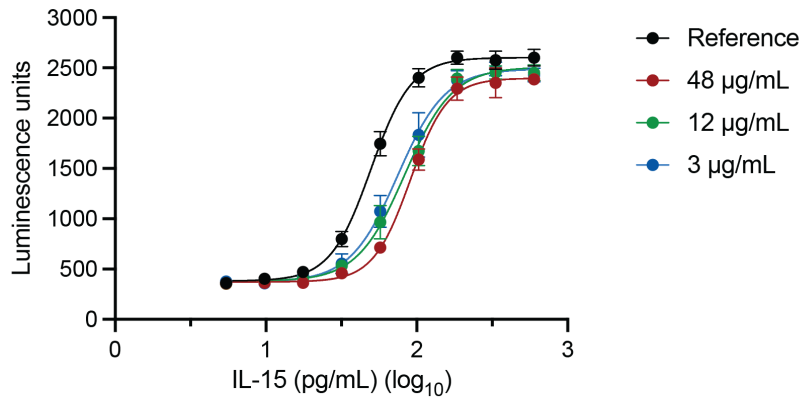
**Appendix Fig. 5. Loading of anti-CD40 in a combinatorial network with IL-15.**

The anti-CD40 protein feed concentration was maintained at 96 µg/mL, and IL-15 feed concentration was varied as indicated. Data represented as mean ± standard deviation. P-values were determined by ordinary one-way ANOVA (ns, not significant,  $p > 0.05$ ).



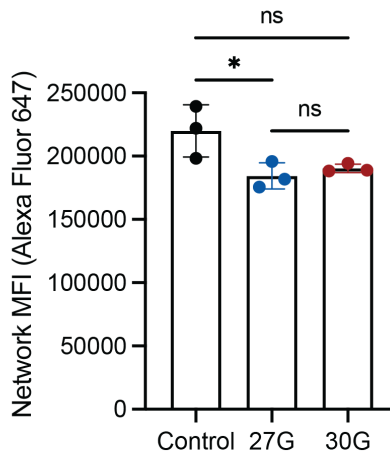
**Appendix Fig. 6. Loading of IL-15 in networks at different TA concentrations.**

Data represented as mean ± standard deviation. P-values were determined by an unpaired t-test ( $*p > 0.05$ ).



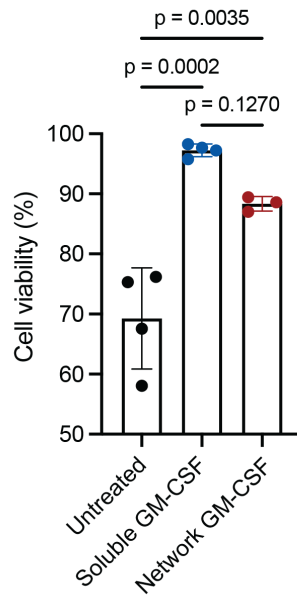
**Appendix Fig. 7. Activity curves of networked human IL-15.**

IL-15 released from networks was quantified and cultured with reporter cells, and activity was measured at the indicated, log-transformed concentrations using a bioluminescent reporter assay. “Reference” indicates soluble IL-15 incubated without TA. Curve fitting was conducted using GraphPad Prism.



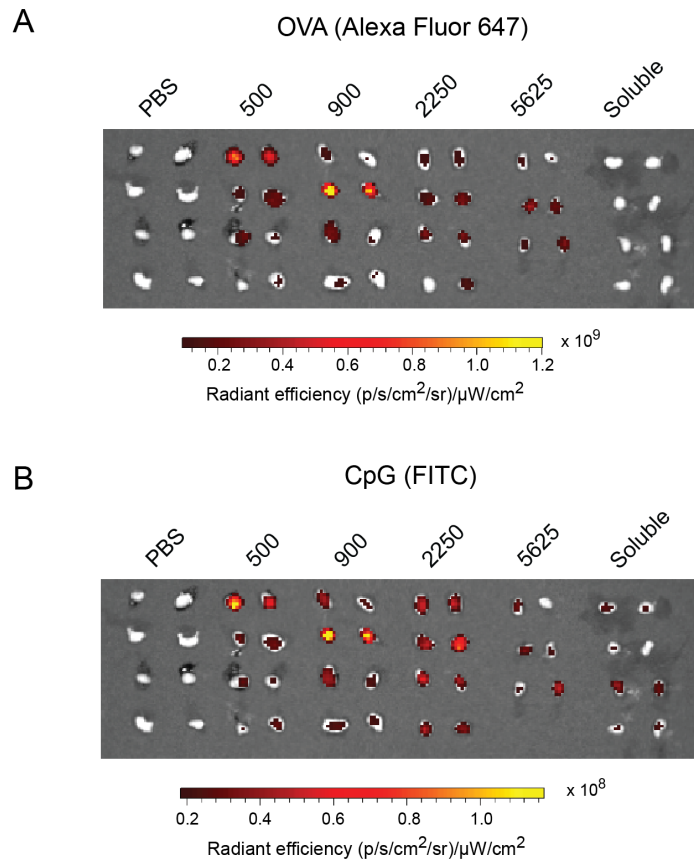
**Appendix Fig. 8. Network stability after application of shear stresses associated with injection.**

Cells were coated with Alexa Fluor 647-labeled BSA and pushed through 27G or 30G needles to simulate injection. Coating fluorescence was quantified using flow cytometry. Data represented as mean  $\pm$  standard deviation. P-values were determined by ordinary one-way ANOVA followed by Tukey’s multiple comparison test (\* $p < 0.05$ ; ns, not significant).

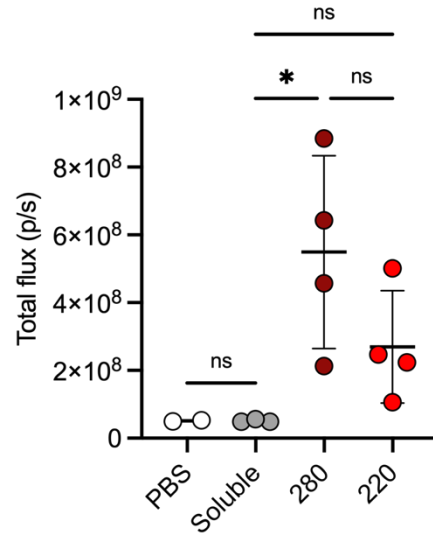


**Appendix Fig. 9. Viability of immature DCs with networks containing GM-CSF.**

Cells were coated with 10% GM-CSF and 90% BSA at a 48  $\mu\text{g}/\text{mL}$  total protein concentration and viability was compared to uncoated cells and uncoated cells cultured with soluble GM-CSF after 24 hours. Viability was assessed via DAPI staining using flow cytometry. P-values were determined by ordinary one-way ANOVA followed by Tukey's multiple comparison test (exact p-values are indicated).

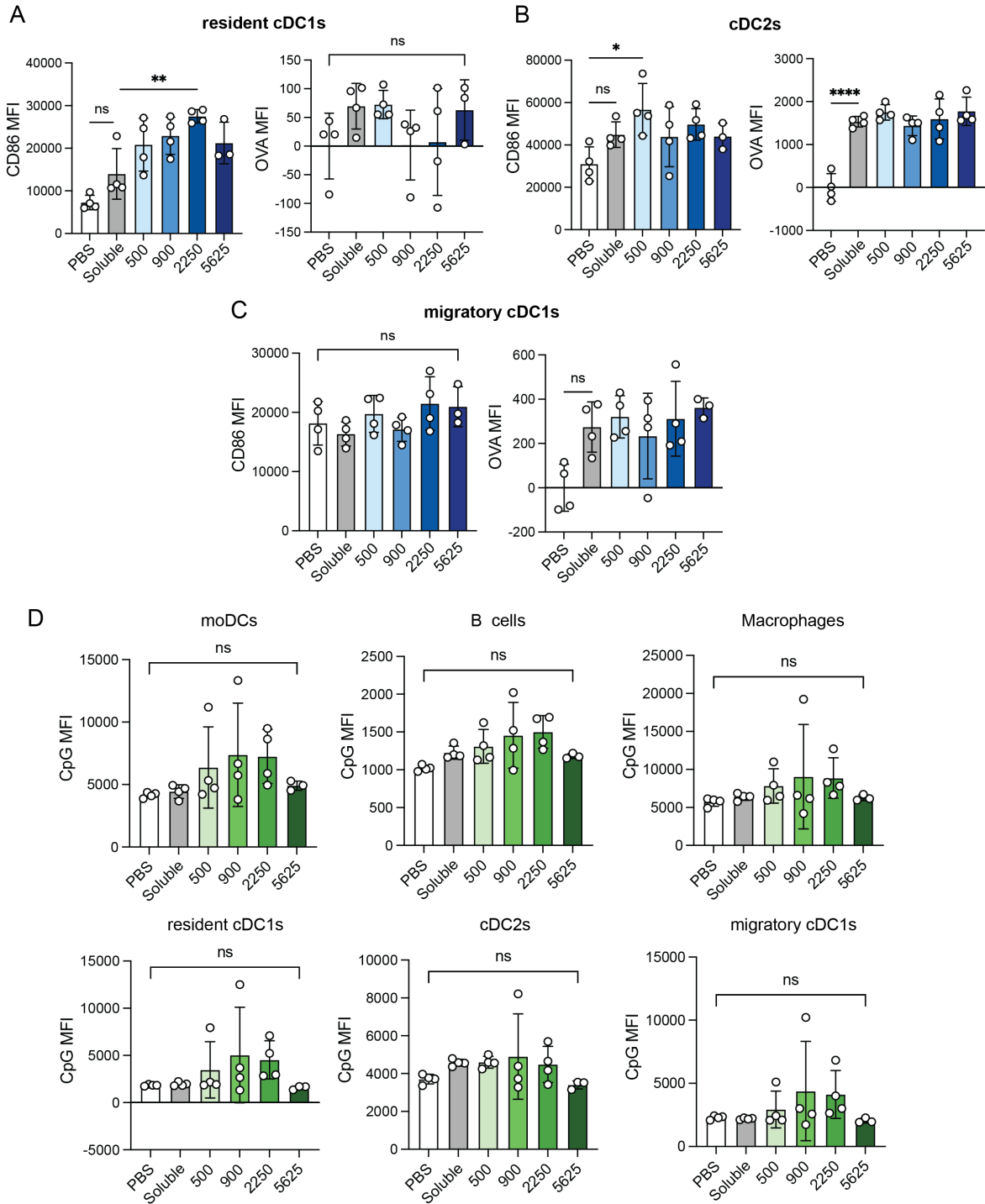


**Appendix Fig. 10. In vivo imaging system (IVIS) images of fluorescent vaccine components in the lymph nodes 48 hours after vaccination.**  
 (A) Alexa Fluor 647-labeled OVA, and (B) FITC-labeled CpG.



**Appendix Fig. 11. Lymph node accumulation of OVA at low TA ratios.**

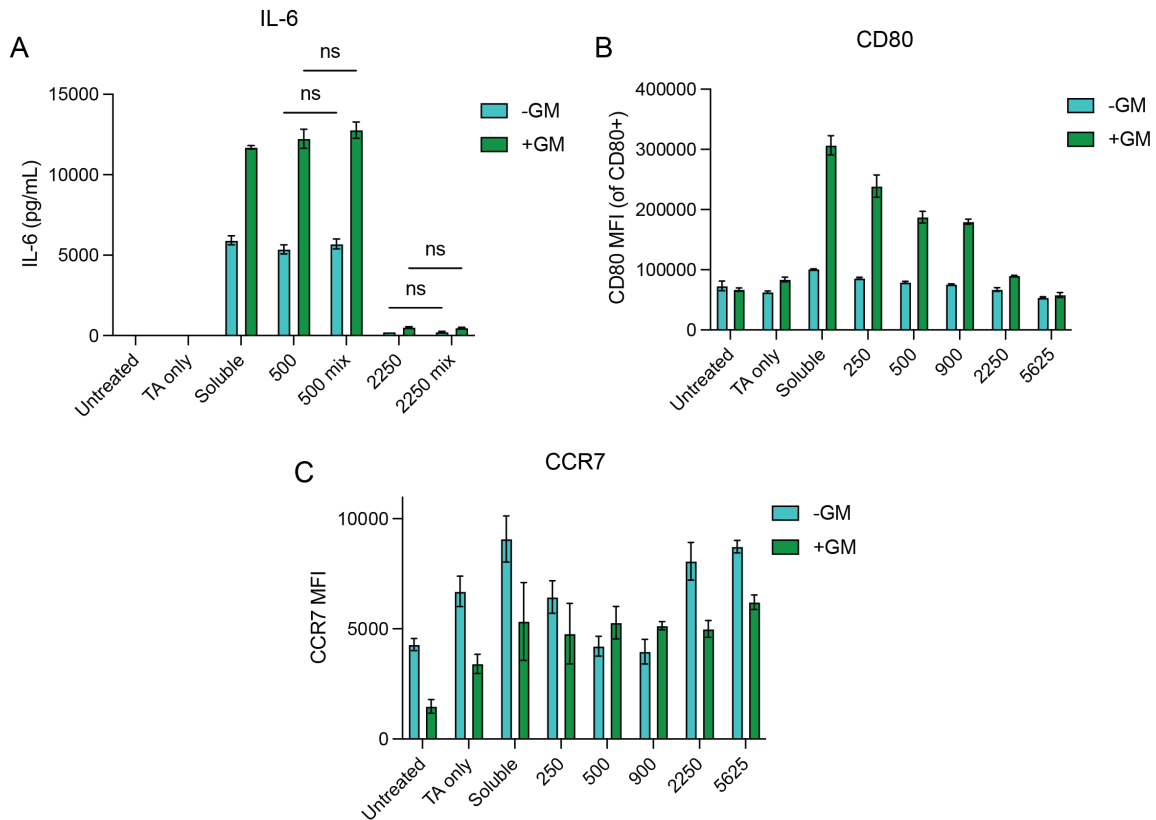
C57BL/6J mice (n=4) were immunized subcutaneously at the tail base with fluorophore-labeled OVA (AF647) (10  $\mu$ g) and indicated ratios of TA (280, 220). After 48 hours, lymph nodes were extracted and arranged for IVIS imaging of fluorescence. Each data point represents a single lymph node.



**Appendix Fig. 12. Vaccine accumulation and phenotype among other relevant cell types.**

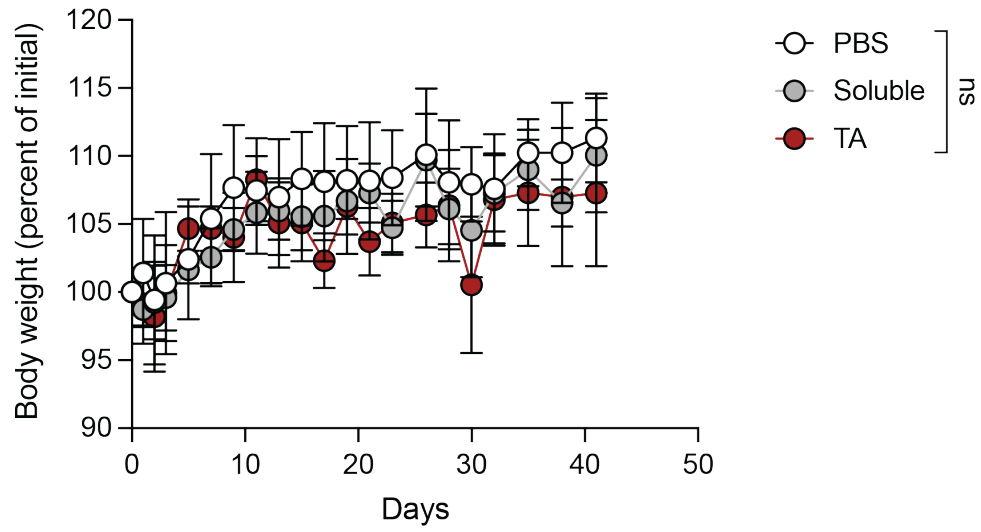
C57BL/6J mice (n=4) were immunized subcutaneously at the tail base with fluorophore-labeled OVA (Alexa Fluor 647) (10  $\mu$ g) and CpG (FITC) (10  $\mu$ g) with different ratios of TA. After 48 hours, lymph nodes were extracted and processed into a single-cell suspension for flow cytometry. (A-C) Median fluorescence intensity (MFI) of CD86 expression and OVA uptake among resident cDC1 (A), cDC2 (B), and migratory cDC1 (C). (D) MFI of CpG uptake among moDCs, B cells, macrophages, resident cDC1s, cDC2s, and migratory cDC1s. For all plots, data were analyzed by one-way ANOVA followed by Tukey's post-hoc test.

ns, not significant, \*\*\*\* $p < 0.0001$ , \*\* $p < 0.01$ . Bars with brackets indicate the result of the one-way ANOVA. Bars without brackets indicate the result of multiple comparisons.



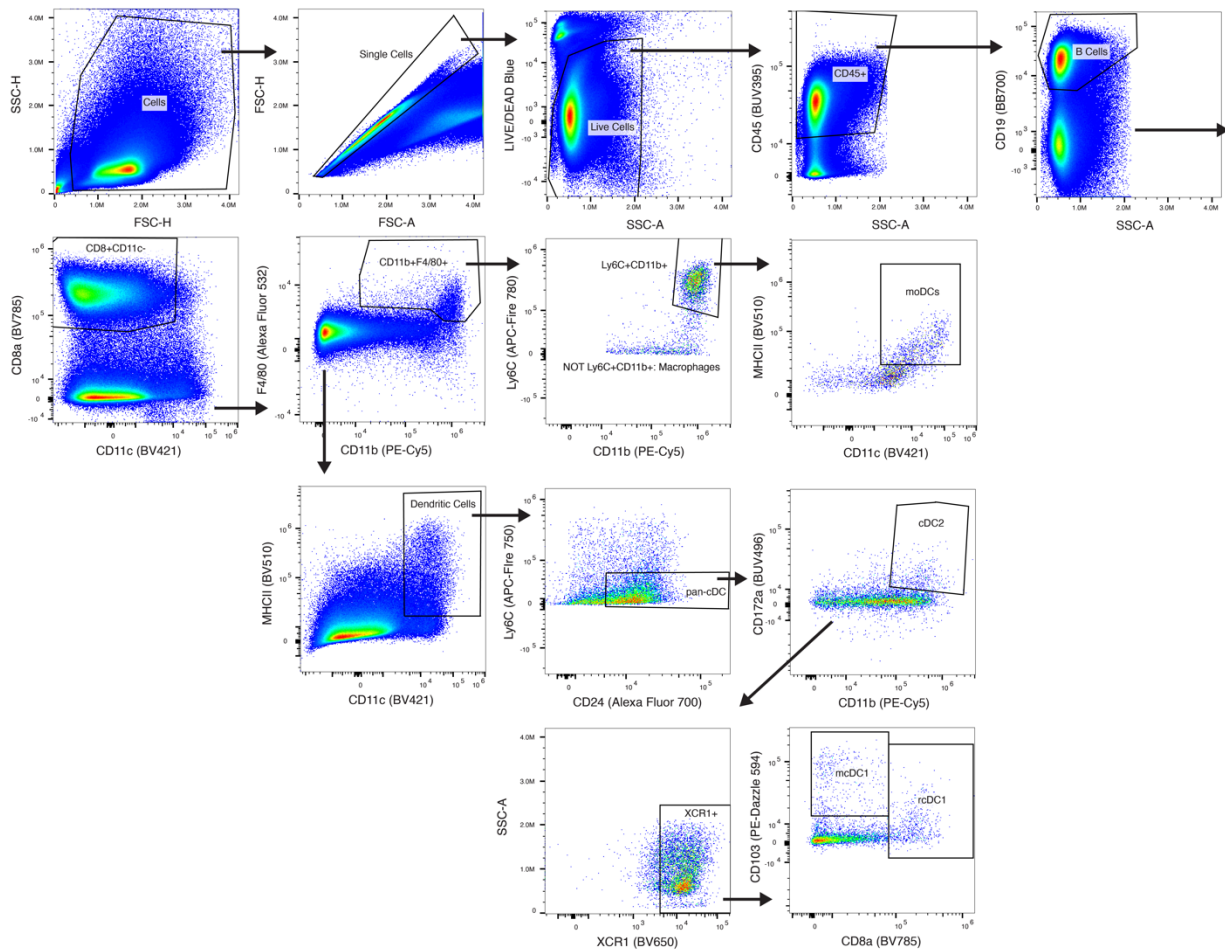
**Appendix Fig. 13. Phenotype of BMDCs cultured with vaccine formulations containing TA.**

BMDCs were cultured with indicated vaccine formulations at a 1:50 dilution in complete media with or without GM-CSF for 24 hours. (A-C) IL-6 secretion by BMDCs. “Mix” indicates a condition in which TA and the vaccine formulation were not complexed prior to addition, and instead added separately to the media. Data were analyzed by two-way ANOVA followed by Tukey’s post-hoc test. ns, not significant. (B) Median fluorescence intensity (MFI) of CD80 among CD80-positive cells. (C) MFI of CCR7 among all cells.



**Appendix Fig. 14. Mouse body weight following RBD vaccination.**

C57BL/6J mice (n=5) were immunized subcutaneously at the tail base with RBD (5  $\mu$ g) and CpG (10  $\mu$ g) either in soluble form or with TA (0.25 mg/mL, 147:1 TA:RBD ratio) for a total of three doses on days 0, 14, and 28. Data were analyzed by two-way ANOVA. ns, not significant.



**Appendix Fig. 15. Representative flow cytometry gating plots of immune cells in the lymph nodes.** Arrows arising within a gate indicate analysis of the gated population in the next plot. Arrows arising outside a gate indicate analysis of the ungated population in the next plot.

### 6.3. Appendix C: Tables

**Appendix Table 1. Examples of current clinical trials for DC/APC vaccines.**

<i>NCT</i>	<i>Phase</i>	<i>Sponsor/Collaborator</i>	<i>Product Name</i>	<i>Indication</i>	<i>Antigen Material</i>	<i>Antigen Type</i>	<i>Antigens</i>	<i>Route</i>	<i>Combination Therapy</i>	<i>Specific Combination</i>	<i>Extra Details</i>
NCT05100641	3	Aivita Biomedical	AV-GBM-1	Glioblastoma	Lysate (autologous)	Lysate	N/A	SC	Chemotherapy, cytokine	Temozolomide, GM-CSF	N/A
NCT01983748	3	University Hospital Erlangen	DCaT-RNA	Uveal melanoma	TTRNA (autologous)	Lysate	N/A	IV	None	N/A	N/A
NCT03059485	2	Dana-Farber Cancer Institute	DC/AML	AML (in remission)	Tumor fusion (autologous)	Tumor fusion	N/A	Unspecified	None	N/A	N/A
NCT03387553	1	H. Lee Moffitt Cancer Center and Research Institute	DC1	Breast cancer	Unknown	TAA	HER2	IN	Chemotherapy, surgery	TCHP	N/A
NCT04912765	2	National Cancer Centre, Singapore	N/A	Liver cancer, colorectal cancer	Peptide	Neoantigen	N/A	ID	Antibody - ICB	Nivolumab	N/A
NCT05127824	2	University of Pittsburgh	alpha-DC1/TBVA	Clear cell renal carcinoma	Peptide	TAA	Tumor blood vessel antigens	ID	Chemotherapy, surgery	Cabozantinib	Alpha type 1-polarized DC
NCT01946373	1	Karolinska University Hospital	N/A	Melanoma (metastatic)	Lysate, peptide	Lysate, TAA	NY-ESO-1	ID	Cell therapy, cytokine	T cells (TIL), IL-2	N/A
NCT03371485	1	Cancer Research UK	AST-VAC2	NSCLC	Unknown	TAA	hTERT	ID	None	N/A	Allogeneic, ESC-derived DC

**Abbreviations:** DC: dendritic cell, APC: antigen-presenting cell, AML: acute myeloid leukemia, NSCLC: non-small cell lung cancer, TTRNA: total tumor RNA, TAA: tumor-associated antigen, SC: subcutaneous, IV: intravenous, IN: intranodal, ID: intradermal, ICB: immune checkpoint blockade, GM-CSF: granulocyte-macrophage colony-stimulating factor, TIL: tumor-infiltrating lymphocyte, ESC: embryonic stem cell

**Appendix Table 2. Indications for DC/APC vaccine clinical trials.**

<b>Indication</b>	<b>Mentions</b>	<b>% of Trials</b>
Brain	30	23.6
Blood	15	11.8
Lung	10	7.9
Skin	10	7.9
Anogenital	8	6.3
Breast	8	6.3
Colorectal	6	4.7
Ovary	6	4.7
Liver	4	3.1
Pancreas	3	2.4
Kidney	3	2.4
Fallopian tube	3	2.4
Peritoneum	3	2.4
Head and neck	3	2.4
Eye	2	1.6
Cervix	2	1.6
Other	6	4.7
Multiple/unknown	5	3.9

**Appendix Table 3. DC/APC antigen identities.**

<b>Antigen</b>	<b>Mentions</b>
WT1	9
HER2	6
Cytomegalovirus pp65	5
Survivin	5
hTERT	4
NY-ESO-1	4
MART-1	3
Tumor blood vessel antigens	2
MAGE-A3	2
HPV16 (E6/E7)	2
MUC1	2
Stem-like cells associated antigens	1
Folate receptor alpha	1
DKK1	1

gp100	1
Tyrosinase	1
PRAME	1
IDO	1
Glioblastoma stem cell-like antigens	1
TRP2	1
KRAS	1
p53	1
HER3	1
CEA	1
MAGE-A4	1
Multi-MAGE	1
MG-7	1
BCR-ABL	1
Proteinase-3	1

**Appendix Table 4. Antibodies used in the lymph node analysis study.**

Target	Fluorophore	Supplier	Catalog #
CD45	BUV395	BD Biosciences	564279
Viability	LIVE/Dead Blue	Invitrogen	L23105
CD172a	BUV496	BD Biosciences	741131
CD86	BUV737	BD Biosciences	741737
CD11c	BV421	Biologend	117343
MHCII	BV510	Biologend	107636
CD69	BV605	Biologend	104530
XCR1	BV650	Biologend	148220
CD80	BV711	BD Biosciences	740698
CD8a	BV785	Biologend	100750
CpG	FITC	N/A	N/A
F4/80	Alexa Fluor 532	Invitrogen	58-4801-82
CD19	Brilliant Blue 700	BD Biosciences	566412
SIINFEKL	PE	Biologend	141604
CD103	PE-Dazzle594	Biologend	121430
CD11b	PE-Cy5	Invitrogen	15-0112-81
CD169	PE-Cy7	Biologend	142412
OVA	Alexa Fluor 647	N/A	N/A
CD24	Alexa Fluor 700	BD Biosciences	564237
Ly6C	APC Fire 750	Biologend	128046

**Appendix Table 5. Antibodies used in the germinal center analysis study.**

<b>Target</b>	<b>Fluorophore</b>	<b>Supplier</b>	<b>Catalog #</b>
Viability	LIVE/Dead Blue	Invitrogen	L23105
CD44	BV510	Biolegend	103043
CXCR5	BV785	Biolegend	145523
CD4	FITC	Biolegend	130308
B220	Alexa Fluor 594	Biolegend	103254
GL7	PE-Cy7	Biolegend	144619
PD-1	APC	Invitrogen	17-9981-82
CD3	Alexa Fluor 700	Biolegend	100215
CD38	APC-Fire 810	Biolegend	102746